MECHANICAL, PIEZORESISTIVE AND FRACTURE BEHAVIOR OF VARIOUS TYPES OF SMART CEMENTS

A Thesis

Presented to

the Faculty of the Department of Civil and Environmental Engineering

University of Houston

In Partial Fulfillment

of the Requirements for the Degree

Master of Science

in Civil Engineering

by

Praveen Ramanathan

December 2014

MECHANICAL, PIEZORESISTIVE AND FRACTURE BEHAVIOR OF VARIOUS TYPES OF SMART CEMENTS

Praveen Ramanathan

Approved:

Chair of the Committee
Cumaraswamy Vipulanandan, Professor,
Civil and Environmental Engineering

Committee Members:

Yi-Lung Mo, Professor,
Civil and Environmental Engineering

Robello Samuel, Adjunct Professor,
Petroleum Engineering

Suresh K. Khator,
Associate Dean,
Cullen College of Engineering

Roberto Ballarini,
Professor and Chairman,
Civil and Environmental Engineering

ACKNOWLEDGEMENTS

First and foremost, I would like to express my sincere gratitude to Dr. Cumaraswamy "Vipu" Vipulanandan for his valuable guidance, kindness, and encouragement throughout the course of this study. His support will never be forgotten. I would also like to extend my appreciations to Dr. Li-Lung Mo and Dr. Robello Samuel for serving on my thesis committee and sharing their valuable suggestions.

I owe my deepest gratitude to the faculty and the staff of Civil and Environmental Engineering Department at the University of Houston for their support and encouragement. I am indebted to the members of the GEM group for their assistance, companionship, and encouragement. Special thanks are extended to Niousha Amani, Kibraeb Gebreselassie, Bahareh Basirat, Sara Ranjbarian, Renuka Pakeetharan, Ahmad Salih, Dongmei Pan, Anudeep Reddy, Chella Ganapathy, Saravanan Ravichandran, Jeannot Ahossin, Shiva Sundar, Ranjith Rajasekaram, Srisothynaathan Pakeetharan and Danistan Joseph for their support and friendship.

The financial support provided by the CIGMAT, THC-IT, and the Department of Civil and Environmental Engineering at the University of Houston is gratefully acknowledged. Finally, I would like to thank my parents, siblings, friends, and relatives for their understanding, unconditional help, endless patience, and encouragement when it was most required. This thesis is dedicated to my parents who have supported me throughout my life.

To My Father

Senathirajah Ramanathan

MECHANICAL, PIEZORESISTIVE AND FRACTURE BEHAVIOR OF VARIOUS TYPES OF SMART CEMENTS

An Abstract

of a

Thesis

Presented to

the Faculty of the Department of Civil and Environmental Engineering

University of Houston

In Partial Fulfillment

of the Requirements for the Degree

Master of Science

in Civil Engineering

by

Praveen Ramanathan

December 2014

ABSTRACT

Cement sheath integrity is an important factor that contributes to the long economic production life of the oil well. Hence there is a need for monitoring the performance of the cement sheath during the entire service life.

This study analyzed a well monitoring system based on electrical resistivity and resistance to effectively monitor the behavior of various classes of cement (API classes A, G and H) sheaths by making them bulk sensing materials. Addition of small amount of carbon fiber enhanced the self-sensing property of the oil well cement making the cement a smart material. Piezoresistivity of the smart cements were studied under various loading conditions up to 28 days of curing. Up to 250% change in resistivity was observed during various types of loading conditions. Mechanical properties also were characterized and the 28 day elastic modulus for different cements varied between $2.7x10^6$ to $3.5x10^6$ psi. Also the Poisson's ratio varied between 0.15 to 0.2. Split tensile strength varied between 230 to 285 psi while flexural strength was in the range of 385 to 430 psi. Fracture properties were characterized for oil well cement. Stress intensity factor K_I was in the range of 0.3 to 0.6 MPa.√m and the Crack Tip Opening Displacement (CTOD) varied between 3 to 6 μm. Impedance characterization of the smart cements used in this study identified them as special bulk material which has resistance only and the capacitance effect was negligible. The monitoring methods studied using lab scale models of oil well were successful in monitoring the placement of different types of fluids used in the well including cement slurry. Also a piezoresistive repair material was developed to repair damaged oil well to regain 90% of strength and self-sensing properties.

TABLE OF CONTENTS

LIST OF FIGURES

LIST OF TABLES

CHAPTER 1 INTRODUCTION

Maintaining the integrity of an oil well is an important factor in economic production of oil and gas during the life of a well. Therefore monitoring the behavior of oil well is of increasing interest of the time. Though improvements happen and new techniques are adopted over the time with respect to monitoring methods of the cement sheath, limitations of the available methods are felt in the industry. Lot of money and effort are invested to continuously improve the available methods for better integrity of the cement sheath. This study attempts to propose an innovative method to monitor the behavior of the cement sheath starting from its placement.

1.1 Problem Statement

Even though very large amount of cement is used in the oil well industry, unlike other construction industries the access to the resulting cement structure, which is cement sheath placed in the annulus of a well between steel casing and formation, is limited to the bare hands and naked eyes. Even though there are limitations in accessibility to the cement sheath, the integrity of the cement sheath highly affects the successful economic life of a well.

So it gets the primary interest of the petroleum industry to monitor and maintain the integrity of the cement sheath. Because of the limited accessibility, monitoring of the well integrity is also limited to the tools and instruments that can be sent or placed at the depth of interest which is generally up to several thousands of feet. Finding an effective solution for the problem of monitoring the behavior of cement sheath within these limitations is of challenge.

Monitoring the behavior of the cement sheath should start from the placement of cement as most of the contaminations with drilling mud, oil and other materials happen during this stage. Mud contamination may leave a mud pocket and all contaminations affect the strength of the material. During the life of the well, cement sheath experiences various pressures applied due to

well operations, pressure test and thermal effect. Monitoring the stress level throughout the depth of the well is therefore important to make sure there are no severe cracks or to identify failures. This study proposes such monitoring system that can be used from the placement of cement throughout the production life of the well.

1.2 Objectives

The general objective of this study was to propose an electrical resistance and piezoresistivity based self-sensing monitoring system to monitor the behavior of cement sheath of oil well. Specific objectives include the following:

- To characterize piezoresistive and mechanical properties of carbon fiber modified oil well cement of different classes
- To study the relationship between fracture formation and piezoresistive behavior
- To study the mode I fracture properties of different classes of oil well cement
- To study the effectiveness of electrical resistance and resistivity based monitoring system in oil well model
- To propose an effective piezoresistive repair method that could regain the strength and the piezoresistivity of cracked or damaged oil well cement sheath

1.3 Organization of the Chapters

This thesis is organized into eight chapters. Chapter 1 is introduction to the study. Chapter 2 summarizes the background and literature review related to cement sheath integrity of oil well and discusses the necessity of a monitoring system which can monitor the behavior of cement sheath. Chapter 3 explains the materials and methodology used in this study. It also explains the experiments conducted in this study. Chapter 4 characterizes different classes of oil well cements used in this study. It includes the mechanical and piezoresistive properties of

different classes of well cement. Impedance characterization is also addressed in chapter 4. Chapter 5 studies mode I fracture properties of different classes of oil well cement and relates the piezoresistivity experimentally to fracture properties. Chapter 6 studies four oil well models of laboratory scale to experiment the effectiveness in electrical resistance and resistivity based sensing method. Chapter 7 consists of proposed repair material and method in regaining strength and piezoresistivity in a damaged cement sheath. Chapter 8 summarizes the conclusions of the study and recommendations are made for future studies.

CHAPTER 2 BACKGROUND AND LITERATURE REVIEW

This chapter provides the background information about the oil and gas well and the related operations during the life of a well. The importance of maintaining and monitoring the integrity of cement sheath is explained by going through the life of the well step by step. It also outlines the challenges faced by the oil and gas industry as reported in the literature with respect to maintaining the integrity of the cement sheath of a well. It highlights the need for an effective real time monitoring system to monitor the health of the well. This chapter also discusses the importance of monitoring the well even during the placement of cement in the annulus and throughout the production life of the well to have an effective control over the health of the well.

2.1 Oil Well

A typical well can be thousands of meters deep, less than a meter wide, and is constructed by using a metal casing surrounded by cement mix which is known as cement sheath that fills the annulus between the outer surface of the casing and the wall formation of the borehole (Lafarge North America Inc.). Life of a well typically lasts around 40 to 50 years which includes different stages before and after oil or gas production (Campbell, 2012).

2.1.1 Life of a Well

The typical life of a well can be divided into five stages namely Pre-exploration, Exploration, Development, Production, and Abandonment (Cairn Energy Plc, 2014, Campbell, 2012). The stages of the well life are shown in Figure 2-1.

Before making an investment and applying for an exploration license, proper due-diligence should be carried out, considering potential safety, social, political and environmental impacts. To be awarded with exploration license, necessary documents explaining legal status, financial capability, technical competence, plans to manage health, safety and environmental

risks, and contributions to local economic development should be submitted to the relevant authorities.

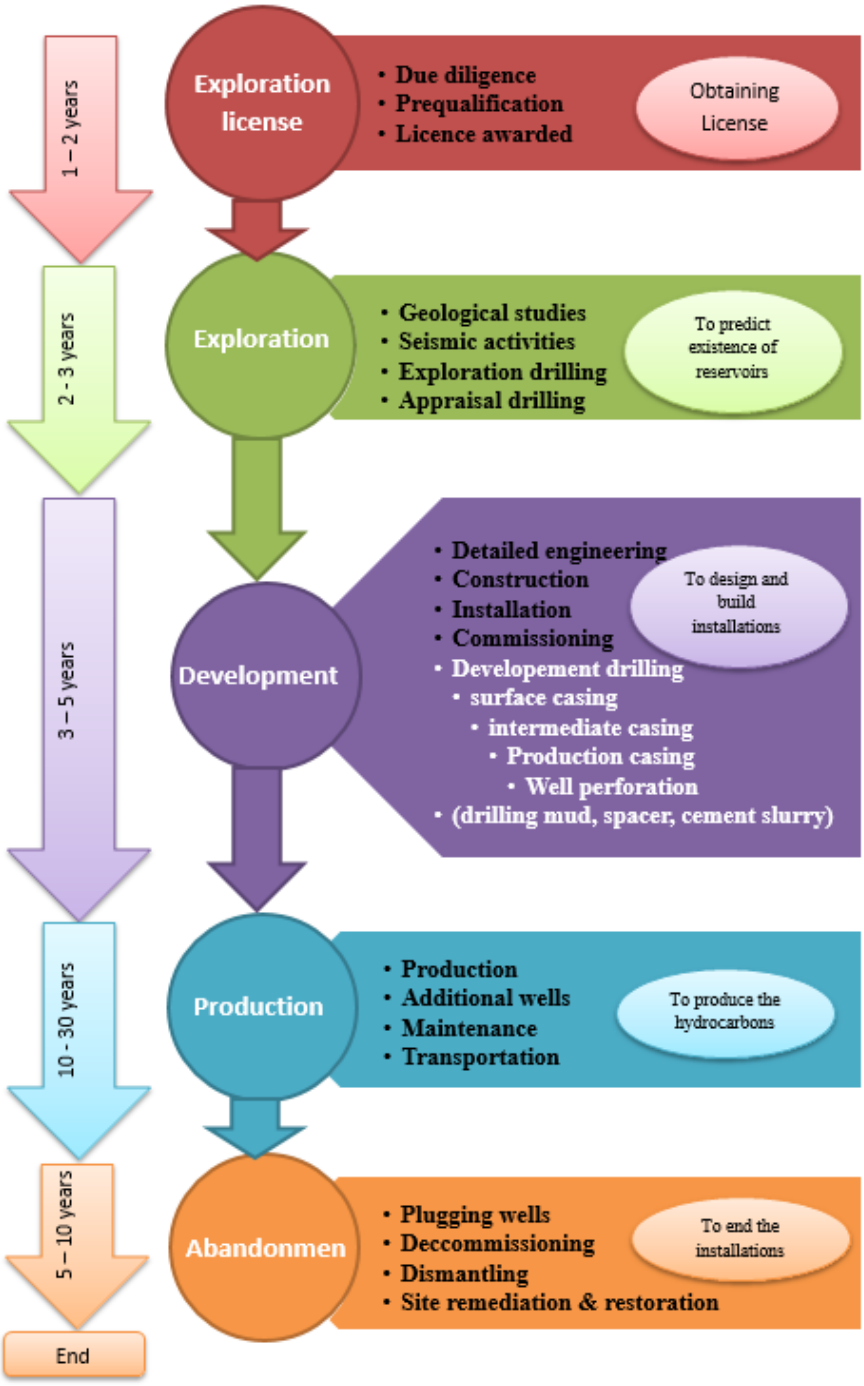

Figure 2-1: Typical Life of an Oil Well

Once exploration stage begins, geological and seismic surveys are carried out to develop a picture of geological structures below the surface. This helps identify the likelihood of an area containing hydrocarbons. Exploration wells are drilled to determine whether oil or gas is present at the selected location. If promising amounts of oil and gas are confirmed during the exploration phase, appraisal wells are used to establish the size and characteristics of the discovery and to provide technical information to determine the optimum method for recovery of the oil and gas.

If appraisal wells show technical and commercial viable quantities of oil and gas, development phase will be started. Drilling and completion are two important phases in constructing the production well in development phase. Completion includes cementing, which ensures the zonal isolation of the well throughout the later life of the well, by leaving a cement sheath in the annular space between casing and formation.

Production phase starts at the end of development stage, and lasts around 30 years (Marathon Oil Corporation, 2010, Campbell, 2012, Cairn Energy Plc, 2014). Production stage is the most important stage of a well's life because it gives the economic benefits. Good primary cement job is necessary for the better performance of a well during the long lasting production life (Calvert, 1990). Number of wells may be increased during this phase based on the need. Products will be transported through pipelines to the desired location for further processing or storage.

A well will be shut-in and abandoned when it reaches an economic limit, where its most efficient production rate does not cover the operating expenses. Permanent plugs and cement will be set in the wellbores to ensure full isolation from the reservoir and to prevent any leaks.

2.1.2 Drilling and completion phase of a well

Drilling and completion is a very important step of development phase which ensures the integrity of the well. Once the drilling rig is assembled on site, drilling

process begins. The drill bit is lowered into the hole by adding sections of drill pipe at the operating surface. A typical drill bit is shown in Figure 2-2.

Drilling fluid is pumped in the pipe and travels down through the bit, and back to the surface, carrying rock pieces, called cuttings (Marathon Oil Corporation, 2010).types of drilling fluids are discussed below.

Figure 2-2: Typical Drill Bit

2.1.3 Drilling Fluids

Drilling a well disturbs long settled and precariously balanced stress. This disturbance should be compensated by using drilling fluids to exert hydrostatic pressure on the formation (Clamart et al., 2008).

The drilling fluid has several functions. As it passes out of the drill bit, it lubricates the cutting surface, reduces friction and wear, and keeps the drill-bit cooler. While traveling back up the hole, the mud also provides pressure to prevent the hole from caving in on itself (Marathon Oil Corporation, 2010).

Commonly available types of drilling fluids are listed below.

- ***Water Based Fluids***: The base fluid may be fresh water, seawater or brine. Water-based fluids are used to drill approximately 80% of all wells (Oilfield Market Report, 2004).

- ***Oil Based Fluids***: Oil-based fluids in use today are formulated with diesel, mineral oil, or low-toxicity linear olefins and paraffin. Oil-based systems were introduced in 1960s to address the problems of water based fluid reacting or swelling formation clays, increasing downhole temperatures, contaminants and stuck pipe, torque and drag
- ***Synthetic-Based Drilling Fluids:*** Synthetic-based fluids were developed out of an increasing desire to reduce the environmental impact of offshore drilling operations, but without sacrificing the cost-effectiveness of oil-based systems.
- ***Pneumatic-Drilling Fluids:*** Compressed air or gas can be used in place of drilling fluid to circulate cuttings out of the wellbore. Pneumatic fluids can be air or gas only, aerated fluid or foam (Negrao, 1999)

Removing drilling mud from the wellbore is critical for successful zonal isolation. Therefore, the borehole should be washed out and during the hole cleaning operation, formation pressure must be contained and drilling fluid must be displaced by a higher density fluid called spacer which is pumped behind the mud and ahead of the cement.

2.1.4 Spacer Fluid

The spacer is designed to keep the drilling fluids and the cement apart while the cement is being pumped through the casing into the annulus, and is generally formulated with the viscosity close to or greater than that of the drilling fluid (Simon and Guillot, 1991, Clamart et al., 2008). Besides maintaining well control, the spacer also serves as a chemical wash to clean the leftover drilling mud from the casing-casing and casing wellbore annuli. If the spacer leaves drilling fluids behind, or if it allows them to mix with the cement, then good bonding between cement and the formation or casing is unlikely (Clamart et al., 2008). Since these contaminations remain in a liquid state, they are liable to form channels of communication between zones along the borehole or casing. (Clamart et al., 2008).

2.1.5 Casing and Cementing

Casing a well is a task performed to ensure the integrity of the wellbore throughout the drilling and production phase. At certain depths, drilling will be stopped to place steel casing into the ground to protect the hole as well as surrounding rock layers and underground aquifers. The casing is fixed in place by pumping cement down the inside of the casing and up the outside annulus between the steel casing and the surrounding rock. Drilling operations are halted until the cement hardens (Marathon Oil Corporation, 2010).

Casing, based on the depth at which it is fixed and the purpose of it, can be divided into three types; surface casing, intermediate casing, production casing. Larger diameter surface casing is used in the uppermost portion of the well to ensure well wall integrity and for well control. Production casing is set when the well is to be brought to production.

Between surface casing and production casings, intermediate casing could be placed based on the depth of the well, depth of the surface casing, and the relative pressure of shallow formation as compared to deeper formation. Figure 2-3 shows a schematic diagram of a cased cemented well.

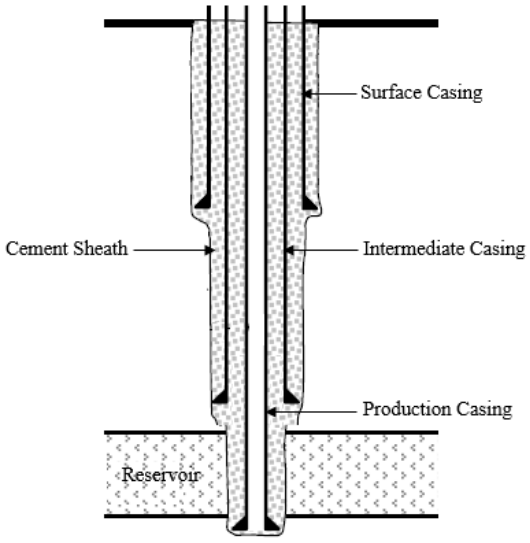

Figure 2-3: Schematic Diagram of a Cased Cemented Well

The casing and cement create a physical barrier between the external formation and the inside of the pipe to stop external fluids from entering the wellbore during drilling and production. It also keeps production fluids and natural gas from escaping the wellbore in the production phase.

To finish the drilling process, a stack of valves is placed on top of the wellhead to allow access to the wellbore for the future use. The casing is pressure tested to ensure integrity, i.e., there is no leak paths.

The wellbore is then perforated at the designed depth by sending a perforating gun which creates holes through the casing and cement into the rock formation allowing the oil and natural gas to flow from the rock formation into the well (Marathon Oil Corporation, 2010). To enhance productivity, a well stimulation process known as hydraulic fracturing is used to create small cracks in the underground geologic formations that in turn allow fluids and natural gas to flow more easily into the well and up to the surface.

2.2 Primary Cementing Job

Primary cementing is the process of placing a cement sheath in the annulus between the casing and the formation (Nelson, 2012). The main objective of a primary cementing is to provide complete and permanent isolation of the formation behind the casing (Simon and Guillot, 1991). The producing performance of a well depends largely on a good primary cementing job (Calvert and Smith, 1990).

In an ideal cement job, there is a complete hydraulic seal between the casing and the formation throughout the zones of interest (Calvert and Smith, 1990). A schematic diagram of primary cement job in progress is shown in Figure 2-4 (Simon and Guillot, 1991).

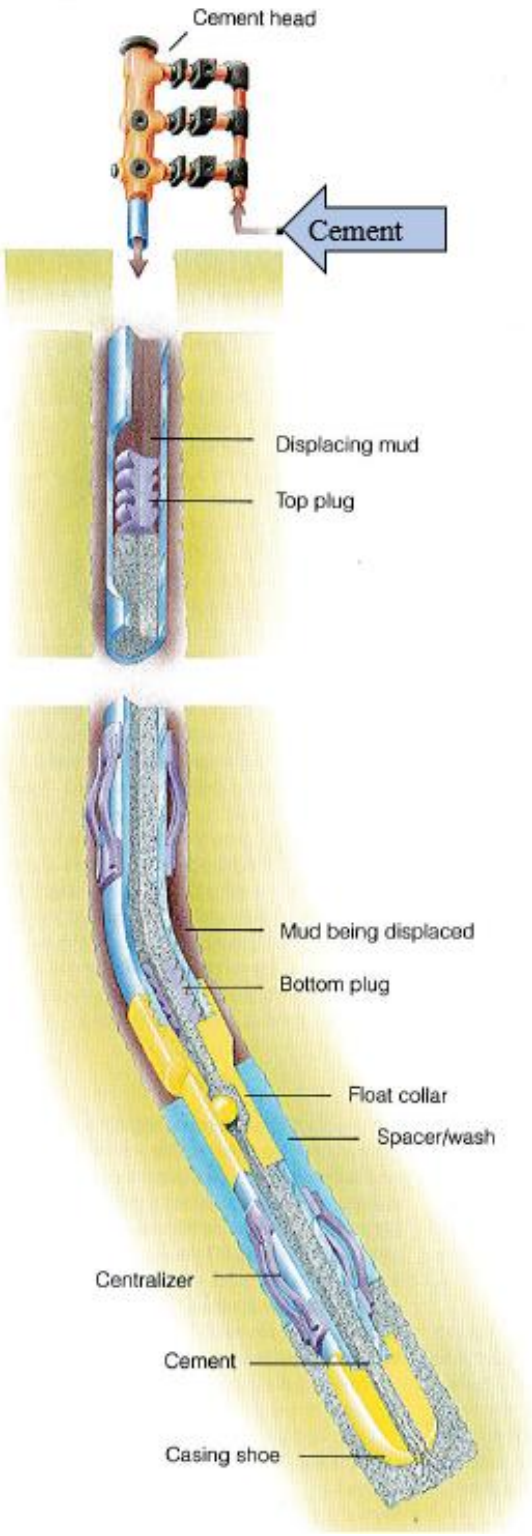

Figure 2-4: Schematic Diagram of Primary Cement Job in Progress

As shown in Figure 2-4, float collar prevents flow back of the cement slurry when pumping is stopped. Without a float collar or float shoe, the cement slurry placed in the annulus could U-tube, or reverse flow back into the casing. A float collar is installed near the bottom of the casing string (Nelson, 2012).

A float shoe attached to the bottom of the casing string prevents reverse flow as a float collar does (Calvert and Smith, 1990). It also guides the casing toward the center of the hole to minimize hitting rock ledges or washouts as the casing is run into the wellbore. By floating casing in, hook weight is reduced (www.glossary.oilfield.slb.com).

Centralizers are the devices that help keep the casing in the center of the wellbore to ensure efficient placement of a cement sheath around the casing string (Calvert and Smith, 1990). If casing strings are cemented off-center, there is a high risk that a channel of drilling fluid or contaminated cement will be left where the casing contacts the formation, creating an imperfect seal (Nelson, 2012).

Top and bottom plugs are rubber plugs used to separate the cement slurry from other fluids and reduce contamination. The bottom plug is launched ahead of the cement slurry to minimize contamination by fluids inside the casing prior to cementing. A diaphragm in the plug body ruptures to allow the cement slurry to pass through after the plug reaches the landing collar. The top plug has a solid body that provides positive indication of contact with the landing collar and bottom plug through an increase in pump pressure (Nelson, 2012; Calvert and Smith, 1990).

Further, scratchers with metal wires can be used to scrape mud cake off permeable zones to help obtain a solid cement column by removing the mud cake.

2.2.1 Good Primary Cementing Practices

Some of the good cementing practices in the literature are summarized below. Most of them meet the requirement of an ideal well.

- The ideal cementable wellbore is 3 in. larger than the casing outer diameter (the absolute minimum is 1 1/2 in. larger), as nearly gauge as possible (without washouts), as straight as possible (without severe doglegs), stabilized and properly conditioned (without sloughing, flowing, or losing circulation) as shown in Figure 2-5 (Calvert and Smith, 1990).
- Minimum strength required for any operation is 500 psi in 24 hours at downhole static temperature (Calvert and Smith, 1990).
- Finely centered casing (Calvert and Smith, 1990, Goodwin, 1997).
- Hole is circulated until a minimum of 85% of the annular volume is circulating (Goodwin, 1997).
- Drilling mud is thinned as much as possible before cementing (Bittleston and Guillot, 1991; Goodwin, 1997).
- Casing is reciprocated or rotated during circulation and cementing (Bittleston and Guillot, 1991; Goodwin, 1997).
- A minimum of 500 linear ft of water (or spacer if required for pressure control) in the annulus is pumped ahead of the cement (Goodwin, 1997).
- Cement slurry is mixed within ± 0.2 lbm/gal accuracy of planned density (Goodwin, 1997).
- Cement is circulated to the surface (Goodwin, 1997).
- Flow or loss circulation problems are solved before cementing (Goodwin, 1997).
- Proper use of centralizers, cement plugs, scratchers and other casing hardware (Bittleston and Guillot, 1991).
- Use of chemical washes and spacers (Bittleston and Guillot, 1991).

Figure 2-5 (Calvert and Smith, 1990) summarizes few good cementing practices for wellbore. It gives the ideal diameter requirement also.

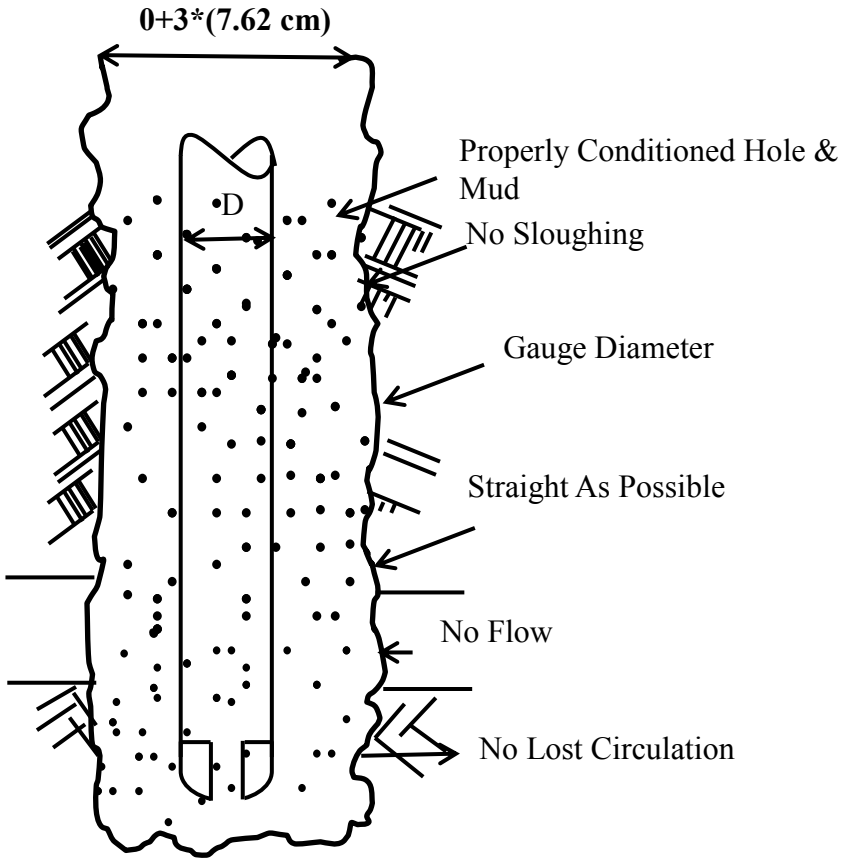

Figure 2-5: Good Cementing Practices for Wellbore

No flow should be permitted for the communication of fluids in and out of the casing to ensure the function of the cement sheath integrity. The vertical edges are expected to be straight as possible.

2.3 Oil Well Cement - Introduction and History

Portland cement is produced by partially fusing powdered blends composed of limestone with materials like clays, shale, blast- furnace slag, siliceous sands, iron ores, and pyrite cinders. From a chemical standpoint, these blends may be considered to be mixtures of the oxides of calcium (CaO), aluminum (Al_2O_3), silicon (SiO_2), magnesium (MgO), iron (Fe_2O_3),

potassium (K_2O) and sodium (Na_2O). During heating to about 2,700°F, these oxides combine to form calcium silicates and aluminates (commonly referred to as "clinker") that can react with water to form a hydrated product with cementitious properties. The paste of Portland cement and water will harden under water and in air. Portland cement is known as hydraulic cement (Bouge, 1947).

Hydraulic cements set and harden by reacting chemically with water, which is known as hydration and forms a stone like mass. Hydration begins as soon as cement contacts water. During the hydration process, each cement particle forms a type of growth on its surface that gradually spreads until it adheres with the growth from other adjacent cement particles which results in progressive stiffening, hardening, and strength development result.

2.3.1 History - The Need of API Specification for Oil Well Cements

Test procedures and specifications for the performance of various types of Portland cement in construction work are maintained by the American Society for Testing and Materials (ASTM). After following ASTM standards for some time period, the oil industry determined that the ASTM tests were inadequate for determining the performance of cements in wells because they were made under conditions unlike those encountered in well cementing - operations (Calvert and Smith, 1990).

In 1952, the national API committee adopted standards for six classes of cements used in oil and gas well cementing operations. The first tentative standard in 1953, designated API Standard 10A, was entitled API Specification for Oil-Well Cements. The standards for six API classes of well cements covered chemical requirements, determined by ASTM procedures, and physical requirements, determined in accordance with procedures outlined in API RP 10B and ASTM. API Specifications represent a realistic method of classifying Portland cement for use in wells by specifying the required properties. Figure 2-6 summarizes the history of oil well cement.

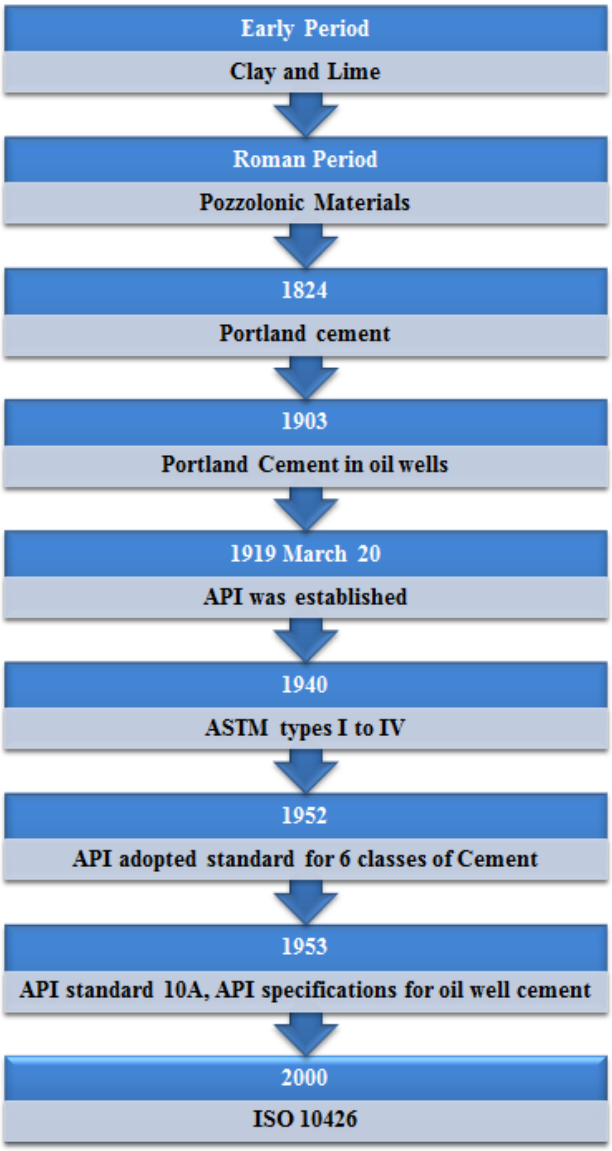

Figure 2-6: History of Oil Well Cement

2.3.2 API classes of Oil well Cement

The API specification has defined nine different classes of cement A, B, C, D, E, F, G, H and J. Specification 10A discuss about the types of cement. A brief summary from the literature on API classification on Portland cement is given in Table 2-1 (J.J. Azar and Samuel, 2007; Halliburton, 1999; Lyons, 2009; Lyons and Plisga, 2011).

Table 2-1: Summary of Different Classes of Oil Well Cement

API Class (ASTM Type)	Applicable Depth	Condition required	API rec'd w:c	Specific gravity	Surface area (cm^2/gm)	Remarks
Class A (Type I)	surface – 6000 ft (0 - 1830 m)	No special properties required	0.46	3.14	1500	Ordinary Portland cement
Class B (Type II)	surface – 6000 ft (0 - 1830 m)	MSR, HSR	0.46	3.14	1600	Ordinary Portland cement
Class C (Type III)	Surface - 6000 ft (0 - 1830 m)	High early strength MSR, HSR	0.56	3.14	2200	High early cement Finer than class A and B
Class D	6000 - 10,000 ft (1830 - 3050 m)	MSR, HSR HPHT	0.38	3.16	1200	Retarded cement
Class E	10,000 – 14,000 ft (3050 - 4270 m)	MSR, HSR HPHT	0.38	3.16	1200	Retarded cement
Class F	10,000 – 16,000 ft (3050 - 4270 m)	HSR Extremely HPHT	0.38	3.16	1200	Retarded cement
Class G	As manufactured intended for surface – 8000 ft (0 - 2440 m)	MSR, HSR	0.44	3.16	1400	Basic well cement Can be used with accelerators and retarders to cover a wide range of well depths and temperatures. No addition other than calcium sulphate or water Class G is ground to a finer particle size than Class H.
Class H	As manufactured intended for surface – 8000 ft (0 - 2440 m)	MSR, HSR	0.38	3.16	1200	Basic well cement, Can be used with accelerators and retarders to cover a wider range of well depths and temperatures. coarser than G No addition other than calcium sulphate or water
Class J	As manufactured intended for 12,000 - 16,000 ft (3600 - 4880 m)	MSR, HSR Extremely HPHT				Can be used with accelerators and retarders to cover a range of well depths and temperatures. No addition other than calcium sulphate or water

Remarks: MSR- Moderate sulphate resistance, HSR- High sulphate resistance, properties to prevent deterioration of the cement from sulfate attack in the formation water, HPHT- High pressure High temperature

The ASTM C 150 specifications cover eight types of Portland cements, Types I, IA, II, IIA, III, IIIA, IV and V. They are manufactured for use at atmospheric conditions. The API classed A, B and C correspond to ASTM I, II, and III respectively. The API class D, E, F, G, and H and J are cements manufactured for use in deep wells and to be subject to a wide range of pressure and temperatures. These do not have corresponding ASTM types (Lyons, 2009).

Although the API defines nine different classes of cement, in general Classes A, B, C, G, and H are available from manufacturers and distributed in the U.S (Calvert and Smith, 1990). Classes G and H currently are the most widely used cements (Smith, 1987). Roughly 65% of the well cement made in the U.S. is Class H (mostly in the gulf coast and midcontinent regions), 15% is Class G (in the California and Rocky Mountain areas), and the rest is either Class A (10%) or C (10%). In international operations, approximately 95% of the well cement used is Class G (Canada, Europe, Middle East, South America, and Far East). Specialty cements constitute less than 1% of the worldwide downhole market (Calvert and Smith, 1990).

Table 2-1 shows the API recommended water to cement ratio for each types of cement. Figure 2-7 shows typical strength variation with water to cement ratio.

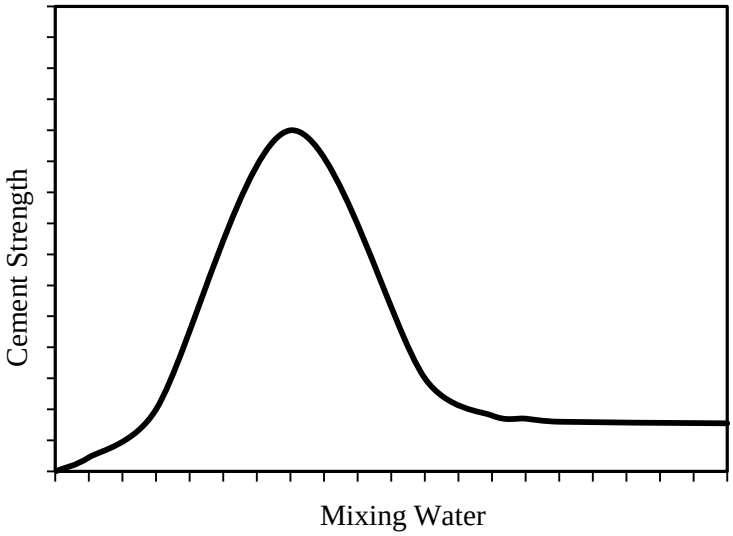

Figure 2-7: Typical Variation of Strength with Mixing Water

Though, the strength changes with the mixing water, strength cannot be the only criteria for selecting the water to cement ratio. Pumpability or flowablity also should be considered to determine the water to cement ratio.

2.3.3 Hydration of Oil Well Cement

The chemical reaction of cement with water that results in hardening of cement is called as hydration of cement. Cement hydration begins as soon as cement comes in contact with water (Smith et al., 1990).

When the cement is mixed with water, the binding phases in Portland cement (Ca_3SiO_5, Ca_2SiO_4, $Ca_3Al_2O_4$, and $Ca_4Al_nFe_2$-nO_7) react in different ways. During hydration of Portland cement, chemical reactions between the clinker components, calcium sulfate and water would take place, which will lead to continuous cement slurry thickening and hardening. In the Portland cement, more than 80% of the total material would be of silicate phase. Calcium silicate hydrate and calcium hydroxide are the products of hydration of both tricalcium silicate (Ca_3SiO_5) and dicalcium silicate (Ca_2SiO_4) as shown in Equation 2-1 and 2-2 (Natarajan, 2005)

$$2\ Ca_3SiO_5 + 7\ H_2O \rightarrow 3\ CaO \bullet 2\ SiO_2 \bullet 4\ H2O + 3\ Ca(OH)_2 \text{ and} \qquad 2\text{-}1$$

$$2\ Ca_2SiO_4 + 4\ H_2O \rightarrow 3\ CaO \bullet 2\ SiO_2 \bullet 4\ H2O + Ca(OH)_2. \qquad 2\text{-}2$$

The resulting product ‘Calcium Silicate Hydrate’ (C-S-H) gel is the principal binder of hardened cement. Also Calcium Silicate Hydrate comprises almost 70% of fully hydrated Portland cement. At short hydration times, $Ca_3Al_2O_4$ (aluminate phases) are the most reactive. Aluminate phases have a significant influence upon the rheology of the cement slurry and early strength development of the set cement. But their presence is relatively small compared to the silicates. Tricalcium aluminates ($Ca_3Al_2O_4$) hydration reactions are shown in the equation below (Natarajan, 2005),

$$2Ca_3Al_2O_4 + 27\ H_2O \rightarrow Ca_2 \bullet Al_2O_3 \bullet 8H_2O + Ca_4 \bullet Al_2O_3 \bullet 19H_2O. \qquad 2\text{-}3$$

The calcium aluminate hydrates (C_2AH_8 and C_4AH_{19}) will be converted into more stable form $Ca_3 \bullet Al_2O_3 \bullet 6H_2O$ from its metastable form by the reaction as shown in the equation below (Natarajan, 2005).

2.4 Functions and Importance of Cement Sheath

Placed between casing and wellbore, a cement sheath is expected to provide zonal isolation throughout the life of a well and to support the casing (Clamart et al., 2008; Goodwin, 1997). It also gives hydraulic seal that prevents fluid communication between producing zones in the borehole and blocks the escape of fluids to the surface. It also protects the steel casing against corrosion by formation fluids (Nelson, 2012).

Over time, stresses are imposed on the cement by pressure integrity tests, increased mud weight, casing perforation, stimulation of well, oil or gas production and increase or fluctuation in wellbore temperature (Jandhyala, 2013). Any of these may damage the sheath. Failure to achieve cement sheath integrity may severely limit the well's ability to reach its full producing potential (Nelson, 2012). Therefore maintaining the integrity of the well becomes very important in the life of the well.

But there are number of challenges in maintaining the integrity of the well starting from the placement of the cement in the annulus throughout the life of the well. If the issue is identified at proper time, remedial action could be taken. This is where the need arises for real time monitoring system.

2.5 Challenges Faced By the Oil Well Industry in Cementing and Cement Sheath Integrity

Wellbore integrity related issues are identified in two stages; pre-production stage and production stage (Carey, 2010). Issues found in the literature are discussed below.

2.5.1 Pre-Production Stage Related Issues

Pre-production stage issues are mainly related to drilling and cementing processes. After hardening of cement, finding out whether the cementing is good or bad does not help to solve the problem. Because, only liquids can be removed from annulus for replacement. If the cement hardens, regardless of its strength (good cement or bad cement) it could not be removed for replacement (1997, Goodwin). It implies the necessity of real time monitoring of cement installation or (placement in the annulus). Some of the pre-production stage issues are listed below.

- Whether the cement occupies 100% of the annulus (1997, Goodwin) or leaving pockets
- Contamination: Cement mixed with drilling mud, spacer or formation fluids in the annulus during and after placement yields a sheath of drastically reduced density and compressive strength (1997, Goodwin).
- Liquid and gas filled channels within the cement sheath or at the cement/formation interface (1997, Goodwin).
- Formation damage or caving (Carey, 2010): Drilling vibrations and unbalanced formation pressure during drilling might cause formation failure.
- Poor casing centralization (Carey, 2010): Poor centralization of casing may lead to incomplete cementing. Cement could not fully displace the mud from the off centered parts of annulus. The cement fills the wide opening of the well leaving pockets in narrow opening.
- Inadequate drilling mud removal (Carey, 2010): Drilling muds form gel-structure when the gel strength is higher than the breaking strength and forms mud cake. It happens when there is no circulation. Entrapped mud and other fluids cause channels and facilitate gas migration causing loss of sheath integrity and zonal isolation.
- Inadequate cement - formation and/or cement - casing bond (Carey, 2010)

- Cement shrinkage (Dusseault, 2000; Carey, 2010)
- Water loss: Under HPHT conditions water loss can occur. The lack of water for hydration will affect the strength.
- Mechanically induced stress: Waiting on cement and other well operations with heavy mud inside the casing about 2 days applies mechanical on cement sheath and casing during pre-production phase.

  Then pressure test will be performed by applying internal pressure along the entire casing string (around 5000 psi) after about 2 days from cement placement (Jandhyala, 2013, Clamart et al., 2008). Formation integrity test will be conducted with around 5400 psi about 2.5 days after cement placement (Jandhyala, 2013). This pressure can expand the casing, causing the cement sheath to experience tensile failure. This may lead to radial cracks and local de-bonding of the cement and casing (Clamart et al., 2008).Hydraulic fracturing, perforation and other well stimulation add more stress to this.
- Thermal induced stress: In the normal life cycle of a well, the wellbore is cooled during drilling and logging, flowed at high temperatures, and cooled periodically for logging or injection testing. This process can place very large stresses on the casing and the cement. Expansion of casing will have an effect on cement sheath too. Loads due to thermal cycling add to these stresses (Petty, 2003).

2.5.2 Production Phase Related Issues

Production stage issues are mainly related to the stresses and impacts on the cement sheath occuring during production stage operation. In a well there will be two types of operational loads, thermal and mechanical (Jandhyala et al., 2013) and stress induced by mechanical and thermal loading should be withstood for successful sheath integrity. Chemical attack is of another concern. Some of the production stage issues are listed below.

- Mechanical stress: Well stimulation during the production stage to increase the production and work over operations. It will cause fracture formation within cement and affect the sheath integrity allowing gas and other formation fluids to leak.
- Thermal loads: During production casing and cement sheath will experience extreme HPHT conditions and cyclic thermal and pressure loading. This causes expansion and contraction of the sheath.
- Formation of micro annulus at casing- cement interface
- Disruption of cement formation bond
- Geochemical attack (Carey, 2010): During the life of the well it may be exposed to aggressive environment. Direct chemical attack on cement sheath will degrade the cement. Sulphate resistant oil well cement serves the purpose of maintaining the integrity. High temperature and exposure to acidic environment (e.g., H_2S or CO_2) induce corrosion of casing and impacts on sheath integrity.

2.6 Cement Failure Modes

There are two mechanisms for loss of cement sheath integrity: damage in cement and de-bodning at the interfaces (Garnier et al., 2007). Damage of the cement sheath could be of following conditions (Ravi and Bosma, 2005, Catalin et al., 2013):

- Cracking of the cement sheath, which could allow radial and vertical migration of fluids (Figure 2-8).

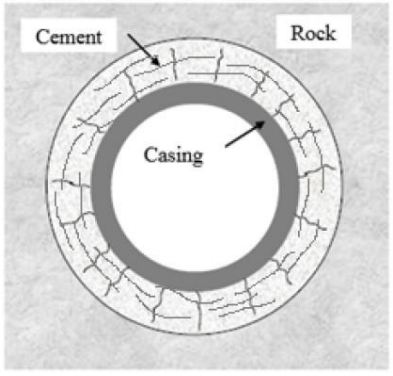

Figure 2-8: Cracks in Cement Sheath

- Plastic deformation in the cement sheath, which could allow radial and vertical migration of fluids (Figure 2-9).

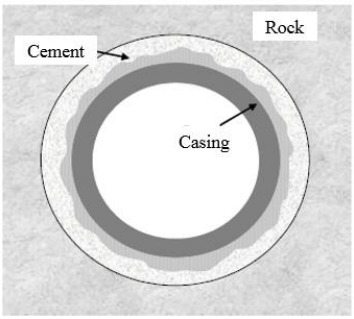

Figure 2-9: Plastic Deformation in Cement Sheath

The stresses induced in wellbore cement are caused by the pressures acting from both sides of the sheath, the outside formation pore pressure and inside pressure transmitted from the inside of the casing and due to other axial loadings. Thermal and mechanical stress, expansion of casing and HPHT fatigue loading conditions can also crack the cement sheath. Shrinkage of the cement could cause crack throughout the cement. The crack in the cement sheath propagates with time. These cracks can be of tensile, compressive or shear and radial, disk type and axial. Plastic deformation is the result of yielding. It usually results in the change of shape of the material. De-bonding of cement sheath can happen at following interfaces (2007, A. Garnier et al., 2005, K. Ravi and M. Bosma, Catalin et al., 2013).

- Rock-cement interface (Figure 2-10)

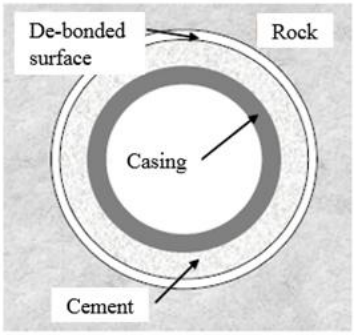

Figure 2-10: De-bonding at Rock – Cement Interface

- Cement-casing interface (Figure 2-11)

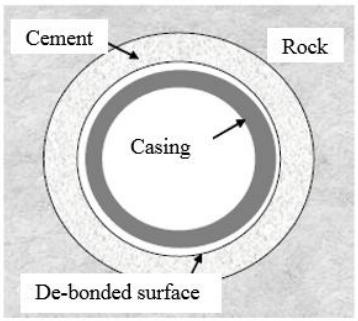

Figure 2-11: Debonding at Casing – Cement Interface

De-bonding of cement can lead to vertical migration of well fluids. De-bonding can be of shear de-bonding failure or tensile de-bonding failure at both interfaces. De-bonding can also occur due to cement shrinkage (Catalin et al., 2013).

2.7 Monitoring the Well Behavior

In contrast to other construction industries, where cement can be physically touched, tested and seen by naked eyes, the cement sheath constructed in oil well industry below the ground till several thousands of feet depth cannot be physically touched and seen by naked eyes (Goodwin, 1997), though oil well industry use bulk amount of cement and the well life highly depends on the cement sheath integrity. Therefore, we are forced to rely on the results of measurements from a variety of electronic downhole tools to define the quality and quantity of cement placed around the casing during the primary cement placement (Goodwin, 1997).

But, according to the literature, mechanisms associated with cement failure are partly because industry lacks appropriate or cost-effective monitoring options (U.S. Department of Energy). Industry lacks real time monitoring system which could be used to track the flow of cement during cement placement in the annulus till the end of the production stage. A real time monitoring system is therefore a challenge of the time.

2.7.1 Real Time Monitoring of Cementing while Placing

If the annulus is packed with bad cement or settled barite from the drilling mud or formation particles, no portion of the particulate matter can be removed and replaced by cement, because they are in solid form (Goodwin, 1997). Only liquids can be removed from the annulus for replacement. Therefore cement should be monitored while being placed and raising in the annulus to ensure good cement is placed and there are no air or mud pockets.

Cement mixed with drilling mud, spacer, or formation fluids in the annulus during and after placement yields a sheath of drastically reduced density and compressive strength. This contamination, especially severe gas influx from the formation, yields a cement sheath that is not recognizable as cement on a bond log measuring system (Goodwin, 1997). Therefore, good monitoring system is necessary to detect contamination during and after placement.

Cement bond log measurements can indicate a total-free-pipe condition; can imply an annular liquid-filled channel (as long as the channel is in contact with the casing) or a micro annulus at the casing-cement interface. They cannot identify channels within the cement sheath or at the cement-formation interface, or particulate-matter fill in the annulus. The bonding index tell us the total-free-pipe condition (Goodwin, 1997). Further, the pulse echo technique has difficulty in differentiating between a drilling fluid and a light weight mud contaminated cement of similar acoustic impedance. But recent ultrasonic tools can detect the presence of channels within the cement sheath through which hydrocarbon can flow (Clamart et al., 2008).

2.8 Challenge of the Time for Innovative Monitoring Method

As discussed above the integrity of the cement sheath is crucial for the life of the well. Proper remedial task can be performed if the deficiency is identified on a timely manner, which can severely improve the well integrity. So it is a timely challenge to develop a monitoring

system which is capable of performing multitasks as discussed below, which can considerably increase the efficiency of currently available monitoring systems by incorporating them.

- Monitors the placement and rising of cement in the annulus
- Gives some alarm when something goes wrong on a certain depth during and after placement
- Detect the contamination during and after placement of cement
- Detects the free water level
    - Detect mud or air pocket
    - Gives some alert on water loss or density change
    - Gives approximate stress level at specified depth
    - Indicates crack and the corresponding range of depth of crack

The proposed monitoring system based on resistivity in this thesis closely analyses the above factors.

2.8.1 Electrical Properties Based Oil Well Monitoring System

The proposed method in this thesis is based on electrical properties based monitoring system which includes resistivity, impedance spectroscopy and piezoresitivity. Resistivity is a material property and for cement it changes with curing time. By monitoring resistivity many properties like hydration of the cement can be predicted (Backe, 2001). Though there is no or limited literature found, this study proposes a method of real time monitoring of the level of the cement during its placement in the annulus.

Impedance spectroscopy is a method of characterizing the electrical properties of materials and their interfaces (Campo, 2002). Based on the equivalent circuit, impedance measurement helps finding out the contact resistance and bulk resistance (Vipulanandan and Prashanth, 2013).

The piezoresistive effect is a change in the electrical resistivity of a semiconductor or metal when mechanical strain is applied. The change in resistivity with the applied stress was several times higher than the change in strain of the materials which makes the material self-sensing smart material (Vipulanandan et al., 2004, 2006-2012). Therefore, change in resistivity has the potential to be used to determine the integrity of the cement sheath.

Summary

Background and related literature were discussed in relation to oil well cement sheath integrity. The following summarizes the chapter.

1. Life of a well can be subdivided into pre exploration, exploration, development, production and abandonment phases.
2. During the development phase, the well is drilled, cased and cemented in a step by step process.
3. Main purpose of the cement sheath is to provide zonal isolation, protecting the casing from corrosion induced by formation fluids and holding the casing in place.
4. Cement sheath integrity is important for the effective economic life of the well.
5. Cement sheath integrity is challenged by several factors starting from cement placement till the end of production phase of the well.
6. An effective monitoring system is necessary to monitor the well health from placement of cement throughout the life of the well.
7. Electrical properties based monitoring system by measuring the resistivity, impedance and piezoresistivity can be a successful monitoring system for maintaining the integrity of the cement sheath of the well.

CHAPTER 3 MATERIALS AND METHODOLOGY

It is important to identify the materials used and the experimental methodology adopted for this study. Also preparation of sample for different types of experiments conducted, curing conditions, types of tests performed to characterize the electrical and mechanical properties, calibration of the devices and methods used for measurements of electrical properties are summarized.

3.1 Smart Cement

Different types of oil well cements, modified with carbon fiber to enhance sensing properties, were used in this study. Modified cement is called smart cement, because the modified cement sheath can self-sense the stress, strain and damages on it. Figure 3-1 shows the stress strain relationship of class H neat cement cured for 28 days.

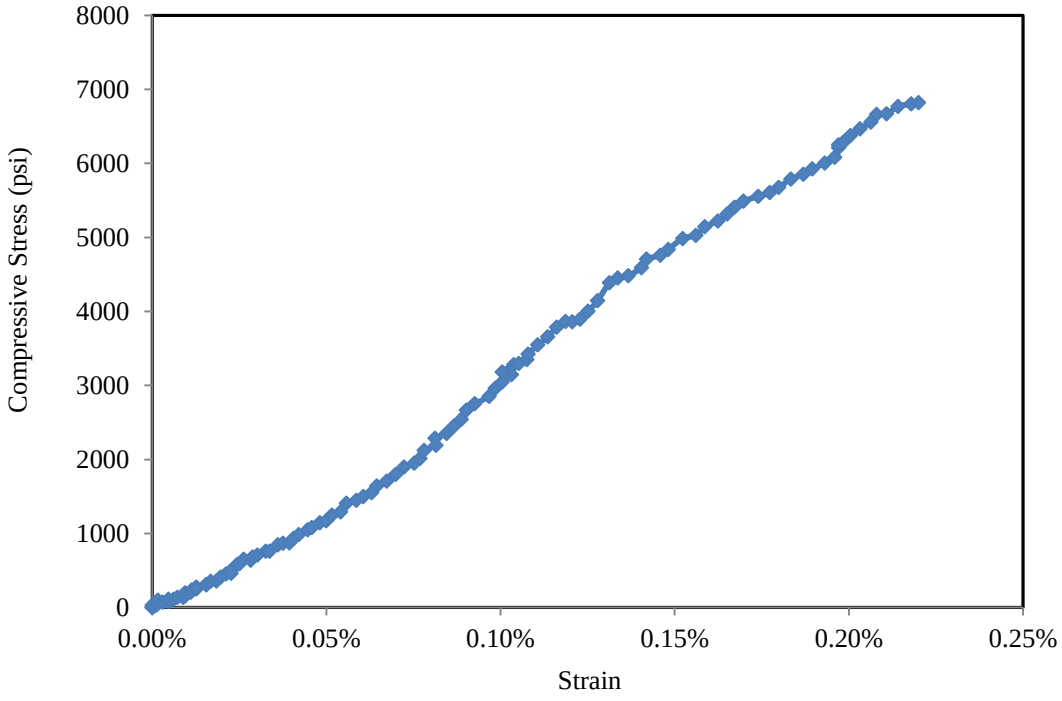

Figure 3-1: Stress Strain Relationship of Class H Neat Cement Cured for 28 Days

At failure strength, the failure strain was about 0.2%. Figure 3-2 shows piezoresistive behavior of carbon fiber modified smart cement and neat cement. Corresponding change in piezoresistivity at the failure strength for this specimen was about 150%, which is 750 times higher than that of strain and about 30 times greater than that of neat cement. Small amount of addition of carbon fiber enhanced the sensing properties and made the cement a smart material.

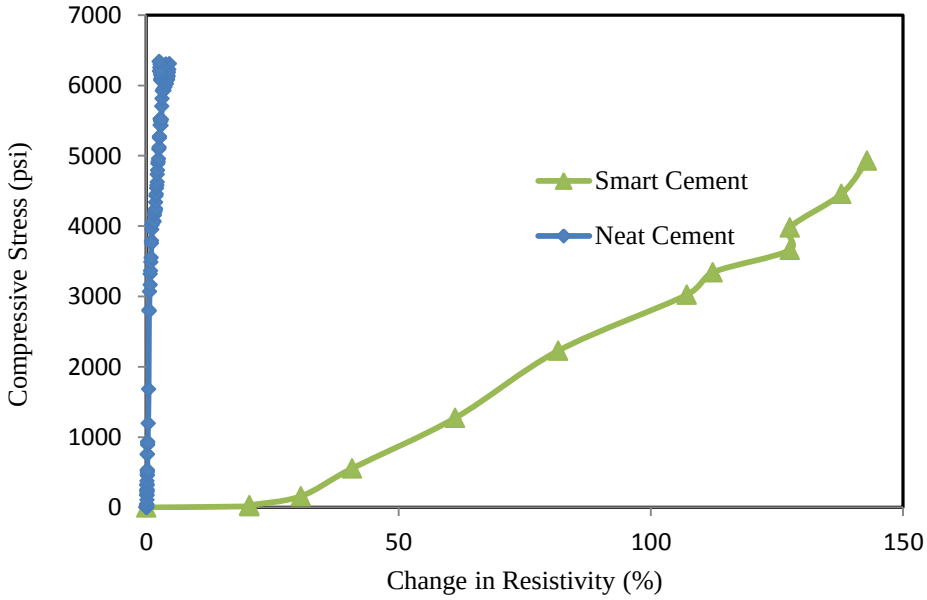

Figure 3-2: Piezoresistive Behavior of Smart Cement and Neat Cement

Commercially available carbon fiber with average length of 0.5 inch was used to modify the cement. The carbon fiber used in this study was pitch-based fiber with diameter of 14.5μm, electrical resistivity of 148 μΩ.m and specific gravity of 1.62.

3.2 Cement Mixing

The types of cements used for this study are API oil well cement class A (which is similar to Portland cement type I according to ASTM C 150 classification), class G and class H. To enhance the piezoresistive property of the cement, the cement was modified by adding 0.075% carbon fiber by weight of the total cement slurry mix.

API Recommended Practice 10B-2 was generally adopted in preparing the samples. The cement slurries were prepared using a high-shear blender type mixer with bottom driven blades. First, measured amount of mixing water was poured into the blender. Then measured amount of carbon fiber was mixed in a slow speed for about 1 minute so that it could be properly dispersed in the mixing water. Cement was then mixed gradually with the water. Final mixing was done with a higher speed for about 4 to 5 minutes to ensure homogeneity. A metal spatula was used to recover material sticking to the wall of the mixing container in the middle of final mixing. Mixing was done at an ambient room temperature of 23±2 ℃. The water-to-cement ratio for most of the studies was 0.38.

3.2.1 Curing Conditions

Specimens were casted in respective molds based on the type of the test to be done and cured in relative humidity box with a relative humidity not less than 95% at room temperature. After 24 hours, specimens were demolded and again kept in the same condition till the test. The instrument that was used to monitor the relative humidity is shown in Figure 3-3.

Figure 3-3: Instrument Used to Measure the Relative Humidity and Temperature

Before and after demolding, resistances were monitored to make sure demolding process does not affect the resistance of the specimen. The average change in resistance before and after demolding was less than 3%. Figure 3-4 shows the average resistance of cement in 2”x4” cylindrical mold before test for each class of cement tested.

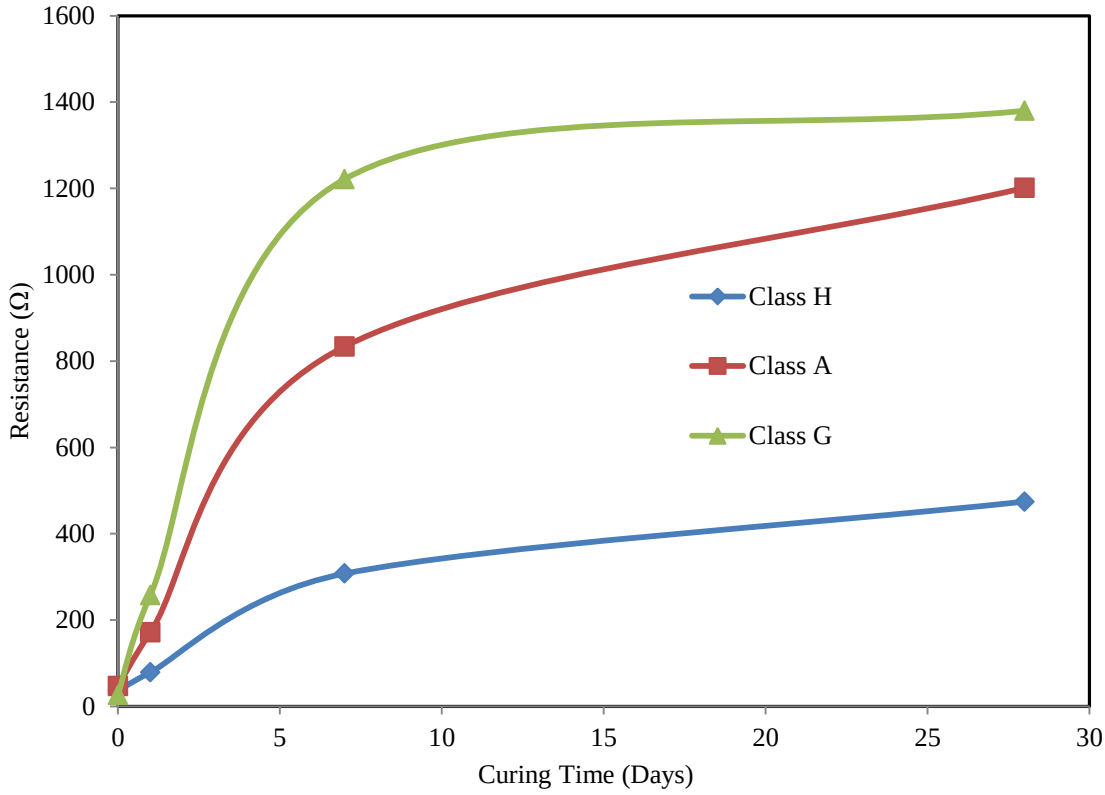

Figure 3-4: Average Resistance of Different Classes of Cement before Test

The average 7 day resistance was highest for class G cement while it was minimum for class H cement. The same trend was observed for average 30 day resistance also.

3.2.2 Density

The density of the slurry plays a major role in providing hydrostatic pressure in the wellbore while it displaces the drilling mud. Density of slurries was calculated using weight and volume after mixing the cement.

The change in density over the period of curing was monitored by measuring the density before the test. Figure 3-5 shows the density of the specimen immediately after mixing and before test.

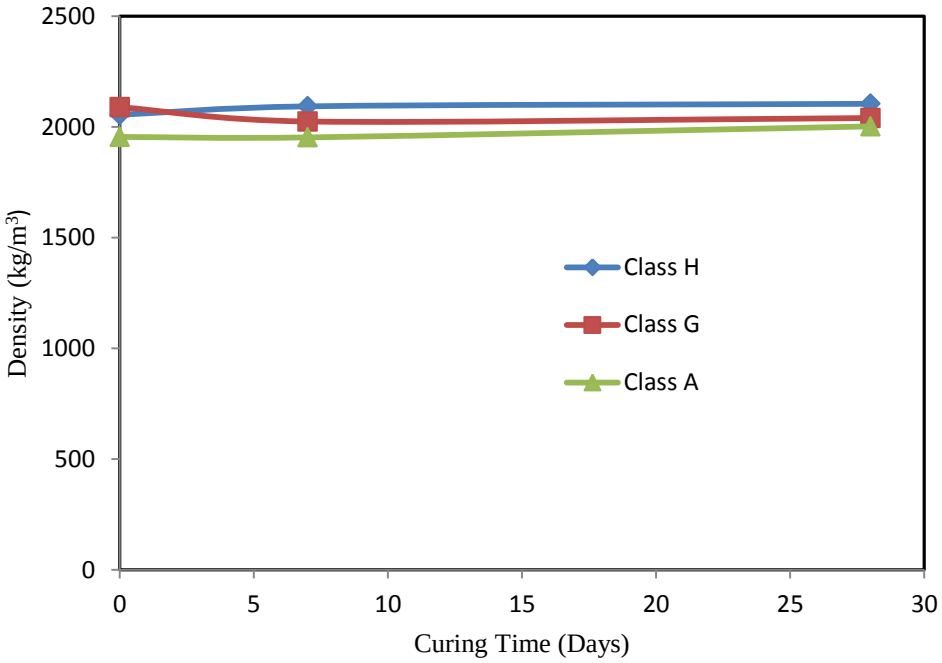

Figure 3-5: Density of Specimens Immediately after Mixing and Before Test

The average densities of each type of cement are tabulated in Table 3-1. With time density increased in general based on the method of curing. Water loss and volume change are the factors affecting the density change.

Table 3-1: Average Density and Resistance of Different Classes of Oil Well cement

Class	Density (kg/m^3)			Resistance (Ω)			
	After mixing	7 days	28 days	After mixing	1 day	7 days	28 days
A	1955	1953	2002	47	172	834	1201
G	2090	2025	2040	26	258	1221	1380
H	2055	2093	2104	37	79	308	474

3.2.3 Setting Time

The Vicat setting test (ASTM C191) was used to determine the initial and final setting times for different API class of hydrating cementitious mixtures. It measures the change in the

penetration depth of a plunger with a diameter of 1.13±0.05 mm under a constant applied load (300 g) as increasing structure formation acts to reduce the extent of penetration into the specimen. Figure 3-6 shows the testing apparatus used for setting time.

Figure 3-6: Setting Time Test – Vicat Needle Apparatus

The test identifies initial and final sets at penetration depths of 25 mm and 0.5 mm respectively. Final setting time of class H cement was 6 hours and 15 minutes, class G was cement 5 hours and 10 minutes and Class A was 5 hours and 10 minutes.

3.2.4 Shrinkage

Approximate values of shrinkage were measured using 15mm diameter plastic tubes. Figure 3-7 shows the experimental setup used to measure shrinkage.

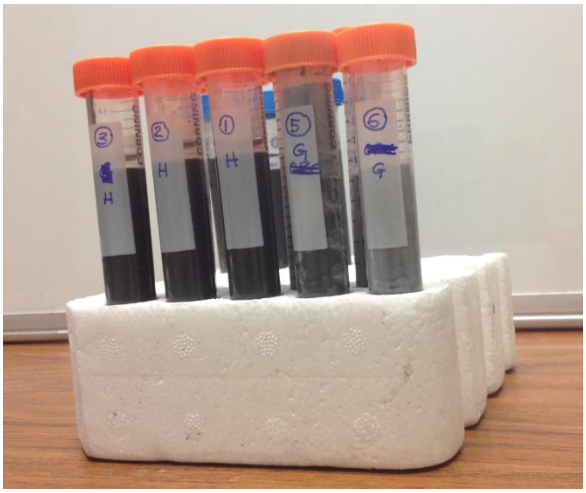

Figure 3-7: Experimental Setup for Quick Shrinkage Test

This experimental method was easy to conduct and results were reasonably close to the literature values. Figure 3-8 shows the variation of shrinkage with time.

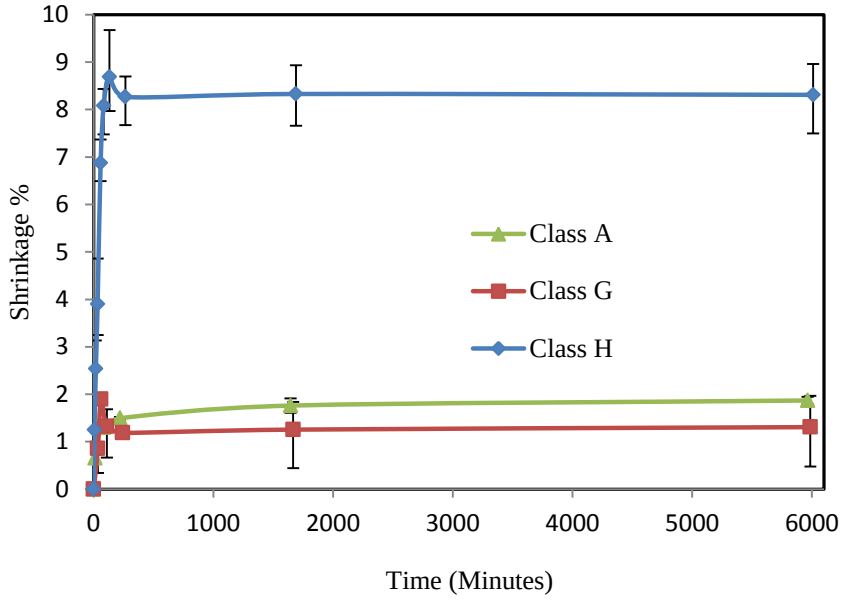

Figure 3-8: Variation of Shrinkage with Time (Different Classes of Cement)

3.3 Experiments Conducted for Characterization of the Materials

Cement was tested on most of the failure modes of cement sheath discussed in Chapter 2. Generally for one criterion, at least three specimens were tested and average value is reported in the following chapters.

A data acquisition system was used to collect the load and strain relationships. Also data output for crack mouth opening displacement and load point deflection were collected using data acquisition system. Dimensions of the specimen were measured using a Vernier caliper instrument for stress calculations. The data acquisition system used is shown in Figure 3-9.

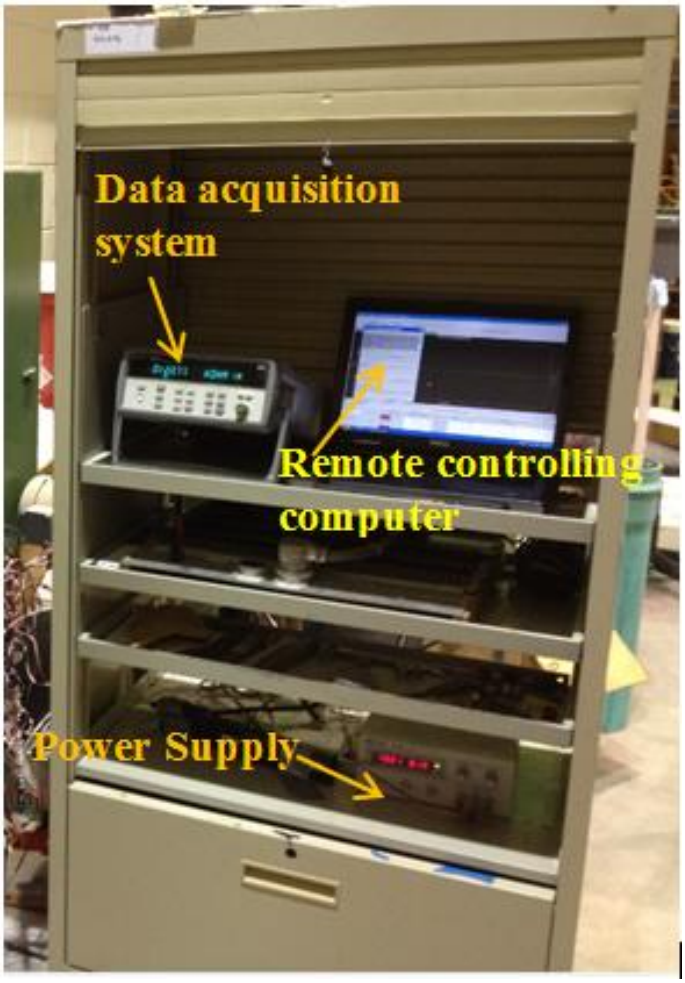

Figure 3-9: Data Acquisition System to Collect Data

Applied load was calibrated from voltage output from load cell. Strain was obtained from two wire DC resistance output from strain gauge or voltage output from extensometer. Data acquisition was used for data collection.

3.3.1 Compression Test

The plastic mold shown in Figure 3-10 was used to prepare specimen to measure compression strength of the material and piezoresistive behavior. The insulator coating was removed from the tips of the wire to make it conductive.

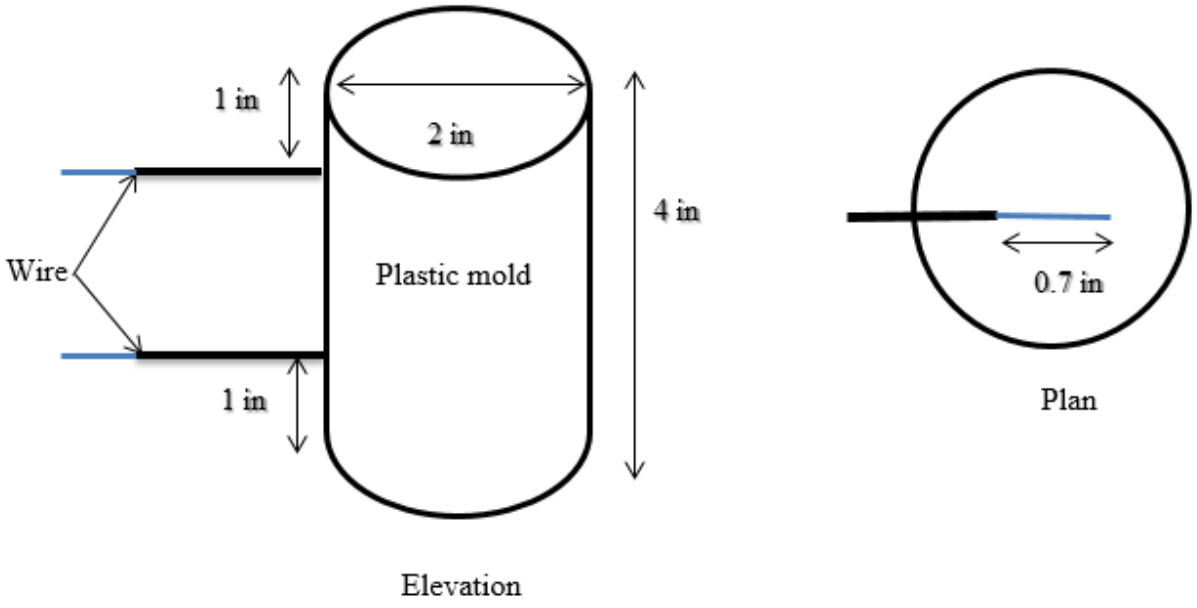

Figure 3-10: Mold Used to Prepare Compression Specimen

The molds were cylindrical in shape with diameter of 2 inches and height of 4 inches. Two conductive wires were placed in the middle of the specimen as shown to measure the electrical resistance of the specimen during loading. The vertical distance between two wires was approximately two inches.

Specimens were instrumented with strain gauge for measuring lateral strain and an extensometer to measure axial strain as shown in Figure 3-11 also to determine the Poisson's ratio. Accuracy of the extensometer was checked with axial strain gauge.

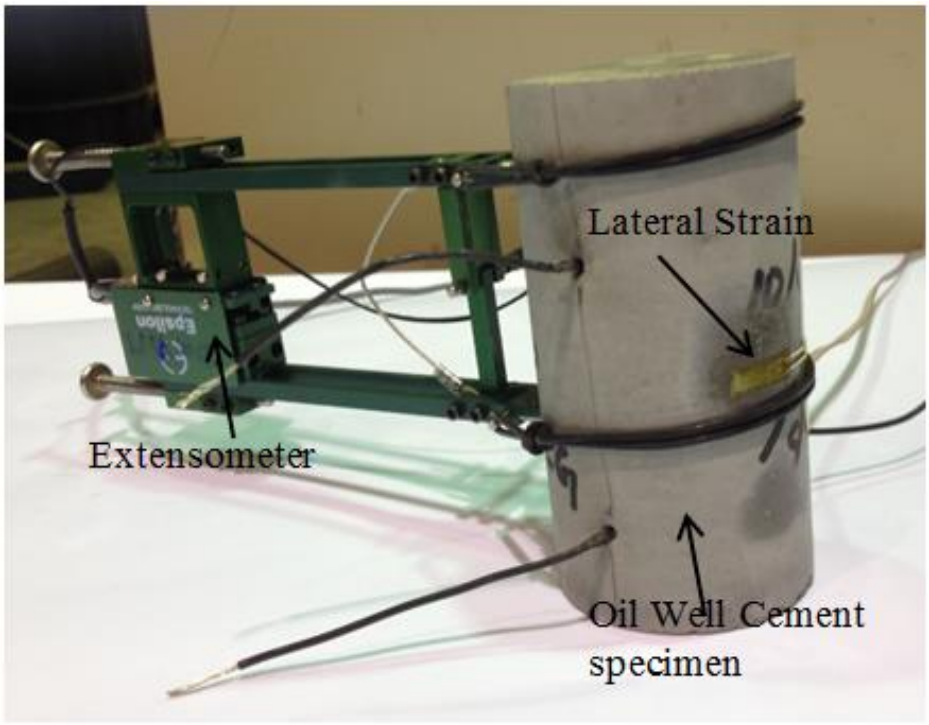

Figure 3-11: Specimen Instrumented with Lateral Strain Gauge and Extensometer

The cylindrical specimen was capped and tested at 0.01in/min displacement rate and Compressive strength of the specimen was determined. Tests were performed on different types of cement samples at various curing ages. The change in resistivity with load also was monitored.

3.3.2 Split Tension (Splitting Tensile Test)

The mold shown in Figure 3-12 was used to prepare specimen to measure tensile strength of the material and piezoresistive behavior using indirect method. The wires were embedded into the specimen as shown in the figure to measure the piezoresistive behavior.

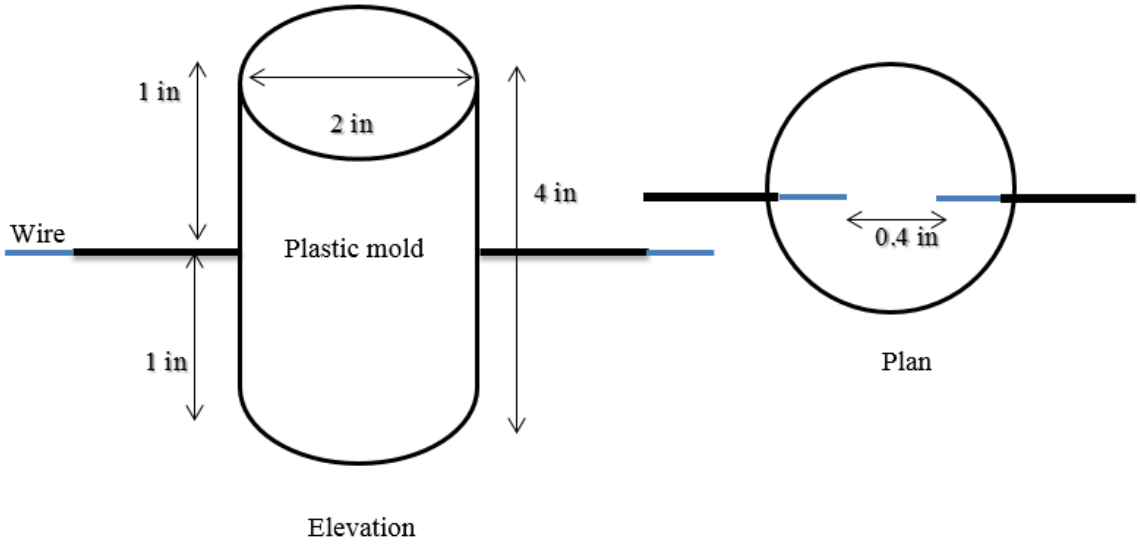

Figure 3-12: Split Tension Specimen Mold

Load, strain and electrical resistance were measured during the tests. The tensile capacity of the specimen was calculated using the Equation 3-1 given in ASTM C 496 – 96,

$$\sigma_t = 2P/\pi ld \,, \qquad 3\text{-}1$$

where, σ_t is splitting tensile strength, P is applied load, l is length and d is diameter. Sample was tested as shown in the Figure 3-13.

Figure 3-13: Split Tensile Specimen

Variation of tensile stress versus change in resistivity was monitored and discussed in Chapter 4. Embedded wires were used to monitor the resistance changes.

3.3.3 Flexural Test

Three point bending test was conducted according to ASTM C293/C293M − 10. Figure 3-14 shows the dimensions of the mold used to prepare the specimen.

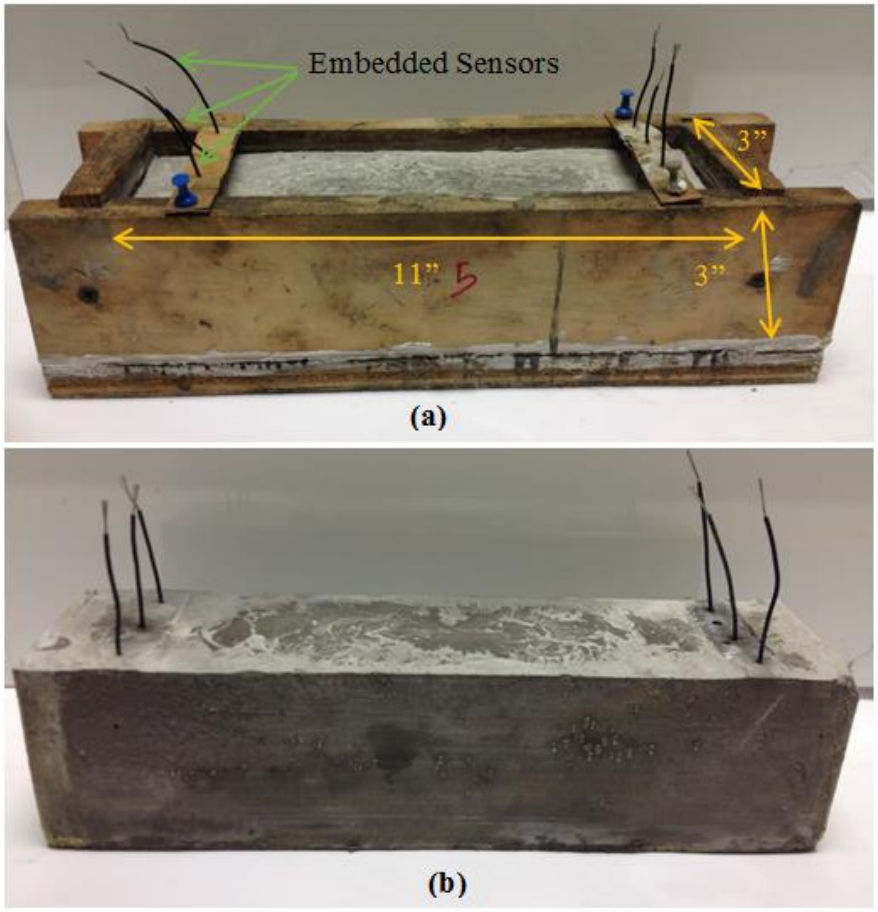

Figure 3-14: (a) Mold Used to Prepare Flexural Specimen (b) Beam Specimen

Wires were used to capture the change in resistance during loading, near compression and tension fibers. Strain gauges were fixed on both tension and compression fibers close to the midpoint to monitor the strains at extreme fibers from neutral axis. Figure 3-15 shows the experimental setup.

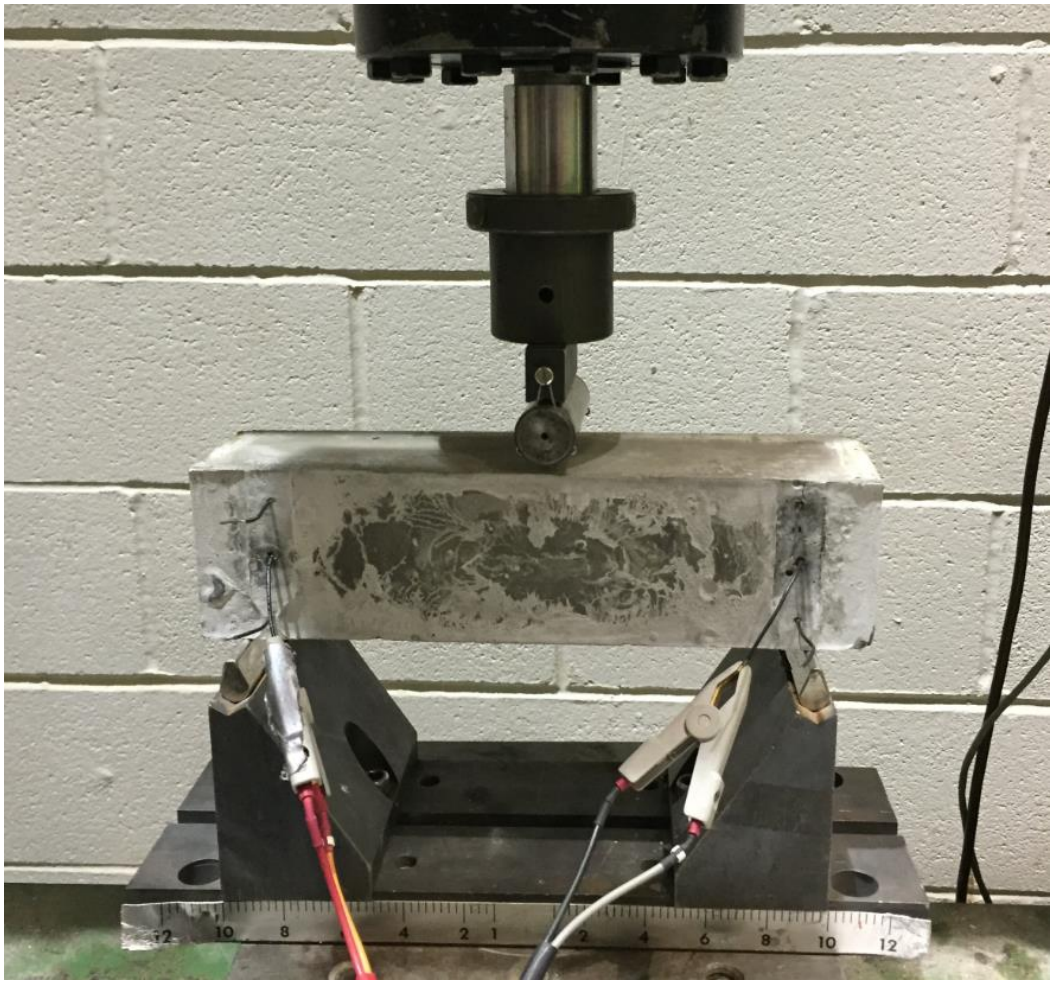

Figure 3-15: Three Point Loading Flexural Test Setup

The Equation 3-2 that was used to calculate the stress is

$$\sigma_f = \frac{3PL}{2bd^2}, \qquad 3\text{-}2$$

where σ_f is flexural stress, P is applied load, L is span length, b is average width of specimen and d is average depth of specimen.

3.3.4 Fracture Toughness and CTOD

Beam specimen explained in Figure 3-13 was used to study mode I fracture properties. A notch with a thickness of 2.5 mm was made with band saw as shown in Figure 3-16.

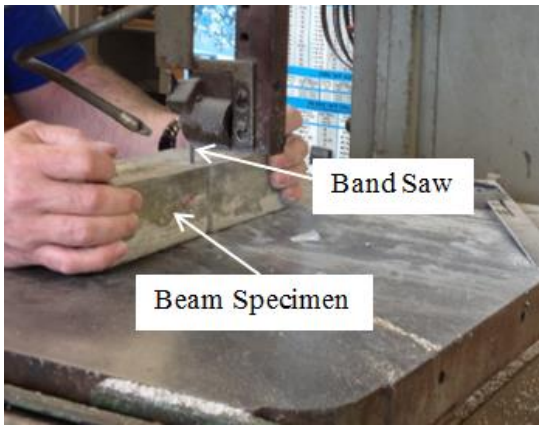

Figure 3-16: Making Notch in the Specimen Using Band Saw

A three point loading setup was used to find the fracture toughness and crack tip opening displacement (CTOD) of different types of oil well cement. Figure 3-17 shows the experimental setup of fracture test.

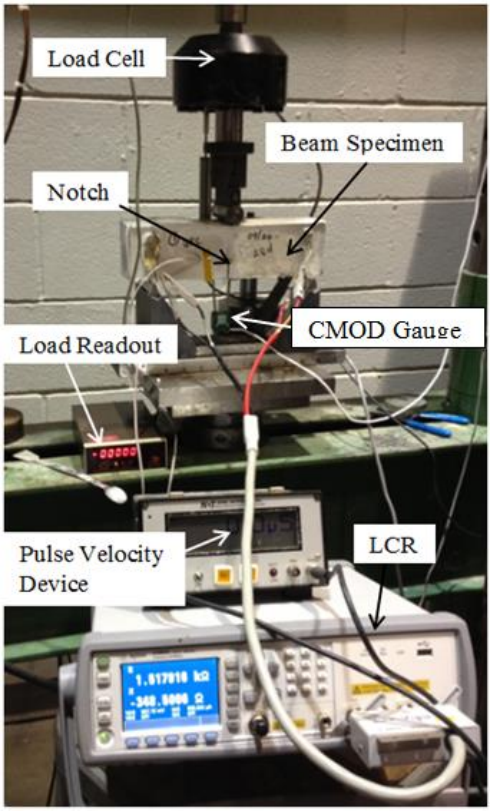

Figure 3-17: Experimental Setup for Three Points Loading Fracture Test

A clip on CMOD gauge was used to measure crack mouth opening displacement. Knife edges were used to clip the CMOD gauge to the pre crack. At the same time resistance and pulse velocity also were monitored to characterize the crack using nondestructive method. Mid span deflection also was monitored using LVDT. Figure 3-18 shows the calibration of LVDT to convert the voltage output from LVDT to displacement.

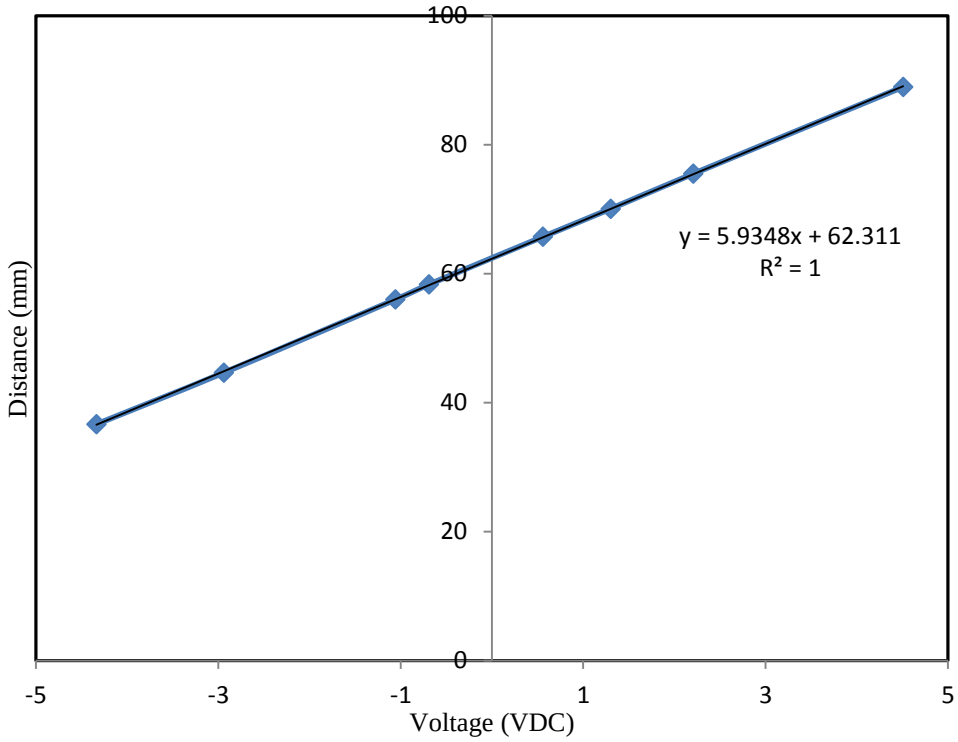

Figure 3-18: Calibration of LVDT (Voltage versus Displacement)

A linear relationship was found between displacement and output voltage. Variation of displacement was found with applied load. Calculation and assumptions made are shown in Chapter 5.

3.3.5 Bonding between Steel - Cement and Rock – Cement

The shear bonding between steel casing and cement was measured using the specimen showed in Figure 3-19. Class H cement was used for this study.

Figure 3-19: Specimen to Measure Shear Bonding Between Steel Casing and Cement

The experimental setup to measure shear bonding between steel casing and cement is shown in Figure 3-20. Load was applied on the steel casing until it reaches the level of cement. Applied load pushed the casing through the cement sheath.

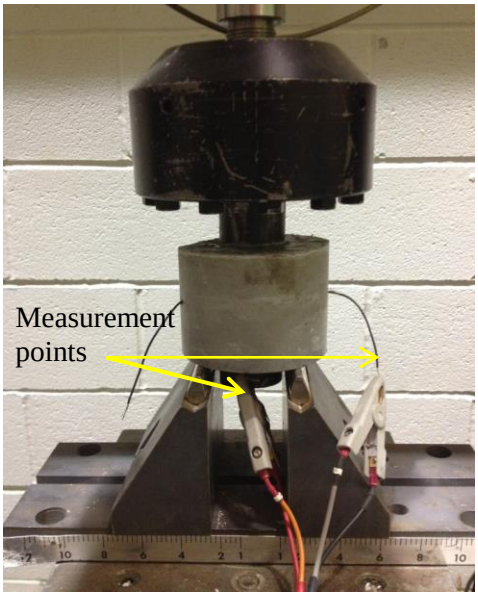

Figure 3-20: Experimental Setup to Measure Shear Bonding between Steel Casing - Cement

Figure 3-21(a) shows the specimen after the test. The steel casing was moved to one side. After de-bonding from cement sheath, applied load acted against the friction between steel-cement interface. Figure 3-21(b) shows the variation of stress with change in resistance.

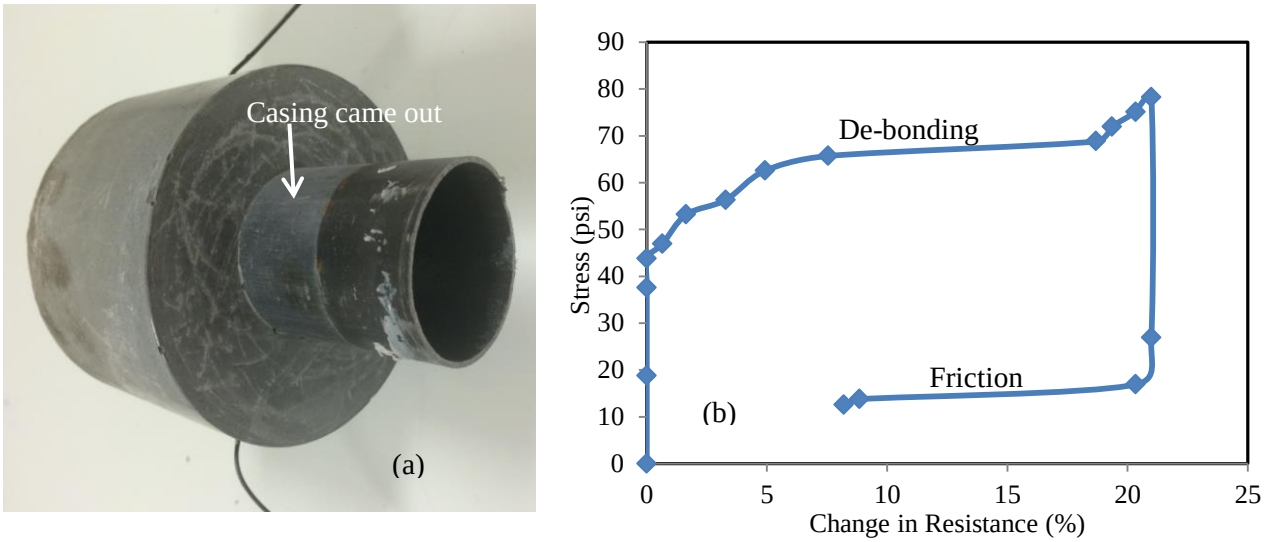

Figure 3-21: (a) Specimen after Interface Bonding Failure (b) Stress versus Resistivity

3.4 Electrical Resistivity Measurements

In this study electrical resistivity of the cementitious material was used to sense the stress level in the hardened cement sheath and real time monitoring of the level of slurry in the oil well model. So measuring the resistance and resistivity of both cement slurry and hardened cement were important to quantify. Measuring the resistivity of the hardened cement was a challenge because there were uncertainties in the electrical current conducting path. Following sections explains methods used in measuring the resistivity of slurry and hardened cement.

3.4.1 Resistivity of Cement Slurry

Two different instruments were used for resistivity measurements of cement slurries. The digital resistivity meter measured the resistivity directly and the other device, conductivity meter, measured the conductivity of the cement slurry and later resistivity was calculated.

3.4.1.1 Resistivity Meter

Figure 3-22 shows the digital resistivity measuring device that was used in this study. This device conforms to API 13-B recommended practices.

Figure 3-22: Digital Resistivity Meter

The range of the device is 0 to 400 Ω.m. Minimum possible reading is 0.01 Ω.m. Suction bulb was used to fill the slurry into the Lucite cell. Slurry was filled and discharged several times before the final fill to avoid air bubble in the sample. Then the sample cell was reattached onto the conductive pins on the meter and reading was taken. Three fills followed immediately after one another were used to calculate the average resistivity at any time.

3.4.1.2 Conductivity Meter

Figure 3-23 shows the probe type conductivity meter that was used to measure the conductivity (1/resistivity) of the cement slurry in this study.

Figure 3-23: Conductivity Meter

Conductivity meter was first calibrated using standard solution with a known value of conductivity. After calibration, the device was double checked with another standard solution for consistency. The resistivity of the cement slurry was calculated using Equation 3-3,

$$\rho\ (\Omega.m) = \frac{1}{measured\ conductivity(\frac{mS}{cm})} \times 10. \qquad 3\text{-}3$$

The range of the device was 0.1µS/cm to 1000 mS/cm, which has the equivalent resistivity of 10,000 Ω.m to 0.1 Ω.m. The least count of the device was 0.1 µS/cm. Conductivity of the cement slurry was measured up to about 4 hours or until when the probe could easily penetrate into the slurry. This data was later used with resistance readings, to find out the resistivity of the hardened cement with some assumptions.

3.4.2 Resistivity of Hardened Cement

Measuring the resistivity of the hardened cement was a challenge because the availability of such devices are limited. Also calculating the resistivity from measurable parameters was also a challenge because of the uncertainty in actual conductive path of the current inside the specimen.

Therefore an approximate method had to be used to find out the resistivity of the hardened cement. Because the resistivity of the material is a material property, once it is calculated it can be used for similar slurries with same water to cement ratio, same additives and same mixing procedure for the same curing time.

Electrical resistivity of a material is given by Equation 3-4

$$R = \rho \frac{L}{A}, \tag{3-4}$$

where R is electrical resistance, L is distance between measuring points, A is cross sectional area.

Because the effective electrical current passing area and length of the carbon fiber modified cement have uncertainties in determining, these geometrical factors have to be found for each time applications. The geometrical parameter called K-factor is given in Equation 3-5 as

$$\mathrm{K} = \frac{L}{A}. \tag{3-5}$$

By finding this K-factor, the resistivity can be calculated with the measured resistance. Calculation of K-factor is explained below for a given mold.

3.4.2.1 K-factor of a Given Mold

Figure 3-24 shows the variation of K-factor with time for a 2”x4” cylindrical specimen with 0.075% carbon fiber by weight and water to cement ratio of 0.38. K-factor was calculated for about 4 hours.

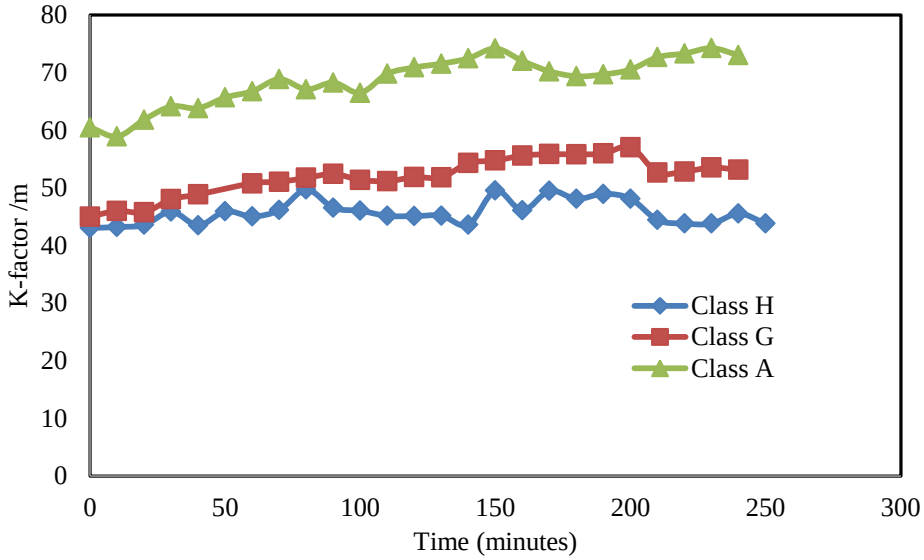

Figure 3-24: Variation of K-factor with Time

Though ideally the geometric factor K is expected to be constant, during initial hydration phase it shows small fluctuations, and with time it reaches a constant value. The constant value it reached with time was considered as the K-factor of the mold.

The K-factor was found from resistance and resistivity measurement from the same mold. Figure 3-25 shows the change of measured resistance with time which was used to measure K-factor.

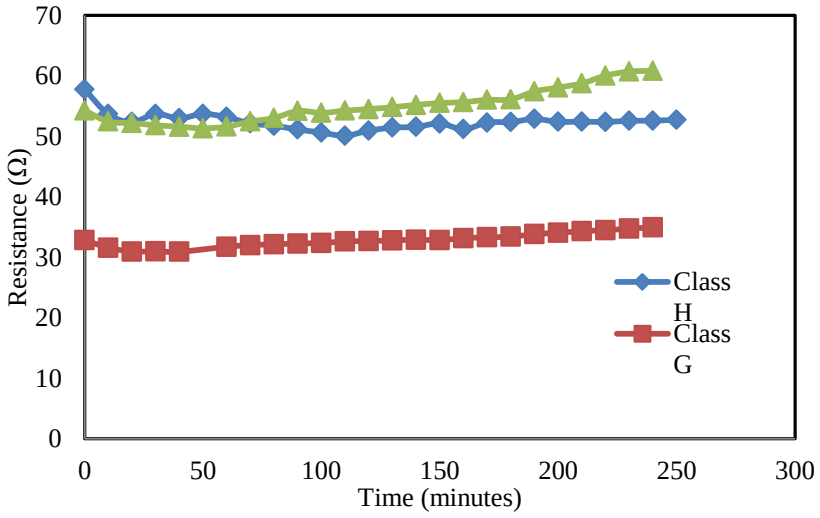

Figure 3-25: Measured Resistance with Time for 2”X4” Mold

Figure 3-26 shows the variation of measured resistivity with time for the same cement slurry. Different classes of cements are used.

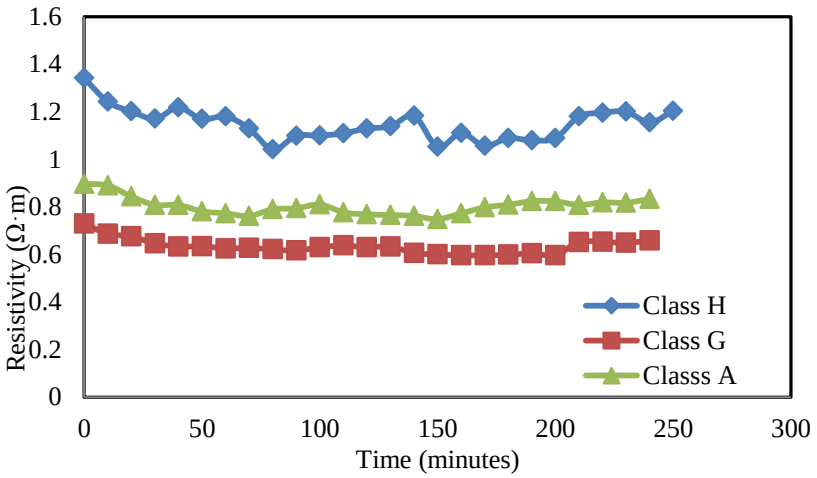

Figure 3-26: Variation of Resistivity with Time

Using Figure 3-25 and Figure 3-26, the K-factor of the mold was calculated with time from Equation 3-6, as shown in Figure 3-24,

$$R = \rho \mathrm{K}\,. \qquad 3\text{-}6$$

Knowing the K-factor of the mold, the resistivity of the hardened cement can be calculated at any curing time. Figure 3-27 shows the resistivity of hardened cement with time which was calculated as mentioned above.

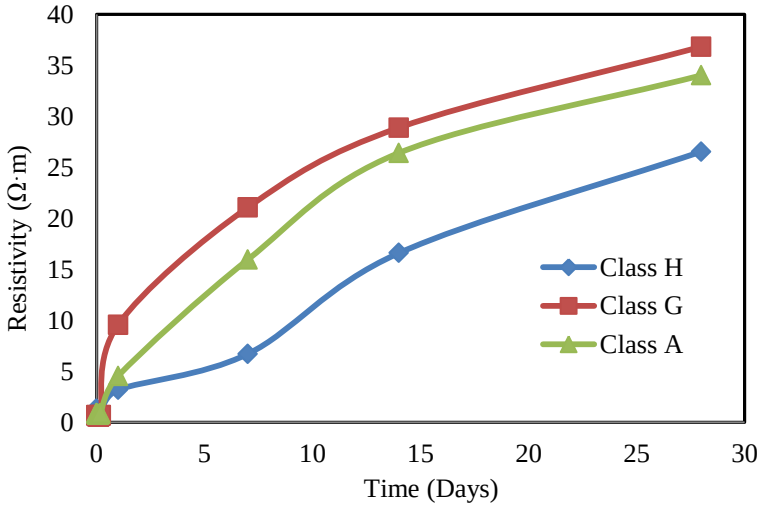

Figure 3-27: Resistivity of Hardened Cement with Time

Knowing the resistivity of the cement with time, the resistance of similar cement slurry can be predicted for real time monitoring of cement slurry placement in the field if the sensing system is calibrated. The schematic of this procedure is shown in Figure 3-28.

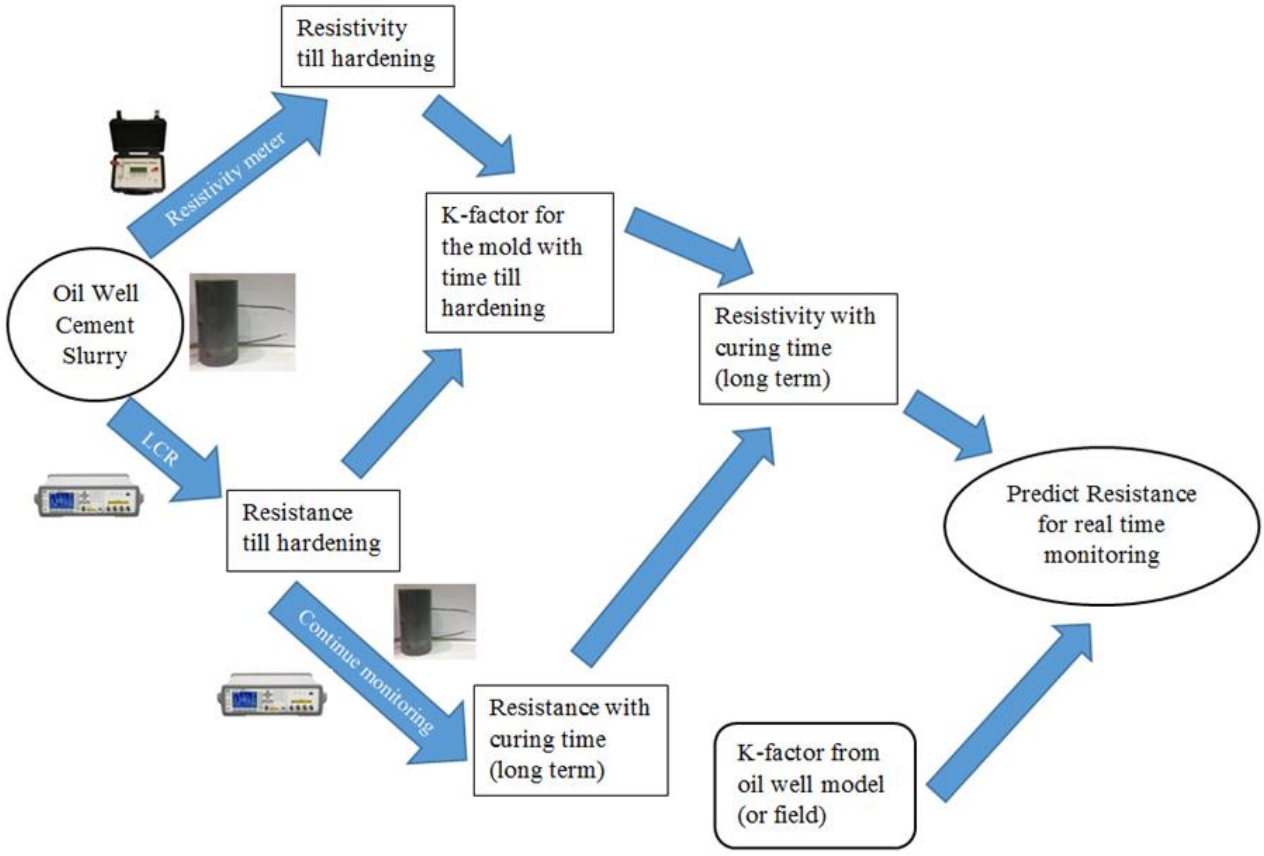

Figure 3-28: Schematic Diagram of Predicting Resistance in the Large Scale Model

However, while the cement sheath is under applied stressed condition, the above method cannot be used to predict the level of stress by piezoresistivity method, because the resistivity of the material varies with strain (under stress) according to piezoresistivity.

Therefore to predict the level of stress in the cement sheath, normalized resistivity is used in this study. The normalized resistivity was calculated from normalized resistance measurements as shown in Equation 3-7

$$\frac{\Delta\rho}{\Delta\rho_0} = \frac{\Delta R}{\Delta R_0} \quad . \qquad 3\text{-}7$$

From the experimental values of piezoresistivity, the level of stress can be estimated in the oil well model or in the field. Very large change in piezoresistive value could be an indicator of cracks.

3.5 Electrical Resistance Measurements

Figure 3-29 shows the high frequency LCR device that was used to measure resistance in this study.

Figure 3-29: LCR Device

This device has a frequency range from 20 Hz to 300 kHz and a least count of 1 μΩ. It also measures several other electrical properties such as impedance, conductance and capacitance.

Resistance values were measured in the maximum range of the device at 300 kHz. Using high frequency minimized many problems reported in the literature such as high contact resistance, polarization and repeatability. Typical impedance versus frequency plot for class G cement is shown in Figure 3-30.

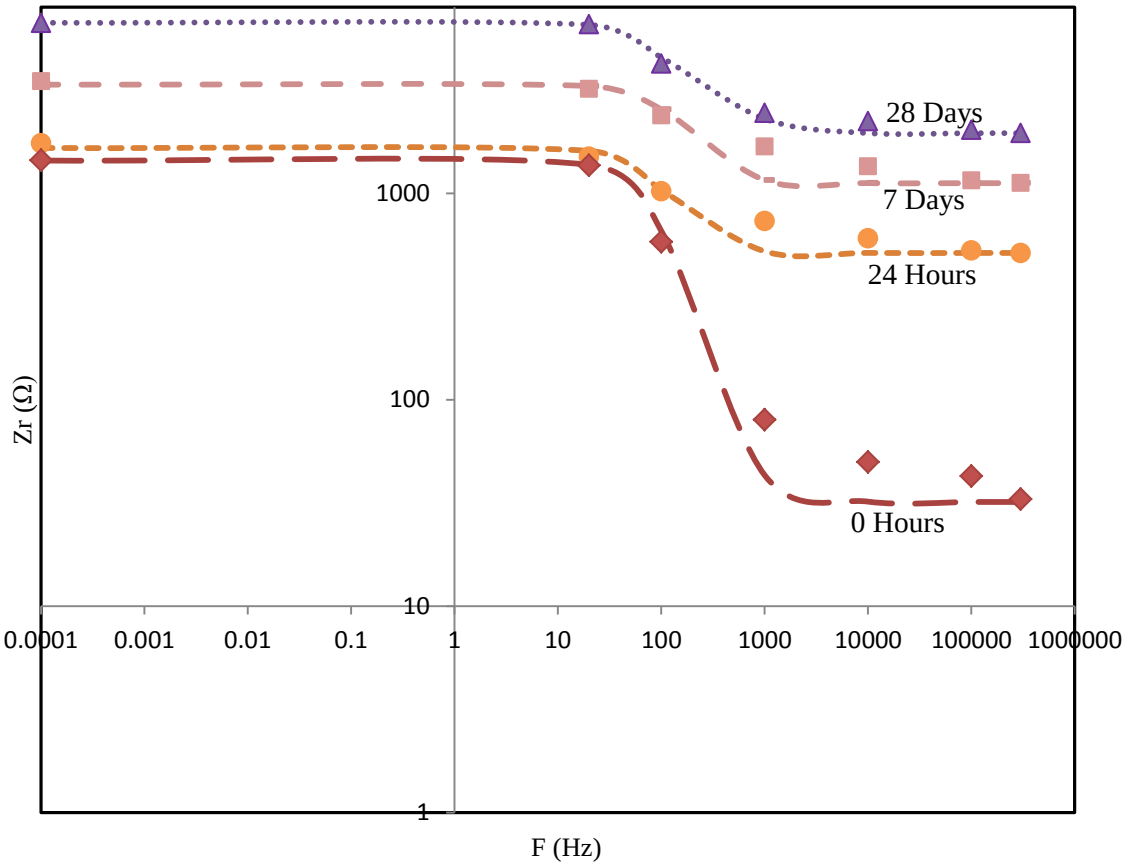

Figure 3-30: Impedance versus Frequency for Class G Oil Well Cement

In all curing ages and for all types of cements, with increasing frequency, resistance dropped drastically thus eliminating the contact resistance. It makes AC resistance measuring methods more reliable and repeatable by measuring only bulk resistance.

Summary

Based on the materials used and the experiments planned to be performed, following observations are advanced:

1. Oil well cement was modified with 0.075% of carbon fiber to enhance the sensing property thus making the cement smart cement.
2. Density, setting time and shrinkage were measured with time for different types of oil well cement.

3. Mechanical and piezoresistive properties were tested by conducting compression, indirect tension, flexural, fracture toughness, steel casing – cement bonding and cement rock formation bonding tests.
4. Resistivity of cement slurry and hardened cement was experimented using K-factor method.
5. A LCR device was used to measure resistance at 300 kHz frequency.
6. A step by step procedure was adopted to predict the cement slurry raise in the oil well model.

CHAPTER 4 CHARACTERIZATION OF OIL WELL CEMENT

This chapter characterizes the mechanical properties of different classes of oil well cement and relates mechanical properties to piezoresistive behavior. Compression test, split tension test and flexural test were conducted to study the mechanical properties. Stress-strain behavior was predicted using p-q model. Piezoresistive behavior was modelled using an analytical model.

Impedance characterization with frequency for different types of cement for different curing times is also discussed in this chapter.

4.1 Impedance Characterization of Oil well cement

Self-sensing property of smart cement discussed in this study is mainly based on piezoresistivity which is a measure of change in resistance. Therefore monitoring the change in resistance is of importance for proper self-sensing. According to literature, researchers have been using two different methods to measure resistance for piezoresistive studies, which are two-probe method and four-probe method. Two-probe method is easy to adopt in the field while four-probe method has limitations in applications.

However, measuring the resistance using two-wire method has some concerns associated with contact resistances at the interface of the wires and cement (Chung, 2006). Hence quantifying contact resistance is important to obtain bulk resistance from apparent resistance to overcome this problem. Impedance characterization of materials is a way to overcome the problem of quantifying the contact resistance and bulk resistance using equivalent circuit representation of the physical system that need to be studied.

4.1.1 Impedance Characterization and Equivalent Circuit

It is essential to identify the most appropriate equivalent circuit to characterize the electrical properties of a material (West et al., 1997).

Based on literature (Vipulanandan & Prashanth, 2013) two possible equivalent electrical circuits for cement-based materials were analyzed in order to find the most suitable equivalent circuit to represent the smart cement.

First possible equivalent circuit is shown in Figure 4-1(Vipulanandan & Prashanth, 2013). In this equivalent circuit, contacts were connected in series with bulk material, and each component of the physical system was represented using a capacitor and a resistor connected in parallel. Rb and Cb are the resistance and capacitance of the bulk material while Rc and Cc are the resistance and capacitance of the contacts.

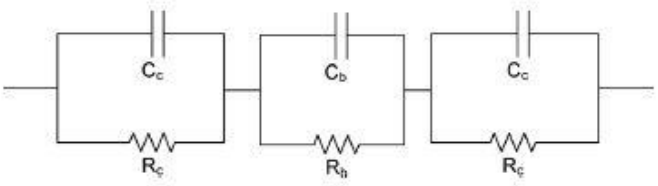

Figure 4-1: Possible Equivalent Circuit 1

The total impedance Z1of this equivalent circuit can be given by Equation 4-1 (Vipulanandan & Prashanth, 2013)

$$Z_1 = \frac{R_b}{1+\omega^2 R_c^2 C_b^2} + 2\frac{Rc}{1+\omega^2 R_c^2 C_c^2} - j\left\{\frac{2\omega R_c^2 C_c}{1+\omega^2 R_c^2 C_c^2} + \frac{\omega R_b^2 C_b}{1+\omega^2 R_b^2 C_b^2}\right\}, \qquad 4\text{-}1$$

where ω is the angular frequency of the applied signal. When ω approaches 0, resulting impedance $Z_1=R_b+2R_c$. When ω approaches infinity then $Z_1 = 0$.

The second possible equivalent circuit can be obtained by assuming the capacitance of the bulk material, C_b, is negligible as shown in Figure 4-2 (Vipulanandan & Prashanth, 2013).

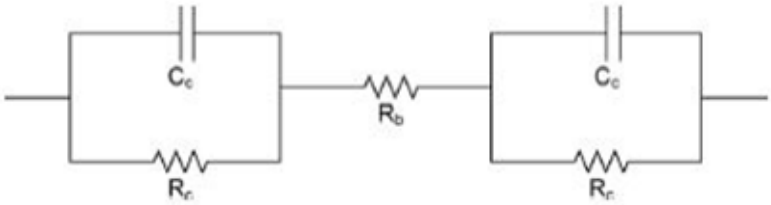

Figure 4-2: Possible Equivalent Circuit 2

The total impedance of the equivalent circuit, Z_2, can be obtained by substituting C_b=0 in Equation 4-1 as shown in Equation 4-2,

$$Z_2 = R_b + 2\frac{Rc}{1+\omega^2 R_c^2 C_c^2} - j\left\{\frac{2\omega R_c^2 C_c}{1+\omega^2 R_c^2 C_c^2}\right\}. \qquad 4\text{-}2$$

When ω reaches 0, resulting impedance $Z_2=R_b+2R_c$. When ω reaches infinity, then $Z_2= R_b$.

Based on these explanation, when ω reaches infinity, if the material shows no impedance (Z=0) then that material is general bulk material (Possible Equivalent circuit 1, contains both resistance and capacitance) and if material shows a constant impedance then that material is special bulk material (Possible Equivalent circuit 2, only resistance). Figure 4-3 (Vipulanandan & Prashanth, 2013) explains both possible equivalent circuit.

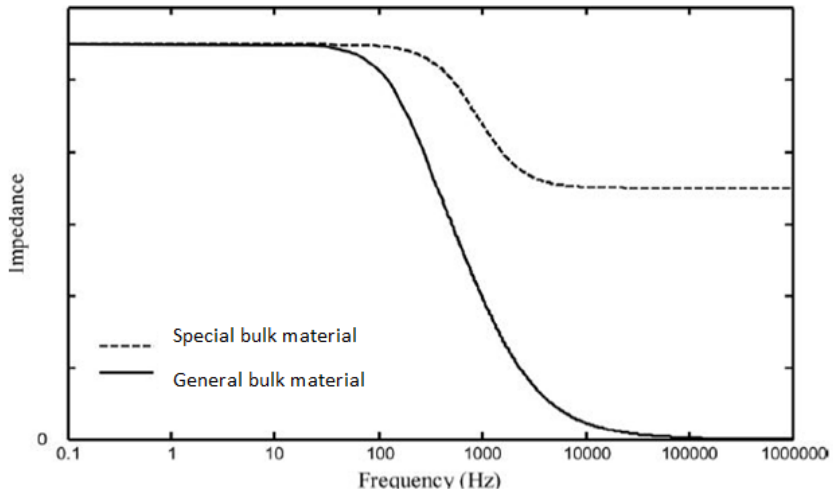

Figure 4-3: Comparison of General Bulk Material and Special Bulk Material

The smart cement used in this study was characterized to find out whether it is general bulk material or special bulk material. LCR device was used for this characterization.

4.1.2 Characterization of the Smart oil well cement used in this study

Different types of cement used in this study were experimented under 20 Hz to 300 kHz AC current using a LCR meter to characterize their properties at different curing ages. Figure 4-4 shows the variation of impedance versus frequency at different curing ages.

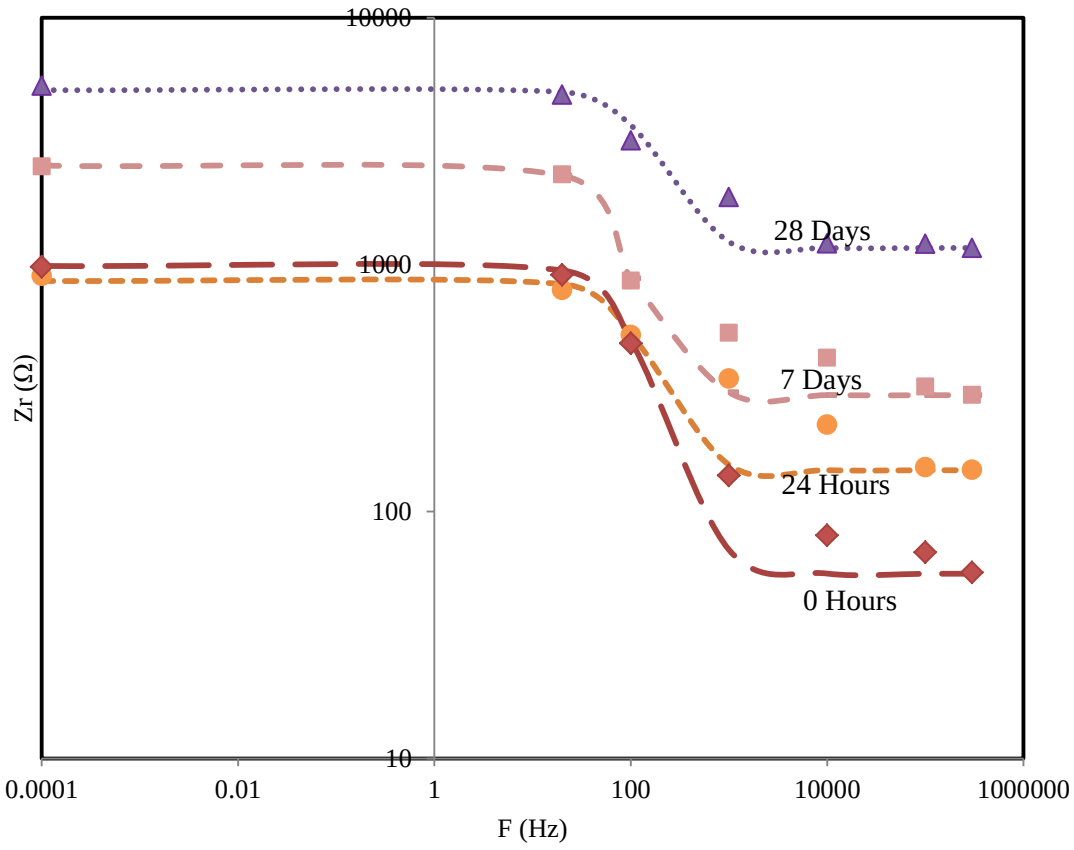

Figure 4-4: Impedance Characterization of Oil Well Cement Class H with Curing Age

All three materials tested in this study at different curing ages showed similar pattern to that of special bulk material (resistance only bulk material). Therefore the different types of oil well cement studied were characterized as special bulk material.

Table 4-1 summarizes the contact and bulk resistances as well as contact and bulk capacitances of the cements studied in this study. Values were obtained from the equivalent circuit equation.

Table 4-1: Model Parameters for Different Curing Ages

Curing Time	Class A (OPC I)	Class G	Class H
0 Hour	Rb = 53 Ω Rc = 345 Ω Cc =5.8 x10^{-6} F	Rb = 32 Ω Rc = 706 Ω Cc =2.5 x10^{-6} F	Rb = 56 Ω Rc = 466 Ω Cc = 3.6x10^{-6} F
24 Hours	Rb = 332 Ω Rc = 1320 Ω Cc =1.5 x10^{-6} F	Rb = 515 Ω Rc = 573 Ω Cc =3.0 x10^{-6} F	Rb = 147 Ω Rc = 356 Ω Cc = 4.2 x10^{-6} F
7 days	Rb = 1164 Ω Rc = 1005 Ω Cc =1.8 x10^{-6} F	Rb = 1122 Ω Rc = 1122 Ω Cc =1.0 x10^{-6} F	Rb = 296 Ω Rc = 1112 Ω Cc = 2.4 x10^{-6} F
28 days	Rb = 2484 Ω Rc = 1730 Ω Cc =1.0 x10^{-6} F	Rb = 1960 Ω Rc = 2378 Ω Cc =6.1 x10^{-7} F	Rb = 1169 Ω Rc = 1961 Ω Cc = 6.1 x10^{-7} F

Figure 4-5 shows the change of each components of impedance with curing time for different types of cements.

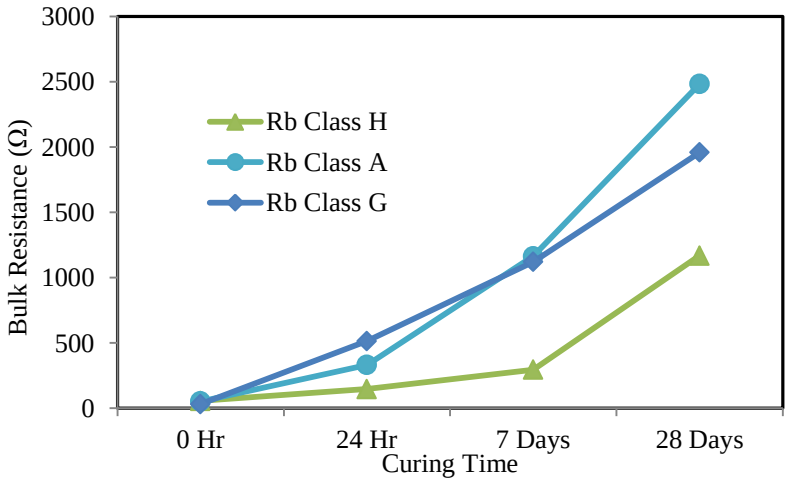

Figure 4-5: Change of Bulk Resistance with Different Curing Age

4.1.3 AC Measurements versus DC Measurements

Above impedance analysis shows DC measurement (at zero frequency) includes contact resistance also in the apparent resistance measured. This contact resistance due to DC measurement may interrupt the piezoresistive property because the contact resistance may also change with applied stress and other conditions.

Therefore, contact resistance should be excluded from the resistance measurement to study the piezoresistive effect caused by the bulk material. As shown in Figure 4-4, AC measurement at high frequency eliminated the contact resistance from the resistance measurement which paves the way to study the piezoresistive effect of bulk material.

Also DC measurement will cause polarization effect in the material being monitored, making the resistance reading unstable with time. Considering all these facts, two-probe AC measurement at 300 kHz was used in this study.

4.2 Compressive Strength and Piezoresistivity

Compressive strength of different types of oil well cement was tested to find out the ultimate compressive strength, modulus and Poisson's ratio. In most of the cases three specimens were tested and average value was considered for calculations. Curing time of the specimens was 28 days from casting.

Figure 4-6 shows the stress- strain variation of class H oil well cement. Axial and lateral strains were measured using extensometer and lateral strain gauge as explained in Chapter 4. These measurements were used to calculate Poisson's ratio and are shown in Table 4-4.

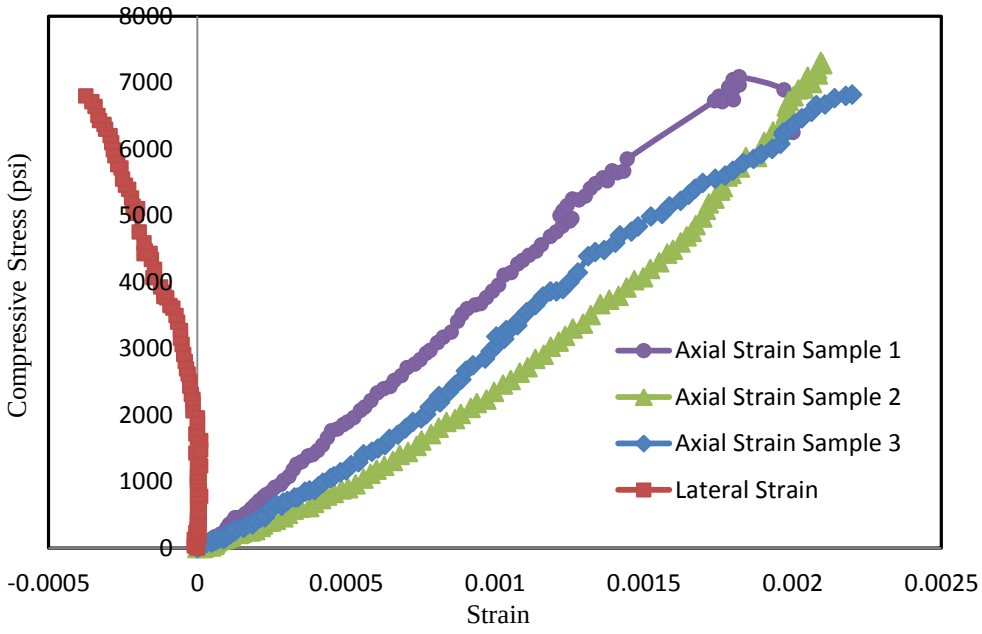

Figure 4-6: Compressive Stress – Strain (Axial and Lateral) Behavior of Class H Cement

The average compressive strength of the material tested was 7100 psi. Figure 4-7 shows the variation of stress versus strain for class G oil well cement.

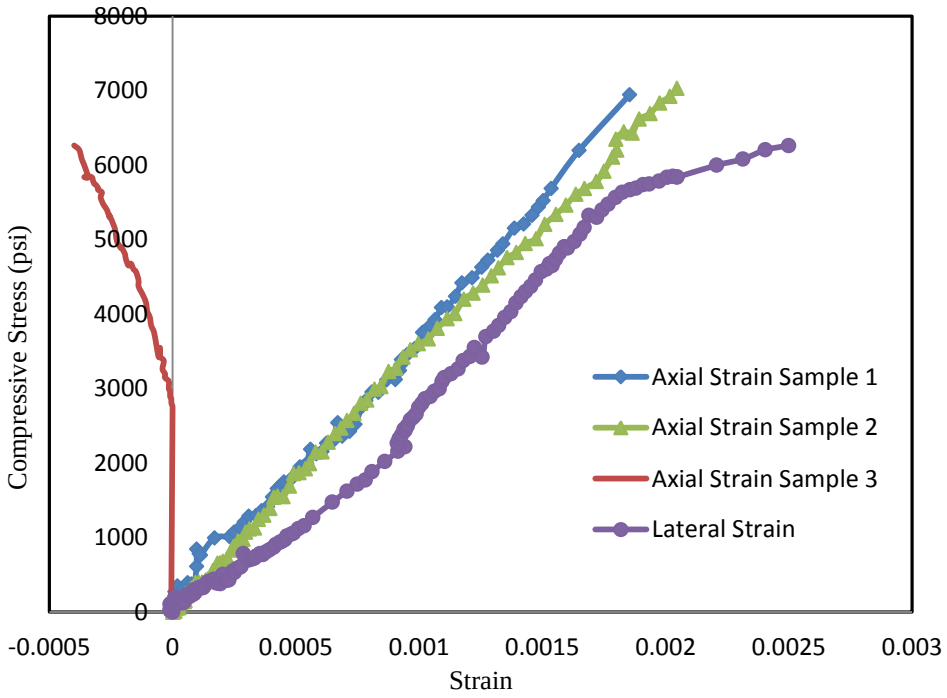

Figure 4-7: Compressive Stress – Strain (Axial and Lateral) Behavior of Class G Cement

The average compressive strength of the material tested was 6750 psi. Figure 4-8 shows the stress strain variation of class A (OPC I) oil well cement (OPC type I).

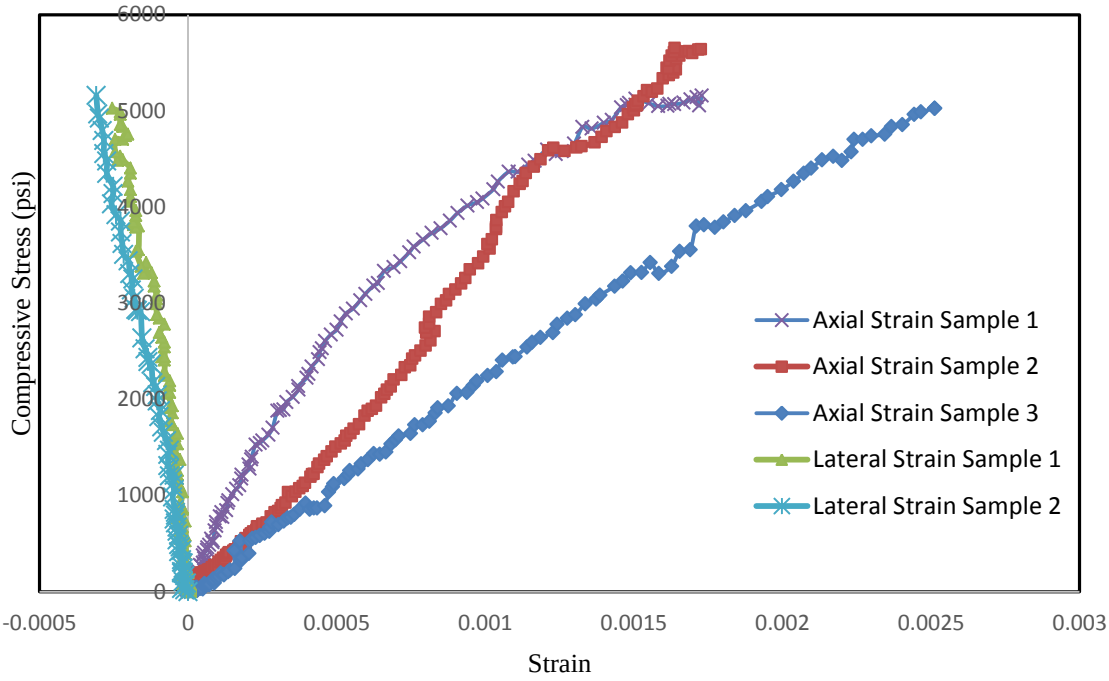

Figure 4-8: Compressive Stress–Strain (Axial and Lateral) Behavior of Class A (OPC I) Cement

The average compressive strength of the tested class A (OPC I) cement was 5250 psi. Table 4-2 summarizes the compressive strength found in this study and compares the values from the literature. The values found from the literature are either experimental values of those studies or the values used for other calculation.

Table 4-2: Ultimate Compressive Strength of Oil Well Cements

Cement	Literature	This study
A (OPC I)	5240 psi (Walter Morris et al., 2003)	5300 psi
Class G	6700 psi (Benjamin Weideman, 2014)	6750 psi
Class H	8700 psi (Catalin Teodoriu, 2012) 4350 psi (Boukhelifa et al., 2004)	7100 psi

While values reported in the literature are in the range of 5240 to 8700 psi, the compressive strength in the current study varied between 5300 to 7100 psi. Table 4-2 summarizes the Elastic Modulus found in this study and compares the values from the literature.

Table 4-3: Elastic Modulus of Oil Well Cement

Cement	Literature	
A (OPC I)	900,000 psi (Walter Morris et al., 2003)	2,730,000 psi
Class G	1,403,000 (Benjamin Weideman, 2014)	2,800,000 psi
Class H	2,500,000 (Catalin Teodoriu, 2012) 1,450,000 psi (Boukhelifa et al., 2004) 1,580,000 (Jandhyala et al., 2013) 1,200,000 (Ravi et al., 2005)	3,500,000 psi

Modulus values reported in the literature for oil well cement varies between 900,000 to 2,500,000 psi. However the modulus found in this study varied between 2,730,000 to 3,500,000 psi. Table 4-2 summarizes the Poisson's ratio found in this study.

Table 4-4: Poisson's Ratio of Oil Well Cement

Cement	Literature	Poisson's ratio
A (OPC I)	0.015 (Walter Morris et al., 2003)	0.15
Class G	0.214 (Benjamin Weideman, 2014)	0.18 to 0.20
Class H	0.2 (Catalin Teodoriu, 2012) 0.15 (Boukhelifa et al., 2004) 0.188 (Jandhyala et al., 2013)	0.19

According to the literature Poisson's ratio of the oil well cement varies between 0.015 to 0.214. The Poisson's ratio according to this study varied between 0.15 to 0.20.

Experimental values are close to the literature though the literature values cover a wide range. Also literature does not clearly mention the curing age of the specimen in many cases.

4.2.2 Piezoresistivity

Change in resistivity with applied stress was calculated from the experimental results to find out the piezoresistivity of the modified oil well cement. Figure 4-9 shows the piezoresistive behavior of modified class H oil well cement.

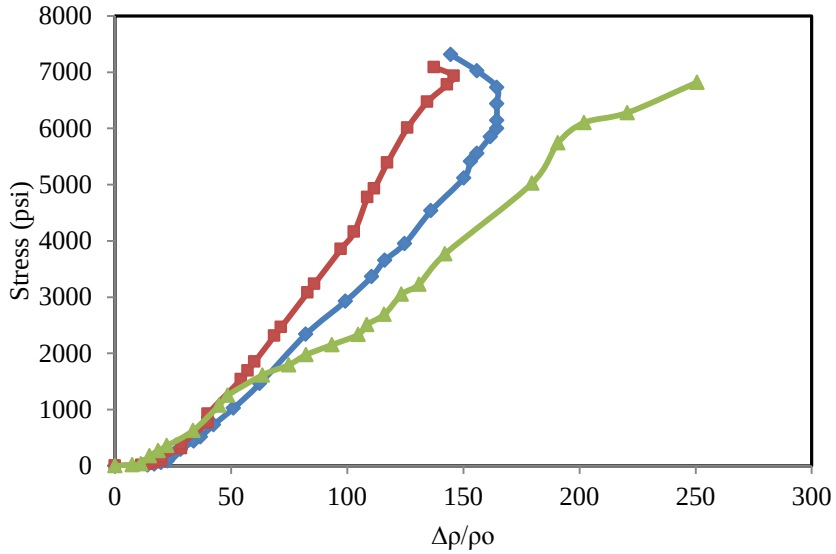

Figure 4-9: Piezoresistive Behavior of Class H Cement

Piezoresistivity of the class H cement varied between 135 to 250 %. Figure 4-10 shows the variation of piezoresistivity for class G oil well cement.

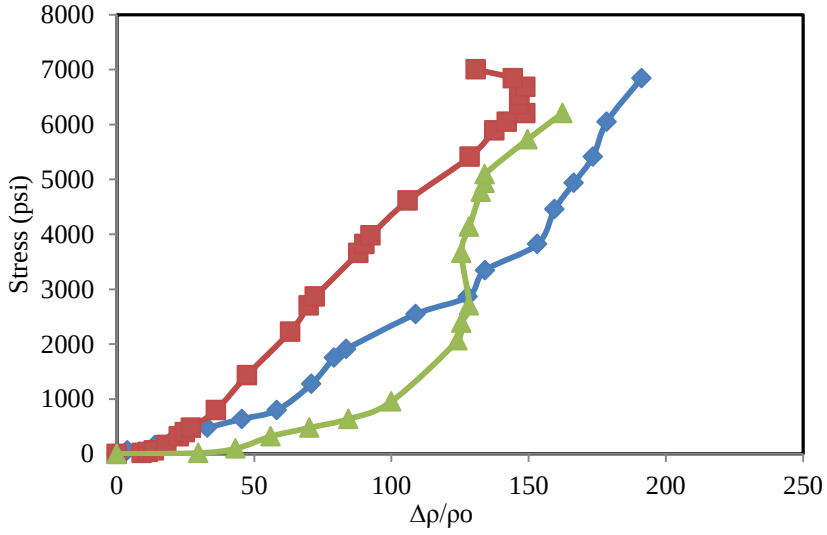

Figure 4-10: Piezoresistive Behavior of Class G Cement

Piezoresistivity of class G cement varied between 145 to 190 %. Figure 4-11 shows the variation of piezoresistivity for class A (OPC I) oil well cement.

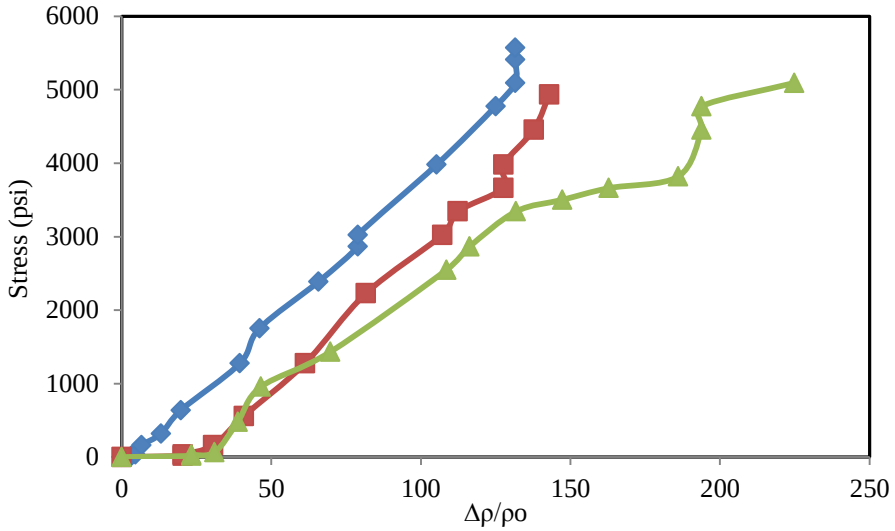

Figure 4-11: Piezoresistive Behavior of Class A (OPC I) Cement

Piezoresistivity of class A (OPC I) cement varied between 130 to 190 %. In general the piezoresistivity for classes H, G and A (OPC I) varied between 130 to 250.

4.2.3 Modelling the Piezoresistive Behavior

Sett and Vipulanandan, 2003 proposed a piezoresistive analytical model to predict the change in resistivity with applied stress for composite polymer matrix. Composite resistivity of carbon fiber reinforced material can be described using percolation theory (Carmona et al., 1987). Percolation theory is

$$\rho_i = A\,\rho^{fiber}\,(\emptyset - \emptyset_{cr})^{-t_i}\,, \qquad 4\text{-}3$$

where ρ_i is the composite resistivity, A is a pre-factor, ρ^{fiber} is the resistivity of carbon fiber, ϕ is the volume fraction of the carbon fibers, ϕ_{cr} is the critical volume fraction of the carbon fibers and t_i is an exponent. Volume fraction of the carbon fibers is represented as

$$\emptyset = \frac{V^f}{V^f + V^p + V^s}\,, \qquad 4\text{-}4$$

where V^f, V^p, V^s are the volume of conducting fibers, polymer matrix and aggregate respectively. The critical volume fraction of a composite can change due to change in microstructure of the composite which can be caused by externally applied stress. Furthermore it was shown by Sett (2003) that the fractional change in electrical resistivity ($\partial\rho/\rho_0$) is given by

$$\left(\frac{\partial\rho}{\rho_0}\right)_i = \left[t_i\emptyset(\emptyset-\emptyset_{cr})^{-1}\left[\left(\frac{1}{K^c\delta_{jk}+B^c_{jk}}\right)_c - \left(\frac{1}{K^f\delta_{jk}+B^f_{jk}}\right)_f\right] + t_i(\emptyset-\emptyset_{cr})^{-1}ZS_{jk}\right]d\sigma_{jk}\,. \qquad 4\text{-}5$$

Here δ_{jk} is the Kronekar delta, S_{jk} is the deviatoric stress tensor, Z is the constant of proportionality, and B_{jk} is the shear parameter. Parameter Z signifies the rate of change of microstructure while parameter B quantifies the volume change of the composite/fiber under deviatoric stress. For an isotropic homogeneous and linear elastic material, the coefficient of volume compressibility (K) can be written in terms of Young's modulus € and Poisson's ratio (μ) as

$$K = \frac{E}{3\,(1-2\mu)}\,. \qquad 4\text{-}6$$

Under uniaxial stress condition, the change in resistivity of linear elastic, isotropic and homogeneous composite can be written in most general form (Sett, 2003) as

$$\left(\frac{\Delta\rho}{\rho_0}\right)_1 = t_1(\emptyset-\emptyset_{cr})^{-1}\left[\emptyset\left\{\frac{1}{\left\{\left(-\frac{E_c^{PC}}{3(1-2\mu_c^{PC})}\right)+B^{PC}\right\}} - \frac{1}{\left\{-\frac{E_c^f}{3(1-2\mu_c^f)}\right\}+B^f}\right\} + \frac{2Z\sigma_{11}}{3}\right]\Delta\sigma_{11}\,. \qquad 4\text{-}7$$

This Equation relates the piezoresistivity of carbon fiber reinforced polymer concrete to the fiber properties (E^f, μ^f and B^f), composite properties (E^c, μ^c, B^c), microstructure (Z), and fiber volume fraction (ϕ). It is the most general equation of piezoresistivity which can be solved incrementally.

Assuming the material is incrementally elastic, in terms of conjugate strain, a common relationship was presented by Sett (2003) as

$$\left(\frac{\Delta\rho}{\rho_0}\right)_i = \prod_{ijk} \Delta\sigma_{jk} = \prod_{ijk} C_{jkmn} \Delta\varepsilon_{mn} = M_{ijk}\, \Delta\varepsilon_{jk}\,. \qquad 4\text{-}8$$

In the Equation, tensor Π_{ijk} is piezoresistivity coefficient, C_{jkmn} is the elasticity matrix and the tensor M_{ijk} is the elasto-resistance tensor known as the gage factor. Piezoresistivity coefficient relates the specific change in electrical resistivity to the change in stress tensor whereas gage factor signifies the sensitivity of change in resistivity measurement to strain measurement.

Since resistance in the material is directional (anisotropic), based on the random distribution of the fibers, the resistivity will be represented as a vector. Hence the piezoresistivity coefficient (Π_{111}) was defined as

$$\left(\frac{\Delta\rho}{\rho_0}\right)_1 = \prod_{111} \Delta\sigma_{11}. \qquad 4\text{-}9$$

Because of Poisson's effect which is given by

$$\varepsilon_{22} = \varepsilon_{33} = -\mu^c \varepsilon_{11}. \qquad 4\text{-}10$$

the strain-resistivity relationship will be

$$\left(\frac{\Delta\rho}{\rho_0}\right)_1 = (M_{111} - 2\mu^c M_{222})\Delta\varepsilon_{11}\,. \qquad 4\text{-}11$$

The applicability of the above model was checked for different types of oil well cement cements. Experimental values were compared with predicted values.

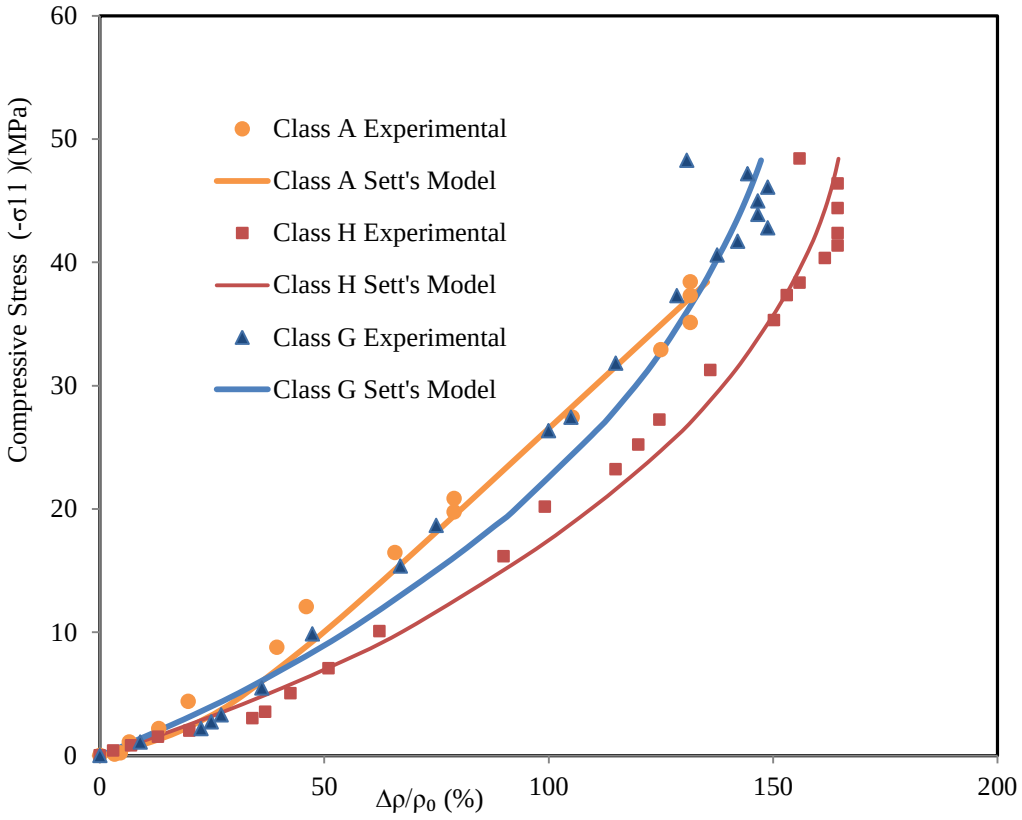

Figure 4-12: Experimental and Predicted Piezoresistive Behavior of Oil Well Cement

The incremental nonlinear analytical piezoresistive model presented by Sett (2003) which is given in Equation 4-7 was used to model the piezoresistive behavior of different kind of cement. From the manufacturer's data, Young's modulus (E) and Poisson's ratio (μ) of the carbon fiber were obtained as 228GPa and 0.3, respectively.

For cement, modulus was obtained from stress-stain relationship and μ was taken as 0.19 for class H and G and 0.15 for class A. Values of K_c and K_f were calculated as 12.97GPa and 190GPa for class H, 10.38GPa and 190GPa for class G and 8.9GPa and 190GPa for Class A.

Piezoresistive behavior of a 0.075% fiber added cement specimen was modeled and is shown in Figure 4-12 along with experimental data. It can be seen that the incremental model predicted the piezoresistive behavior reasonably well. For 0.075% modified fiber added cement

composite, exponent *t* was calculated to be -3.9 for class H and class A and -3.8 for cement G using the percolation Equation 4-3. values of shear parameter (*B*) for composite and fiber were found to be 491GPa and 290GPa for class H, 122 GPa and 249 GPa for cement G and 120 GPa and 250 GPa for cement A. The parameter *Z* which is related to microstructure was found to be $9x10^{-6}$ m^4/N^2 in these cases.

4.3 Splitting Tensile Strength and Piezoresistivity

Specimens of different types of oil well cements cured for 28 days were tested for split tensile strength and piezoresistivity. Figure 4-14 shows the variation of tensile piezoresistivity for class H cement. Specimens were cured for 28 days.

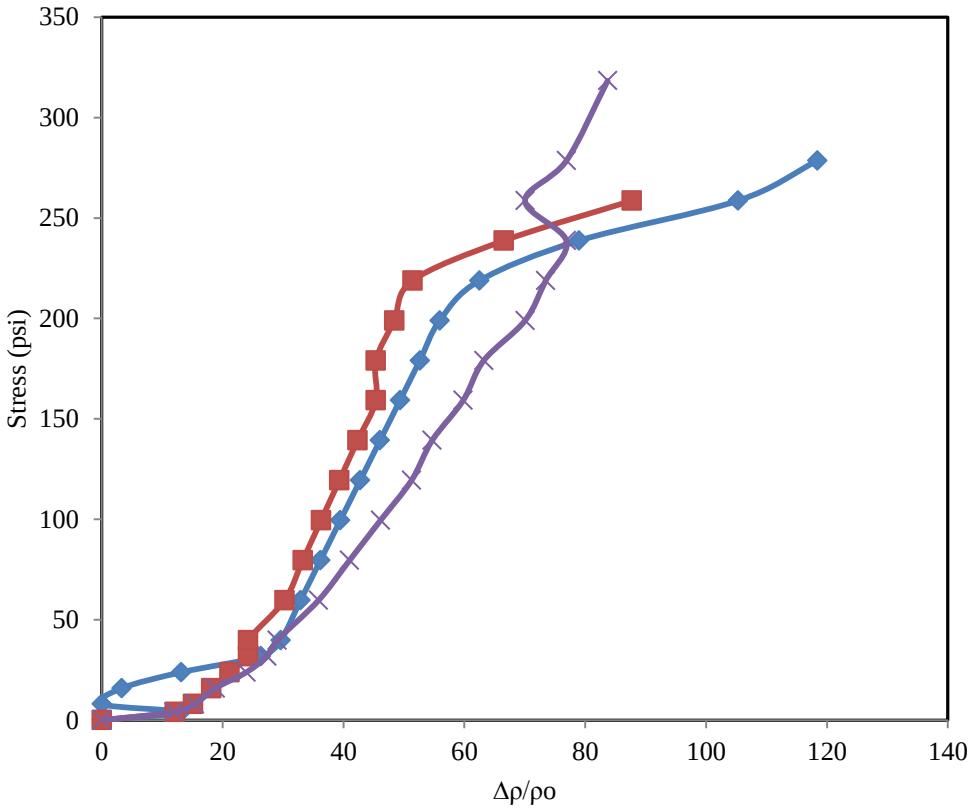

Figure 4-13: Variation of Tensile Piezoresistivity for Class H Cement

The average tensile strength of class H specimen was 285 psi and the piezoresistivity was between 85 and 120%. Figure 4-14 shows the variation of piezoresistivity for class G cement.

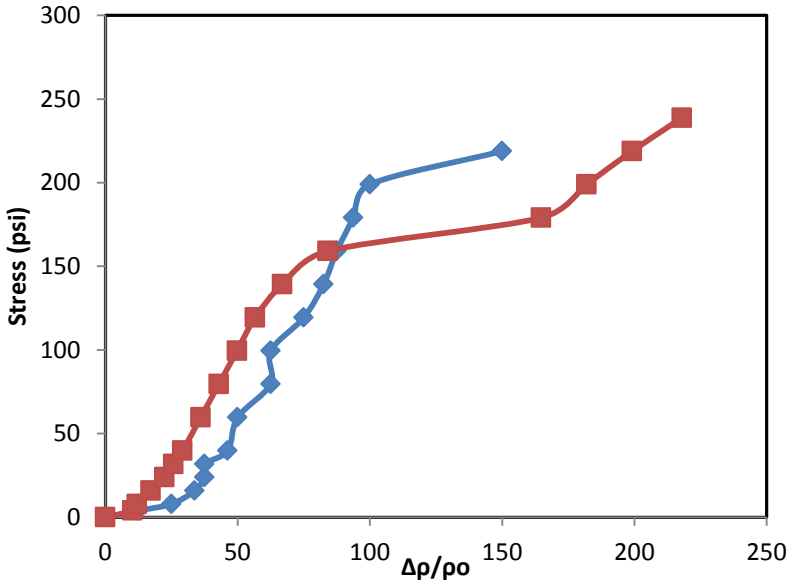

Figure 4-14: Variation of Tensile Piezoresistivity for Class G Cement

The average tensile strength of class G specimen was 230 psi and the piezoresistivity was between 100 and 220%. Figure 4-15 shows the variation of piezoresistivity for class A (OPC I) cement.

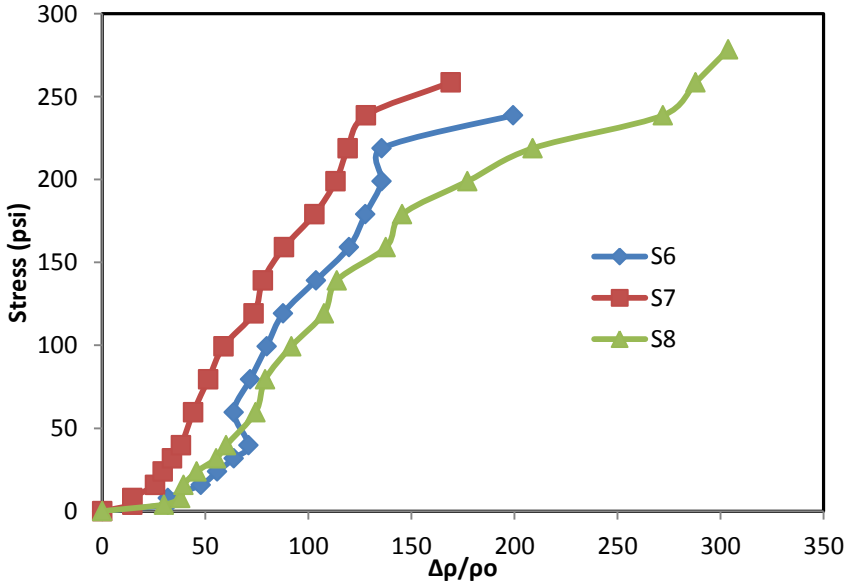

Figure 4-15: Variation of Tensile Piezoresistivity for Class A (OPC I) Cement

The average tensile strength of class A (OPC I) specimen was 260 psi and the piezoresistivity was between 170 and 240%. Table 4-5 summarizes the results of this study and compared with the literature.

Table 4-5: Tensile Strength of Oil Well Cement

Cement	Literature	This study
A (OPC I)	270 psi (Walter Morris et al., 2003)	260 psi
Class G	216 psi (Benjamin Weideman, 2014)	230 psi
Class H	435 psi (Catalin Teodoriu, 2012)	285 psi

According to the literature, the tensile strength varies between 216 and 435 while in the current it varied between 230 to 285 psi.

4.4 Flexural Properties of Different Types of Cement

Beam specimens were tested for flexural stress and strain in the compression and tension fibers. Theory behind stress calculation and experimental results are discussed here.

From simple bending formula, maximum bending stress σ is given as,

$$\sigma_{max} = (M/I)\, y, \qquad 4\text{-}12$$

where M is the maximum bending moment at the middle span, I is the second moment of area about the neutral axis and y is the distance to layer under maximum stress from neutral axis. M and I can be calculated using,

$$M = PL/4 \text{ and} \qquad 4\text{-}12$$

$$I = 1/12\ bd^3, \qquad 4\text{-}13$$

where P is the load, L is the loaded span of the beam, b is beam width and d is the depth of the beam. Combining Equations and the maximum flexural stress σmax can be calculated as

$$\sigma_{max} = 3PL/2bd^2. \qquad 4\text{-}14$$

From the above equation stress was calculated at the tension or compression fiber. Using strain gauges, strain was measured at each fiber. The extreme fiber in the tension region (below the neutral axis in Figure) referred as tension fiber and far fiber in compression region is referred as compression fiber. Figure 4-16 explains the schematic diagram for three point loading test.

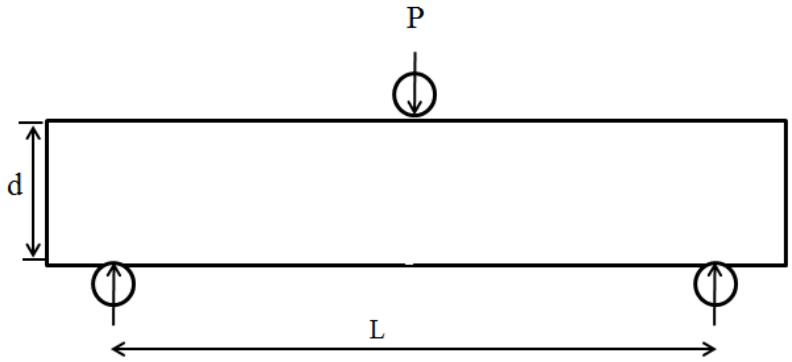

Figure 4-16: Schematic Diagram for Three Point Loading Test

Figure 4-17shows the stress strain relationship at the tensile fiber for class H oil well cement cured for 28 days.

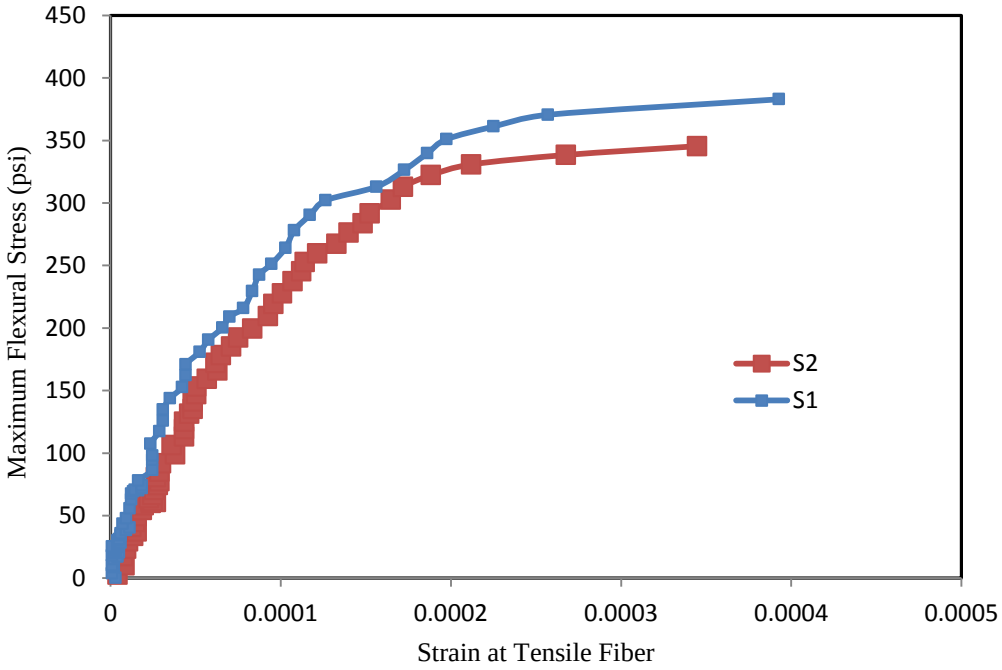

Figure 4-17: Flexural Stress Strain Relationship for Class H Oil Well Cement

The average flexural strength of class H cement was 385 psi. Figure 4-18 shows the stress strain relationship for class G oil well cement.

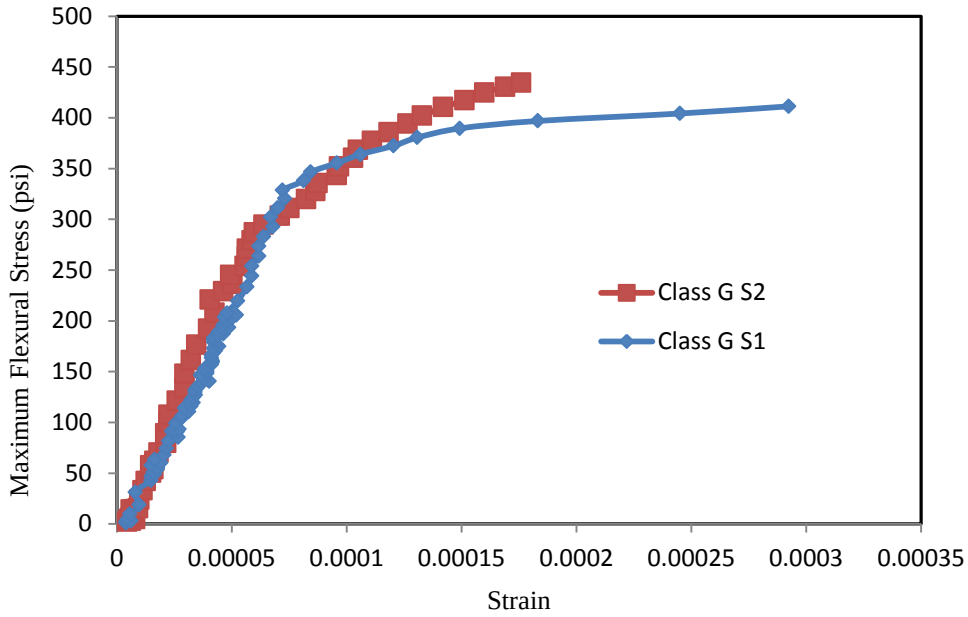

Figure 4-18: Flexural Stress Strain Relationship for Class G Oil Well Cement

The average flexural strength of class G cement was 430 psi. Figure 4-19 shows the stress strain relationship for class A (OPC I) oil well cement cured for 28 days for the tensile fiber.

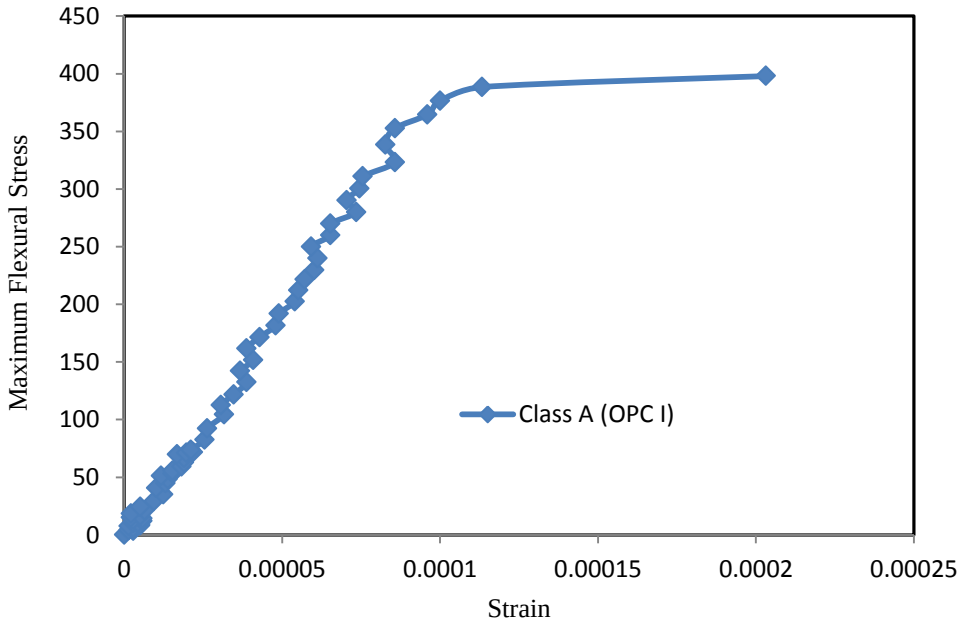

Figure 4-19: Flexural Stress Strain Relationship for Class A (OPC I) Oil Well Cement

The flexural strength of class G cement was 400 psi. Figure 4-20 compares the flexure strength of different types of cement for 28 days with indirect tensile strength.

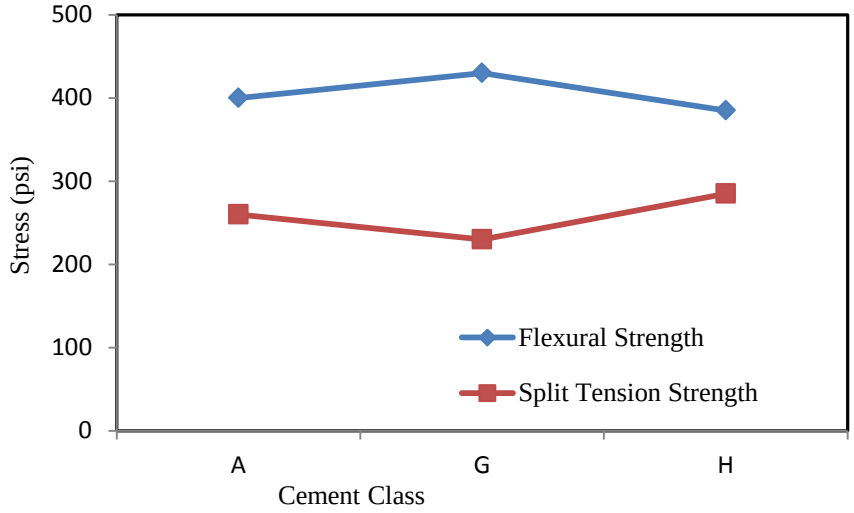

Figure 4-20: Comparison of 28 Days Flexure Strength with Split Tensile Strength

Table 4-6 summarizes results for flexural and split tensile strength for different types of oil well cement.

Table 4-6: Comparision of Flexural and Split tensile strength

Class	Flexural Strength (σ_f)	Split Tensile Strength (σ_s)	Ratio (σ_f/σ_s)
A (OPC I)	400	260	1.5
G	430	230	1.9
H	385	285	1.4

Figure shows the stress variation with change in resistivity for different types of cement.

4.4.1 p-q Model

A stress-strain model which is known as the ‘p-q model’ was developed by Vipulanandan and Paul (1990) to predict the stress-strain behavior of polymer composite materials. Sett (2003)

used the simplified version of the model proposed by Mantrala (1996) to predict the behavior of fiber reinforced polymer concrete. The proposed model is

$$\sigma = \left[\frac{\frac{\varepsilon}{\varepsilon_c}}{q + (1-p-q)\frac{\varepsilon}{\varepsilon_c} + p\left(\frac{\varepsilon}{\varepsilon_c}\right)^{\frac{(p+q)}{p}}} \right] \sigma_c \,, \qquad 4\text{-}15$$

where σ_c is the peak stress, $\mathcal{E}_c$ is strain at peak stress and p, q are material parameters. The parameter q is the ratio between secant and initial tangential moduli. The parameter p was obtained by minimizing the error in predicting the stress-strain relationship.

When q reaches 1, the model predicts a linear material up to peak stress. Therefore the lower value of q represents more non-linear material. On the other hand, the parameter p controls mainly the post peak behavior, although it has little influence in the pre-peak behavior.

Initially q was calculated by estimating the tangent and secant moduli. Then p was optimized so that square of error becomes least.

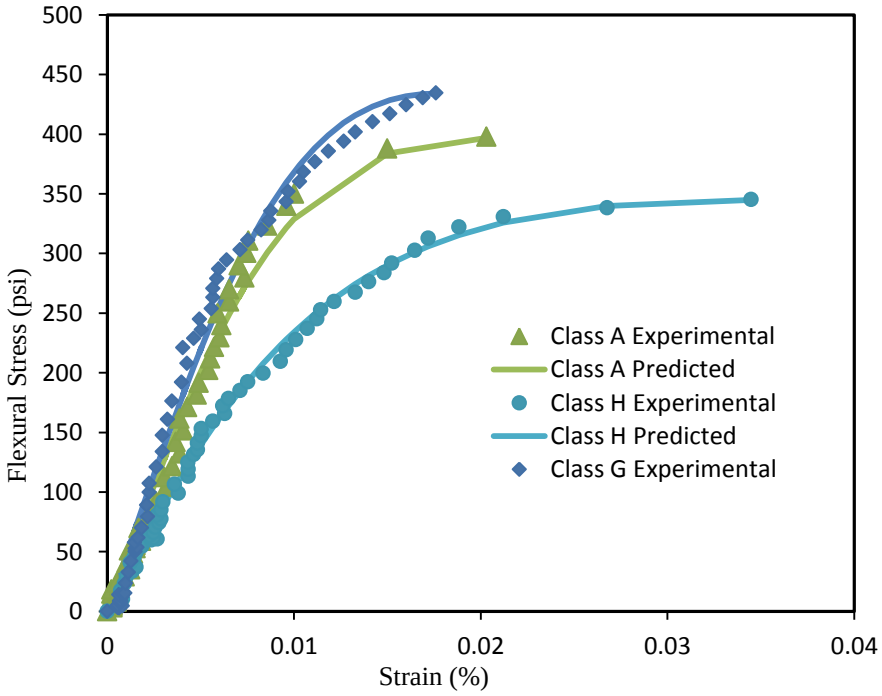

Figure 4-21: p-q model Prediction of Stress versus Strain for Different Types of Cement

Summary

1. Impedence characterization of different types of oil well cement identified the tested smart cements as special bulk materials (resistance only bulk material) at all tested curing ages.
2. Table 4-7 summarizes the mechanical properties of different types of oil well cements at 28 days of curing

Table 4-7: Summary of Mechanical Properties

Cement Class	Compressive strength	Elastic Modulus	Poisson's ratio	Split Tensile strength	Flexural strength
A (OPC I)	5300 psi	2,730,000 psi	0.15	260 psi	400 psi
G	6750 psi	2,800,000 psi	0.18 to 0.2	230 psi	430 psi
H	7100 psi	3,500,000 psi	0.19	285 psi	385 psi

3. At failure, compressive piezoresistive behavior for oil well cement class H was 135-250%, class G was 145-200% and class A (OPC I) was 130-190%.
4. p-q model predicted the stress- strain relationship of smart oil well cement well.
5. Sett's piezoresistive analytical model predicted the piezoresistive behavior of smart oil well cement well.
6. At failure, tensile piezoresistive behavior for oil well cement class H was 85-120%, class G was 100-220% and class A (OPC I) was 170-240%

CHAPTER 5 FRACTURE PROPERTIES OF DIFFERENT TYPES OF OIL WELL CEMENT

This chapter studies the fracture properties of different types of oil well cement used in the oil well industry for specimen cured for 28 days. Crack monitoring systems based on pulse velocity and piezoresistivity are also discussed.

Fracture studies were carried out on specimens with different notch to depth ratios to study mode I crack properties under three point bending loading using Crack Mouth Opening Displacement (CMOD) gauge in order to find out Critical Stress Intensity Factor (K_{IC}), Elastic Crack Mouth Opening Displacement ($CMOD^e$) and Elastic Crack Tip Opening Displacement ($CTOD^e$).

5.1 Introduction to Fracture Mechanics and Fracture Properties of Oil Well Cement

Fracture mechanics is a study of propagation of cracks in materials for which the foundation was first established by Griffith (Budynas 1999). His work especially introduced linear elastic fracture mechanics (LEFM). G. R. Irwin (1948) in 1940s extended the Griffith's LEFM theory to ductile materials by introducing the strain energy release rate (G), stress amplification factor and crack extension resistance curve or R-curve which is known as elastic-plastic fracture mechanics. James R. Rice (1968), developed the J-integral method for non-linear elastic ductile material.

In the literature, researchers have used both LEFM parameters and elastic plastic fracture parameters in characterizing fracture resistance of cement paste, cement mortar, cement concrete, polymer concrete and rocks (Arikan et al., 2004; Atkinson, 1987; Bazant, 1992; Dharmarajah et al., 1988; Vipulanandan et al., 1994; Wecharatna et al., 1982; Ziegeldorf et al., 198).

Three distinct modes of crack propagation are considered in fracture mechanics as shown in Figure 5-1. A tensile stress field gives rise to mode I which is the opening crack propagation mode. Mode II is shearing or sliding mode due to in-plane shear. Mode III is tearing mode, which arises from out-of-plane shear (Budynas 1999).

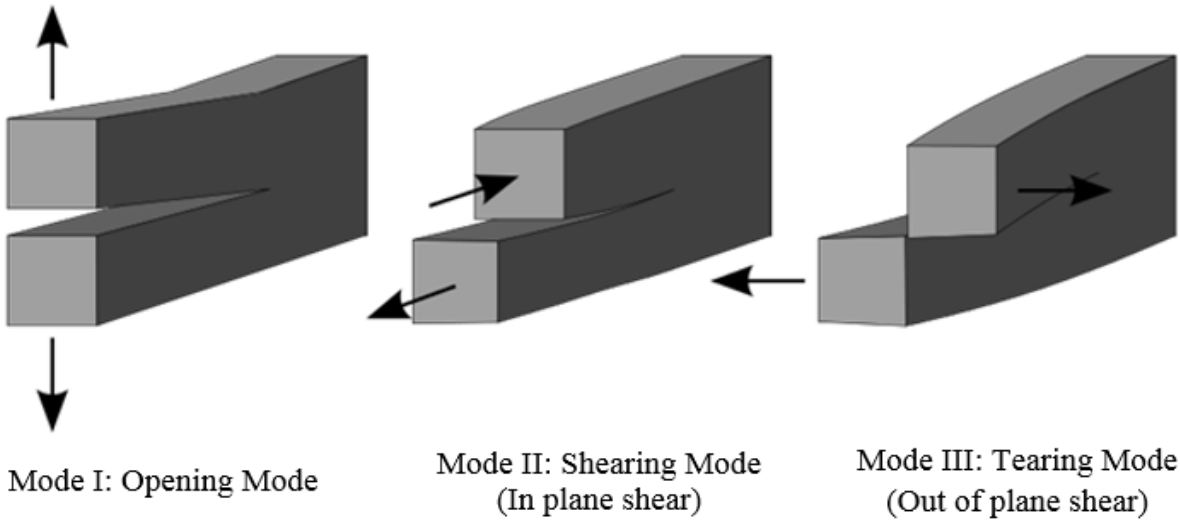

Figure 5-1: Fracture Modes of Materials

The stress state near the tip of a sharp crack was found to be more useful in engineering practice. Stress intensity factor, K_I characterizes the crack tip conditions in a linear elastic material (Budynas 1999). If K_I is known, the entire stress distribution at the crack tip can be computed with some basic equations.

5.1.1 Stress Intensity Factor, K_I (Linear Elastic Fracture Mechanics)

Critical stress intensity factor is one of the most frequently used parameters in the literature to study the fracture properties of materials (Vipulanandan et al., 1994).

Fracture occurs when the stress intensity factor (K_I) reaches its critical stage which is known as Critical Stress Intensity Factor (K_{IC}) or fracture toughness. K_I is proportional to the applied load, while K_{IC} is a material property (Rosler et al., 2007). Prior to fracture, the crack tip

absorbs energy and generates local plastic deformation when the loading is applied. The energy required to propagate the crack needs to overcome the energy absorbed at the crack tip as well as the surface energy (Andrews 1968).

Figure 5-2 (Rosler et al., 2007) shows the propagation of crack, near crack tip. The material near the crack tip plastically deforms and hardens as shown in Figure 5-2 (b). The shape of the crack tip blunts to some extent. Cavities appear in the front of crack tip as shown in Figure 5-2 (c), when the plastic deformation zone enlarges with increasing loads. With increasing applied load, the cavities merge into a continuous crack shape, called crack initiation (Rosler et al., 2007). When the crack length increases, the critical stress is reduced because the energy dissipates.

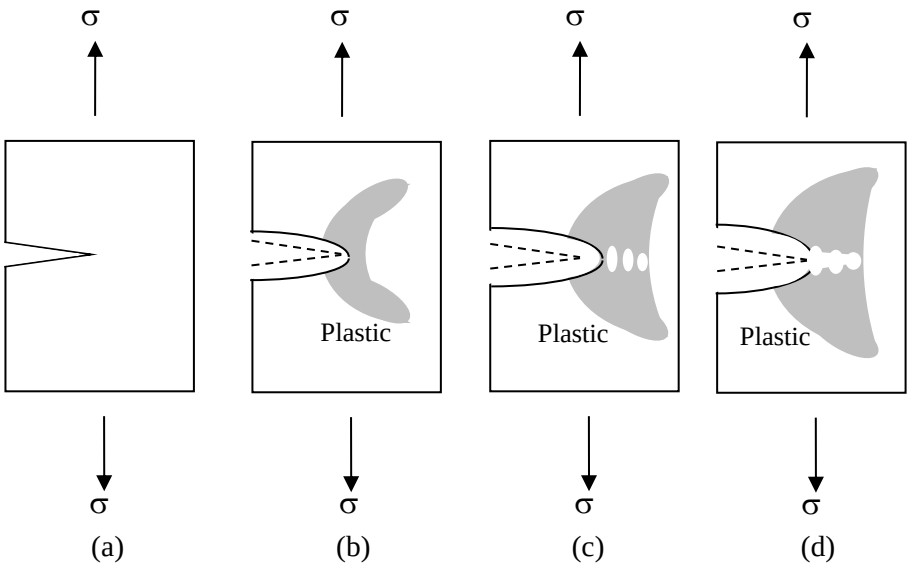

Figure 5-2: Propagation of Crack near Crack Tip

Stress intensity factor, K_I is a constant which is proportional to each stress component at the crack tip shown in Figure 5-33 (Anderson 2004) for elastic materials in the opening mode. The subscript I indicate the crack opening mode.

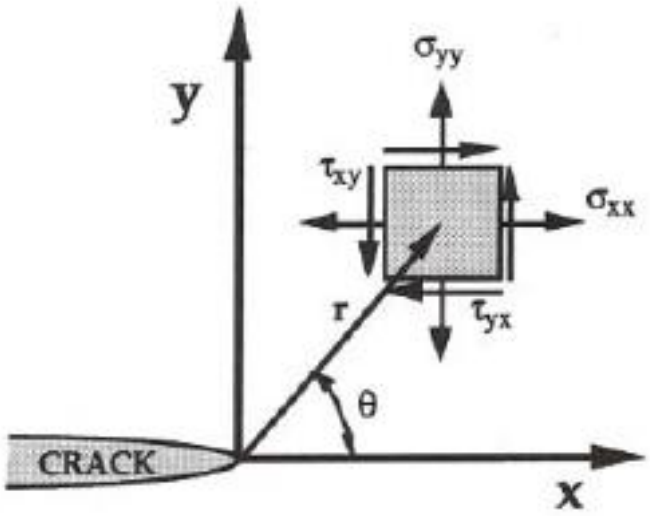

Figure 5-3: Stresses Near the Tip of a Crack for an Elastic Material in Mode I

For distances very close to the crack tip, the relationships between stress components and K_I are given in Equations 5-1 to 5-4 as

$$\sigma_x = \frac{K_I}{\sqrt{2\pi r}} \cos\frac{\theta}{2}\left(1 - \sin\frac{\theta}{2}\sin\frac{3\theta}{2}\right), \quad 5\text{-}1$$

$$\sigma_y = \frac{K_I}{\sqrt{2\pi r}} \cos\frac{\theta}{2}\left(1 + \sin\frac{\theta}{2}\sin\frac{3\theta}{2}\right), \quad 5\text{-}2$$

$$\tau_{xy} = \frac{K_I}{\sqrt{2\pi r}} \cos\frac{\theta}{2}\cos\frac{3\theta}{2}\sin\frac{\theta}{2}, \text{ and} \quad 5\text{-}3$$

$$\sigma_z = \begin{cases} 0 & (if\ plane\ stress) \\ \nu(\sigma_x + \sigma_y) & (if\ plane\ strain) \end{cases}. \quad 5\text{-}4$$

At far distances from the crack tip, these stresses approach their far-field values that would be obtained when the crack was not present.

Beyond a critical stage, the crack becomes unstable and propagates rapidly. The stress intensity factor at this stage is called as critical stress intensity factor, K_{IC}.

This critical stress intensity factor is a measure of material toughness. The fracture toughness or critical stress intensity factor can be related to failure stress and crack length.

Figure 5-4 shows the schematic diagram of experimental setup with clip on CMOD gauge that was used to calculate K_I. knife edge was glued to the specimen.

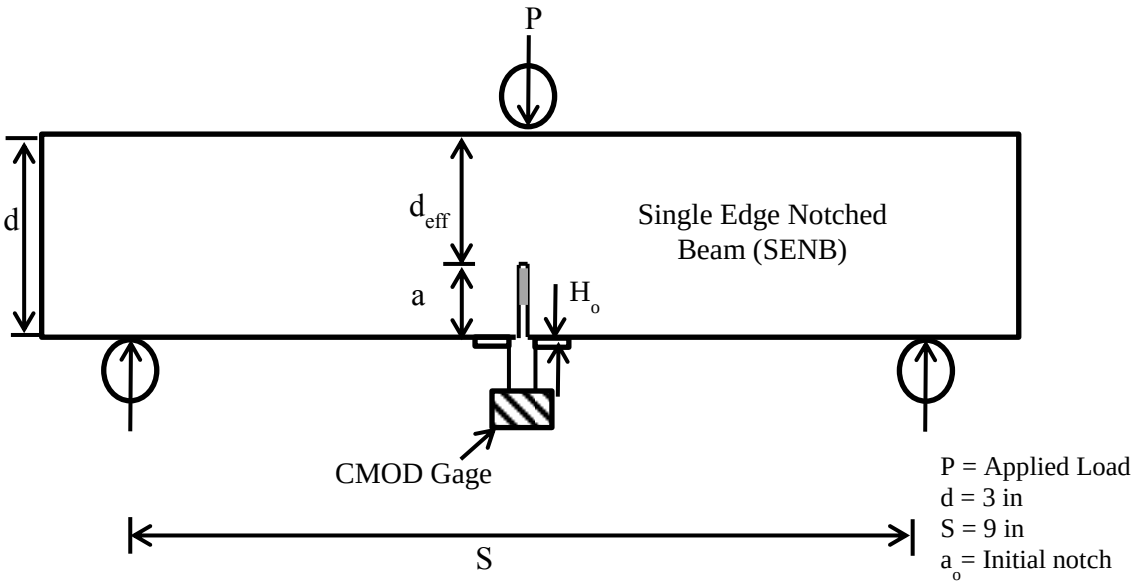

Figure 5-4: Schematic Diagram of Experimental Setup to Find Out KI

The stress intensity factor K_I is given for any geometry as shown in Equation 5-5

$$K_I = \sigma\sqrt{a}F(\alpha), \qquad 5\text{-}5$$

where σ is bending stress calculated as shown in Equation 5-6

$$\sigma = 3PL/2bd_{eff}^2, \qquad 5\text{-}6$$

and F(α) is a correction factor for finite width and loading geometry. For three point loading bending test F(α) is given in the Equation 5-7,

$$F(\alpha) = \frac{\left[1.99 - \alpha(1-\alpha)(2.15 - 3.93\alpha + 2.7\alpha^2)\right]}{\left[(1+2\alpha)(1-\alpha)^{\frac{3}{2}}\right]}, \quad 5\text{-}7$$

where α is a factor depends on crack length. Equation 5-8 defines α as

$$\alpha = \frac{(a + H_0)}{(d + H_0)}, \quad 5\text{-}8$$

where H_0 is the clip gauge holder thickness as shown in Figure 5-3. In the Equation 5-8, 'a' has to be calculated from a numerical iteration procedure using Equation 5-9

$$a_e = a_0 \left[\frac{C_U}{C_0}\right]\left[\frac{V(\alpha_0)}{V(\alpha_e)}\right], \quad 5\text{-}9$$

where initial compliance C_o is given by Equation 5-10

$$Co = \frac{CMOD}{P}, \quad 5\text{-}10$$

unloading compliance C_u was measured at about 95% of the peak load and V(α) is given by Equation 5-11

$$V(\alpha) = 0.76 - 2.28\alpha + 3.87\alpha^2 - 2.04\alpha^3 + \frac{0.66}{(1-\alpha)^2}. \quad 5\text{-}11$$

Variation of load (P) versus Crack Mouth Opening Displacement (CMOD) of class H oil well cement from experiment is shown in Figure 5-5 for initial notch to depth ratio of 0.3.

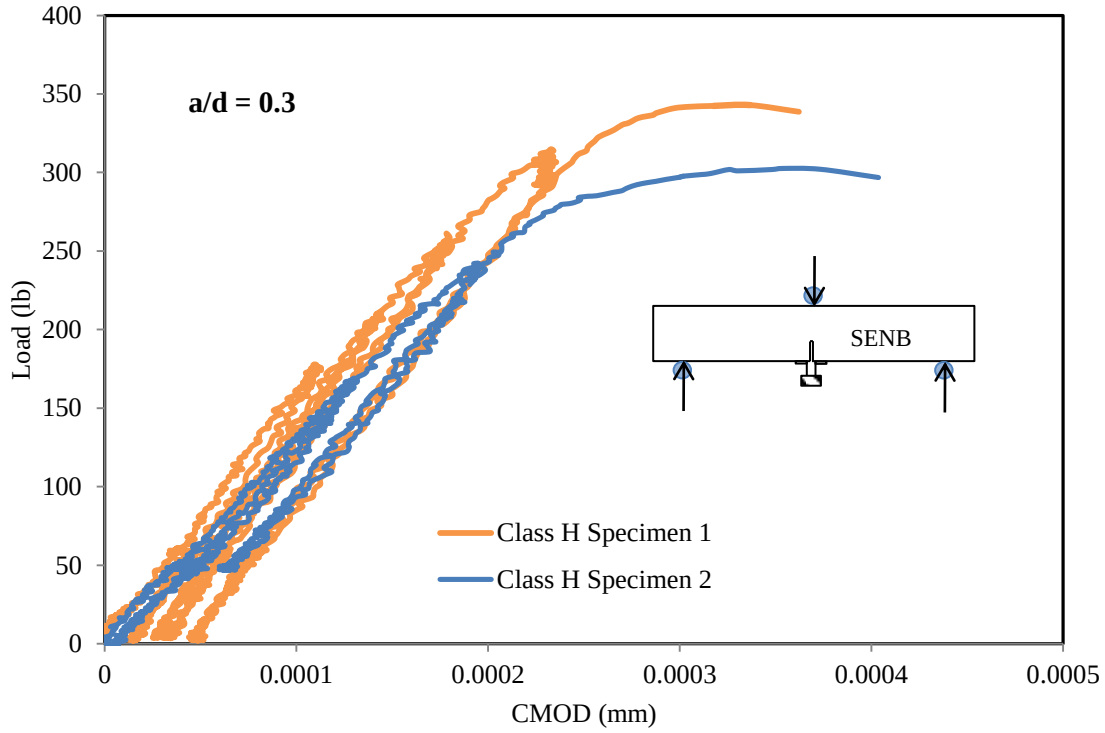

Figure 5-5: Variation of Load versus CMOD of Class H Oil Well Cement for a/d = 0.3

Variation of load versus CMOD of class H cement is shown in Figure 5-6 for a/d ratio of 0.4.

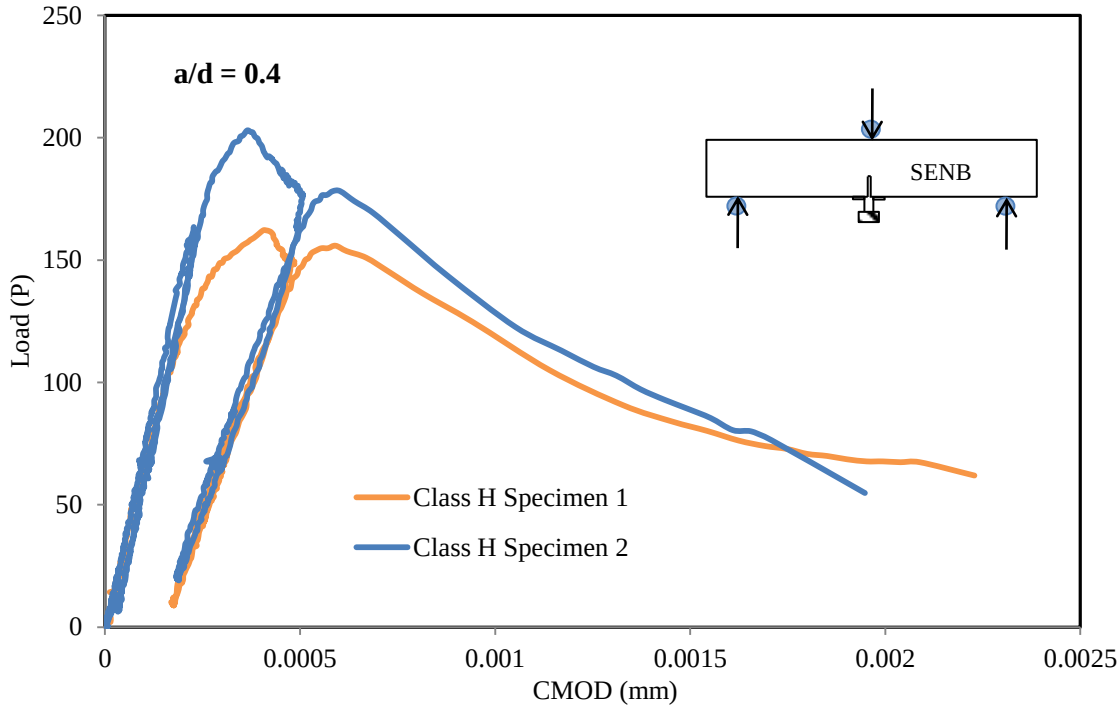

Figure 5-6: Variation of Load versus CMOD of Class H Oil Well Cement for a/d = 0.4

Variation of load versus CMOD of class H cement is shown in Figure 5-7 for a/d ratio of 0.5.

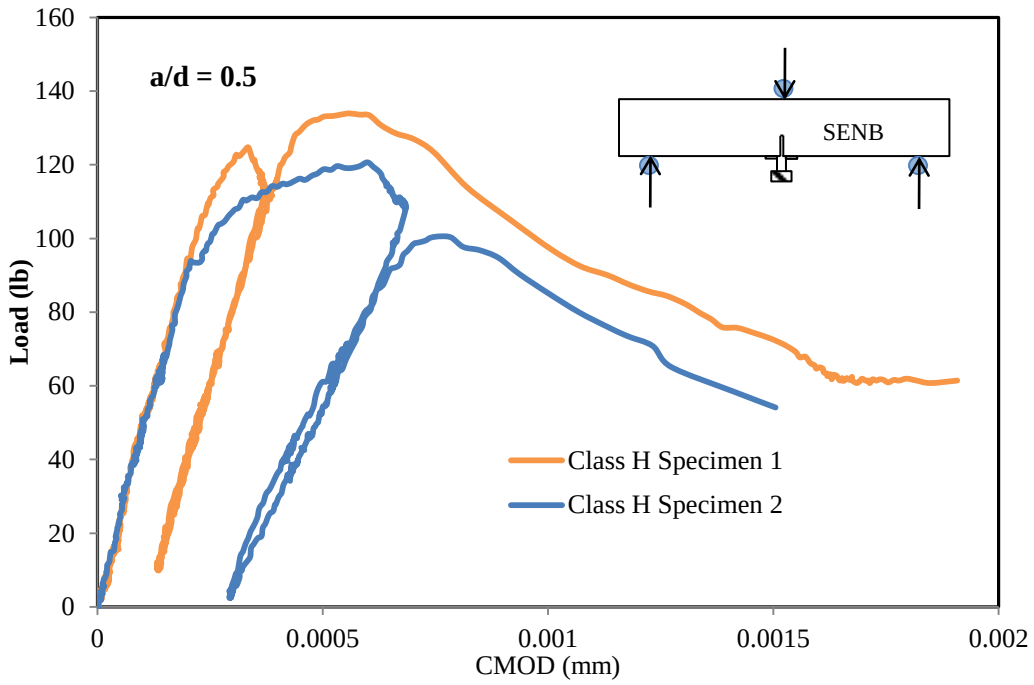

Figure 5-7: Variation of Load versus CMOD of Class H Oil Well Cement for a/d = 0.5

Variation of load versus CMOD of class G cement is shown in Figure 5-8 for a/d ratio of 0.3.

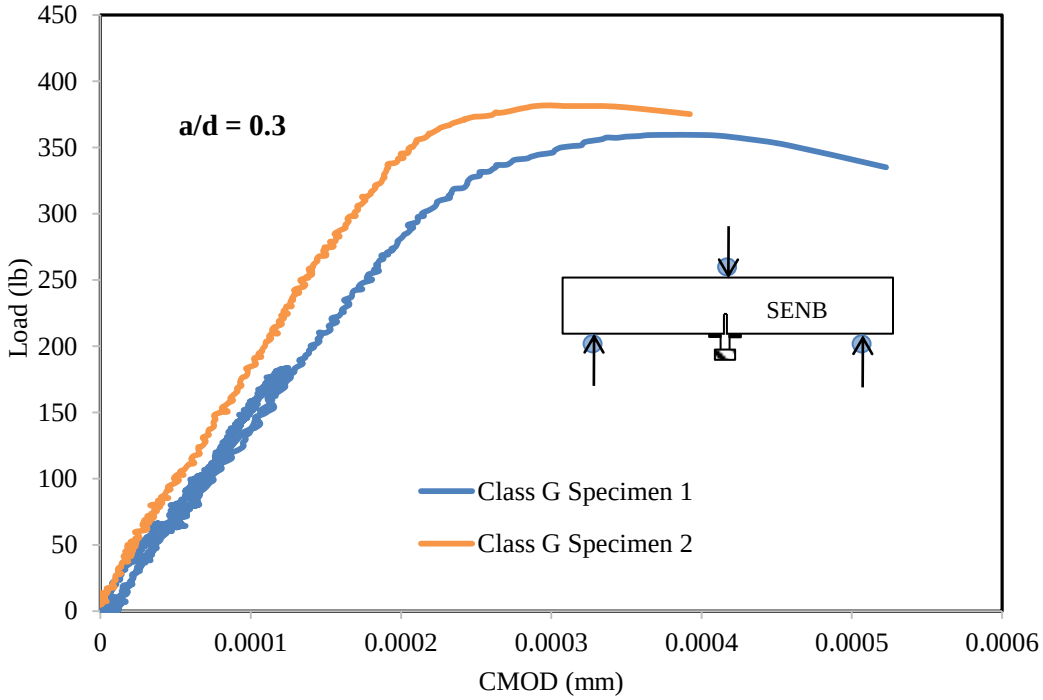

Figure 5-8: Variation of Load versus CMOD of Class G Oil Well Cement for a/d = 0.3

Variation of load versus CMOD of class G cement is shown in Figure 5-9 for a/d ratio of 0.4.

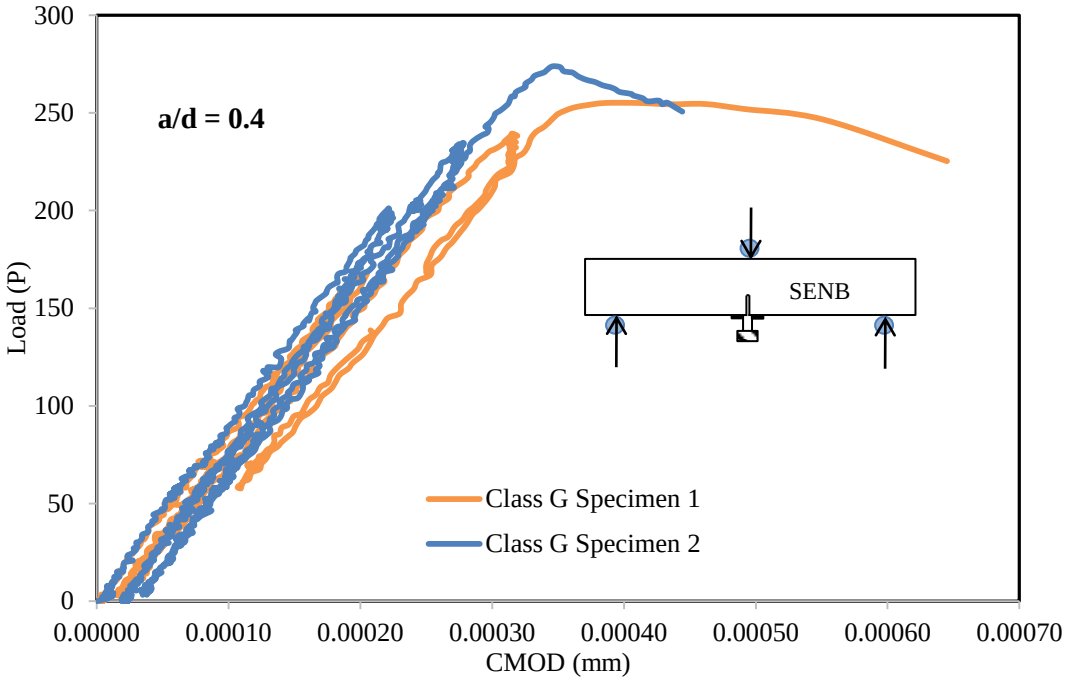

Figure 5-9: Variation of Load versus CMOD of Class G Oil Well Cement for a/d = 0.4

Variation of load versus CMOD of class G cement is shown in Figure 5-10 for a/d ratio of 0.5.

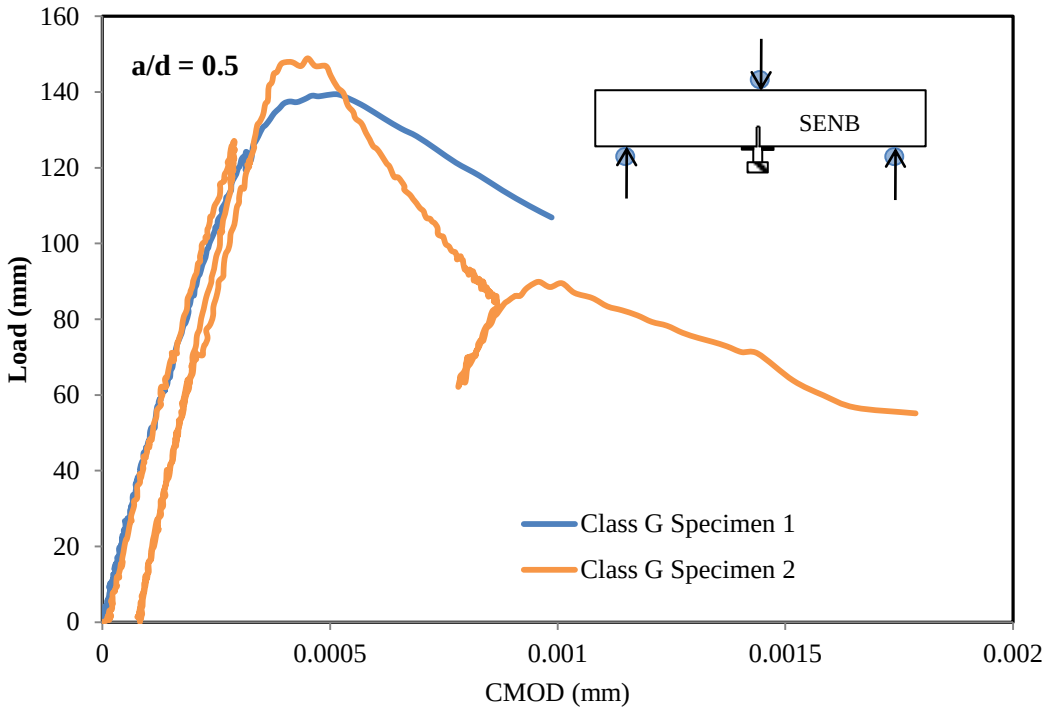

Figure 5-10: Variation of Load versus CMOD of Class G Oil Well Cement for a/d = 0.5

Variation of load versus CMOD of class A cement is shown in Figure 5-11 for a/d ratio of 0.3.

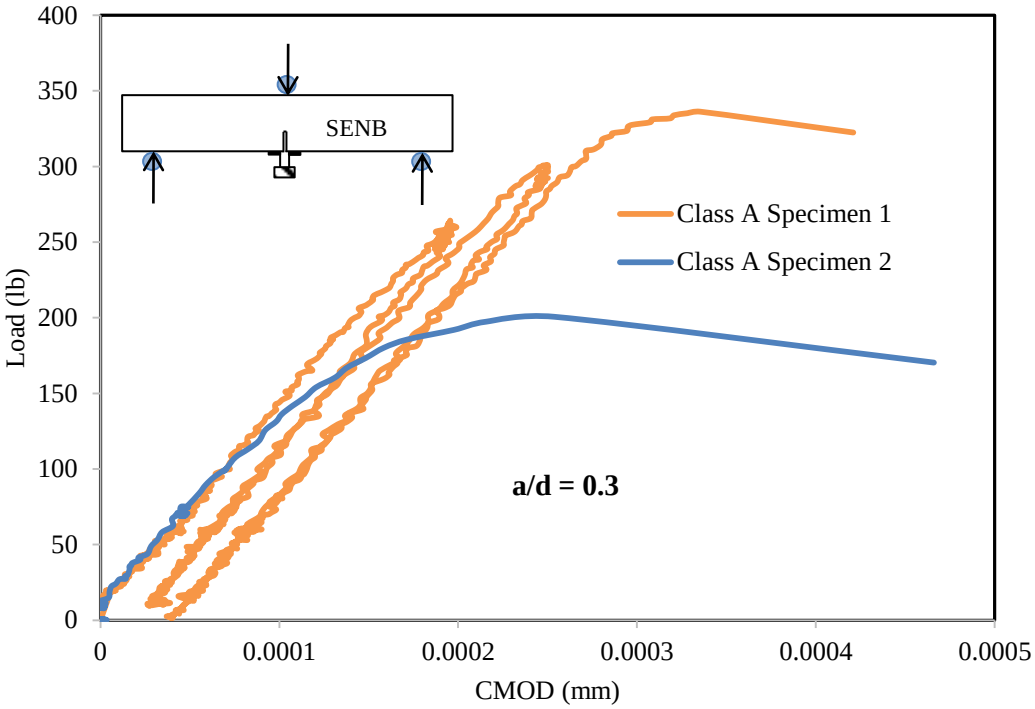

Figure 5-11: Variation of Load versus CMOD of Class A Oil Well Cement for a/d = 0.3

Variation of load versus CMOD of class A cement is shown in Figure 5-12 for a/d ratio of 0.4.

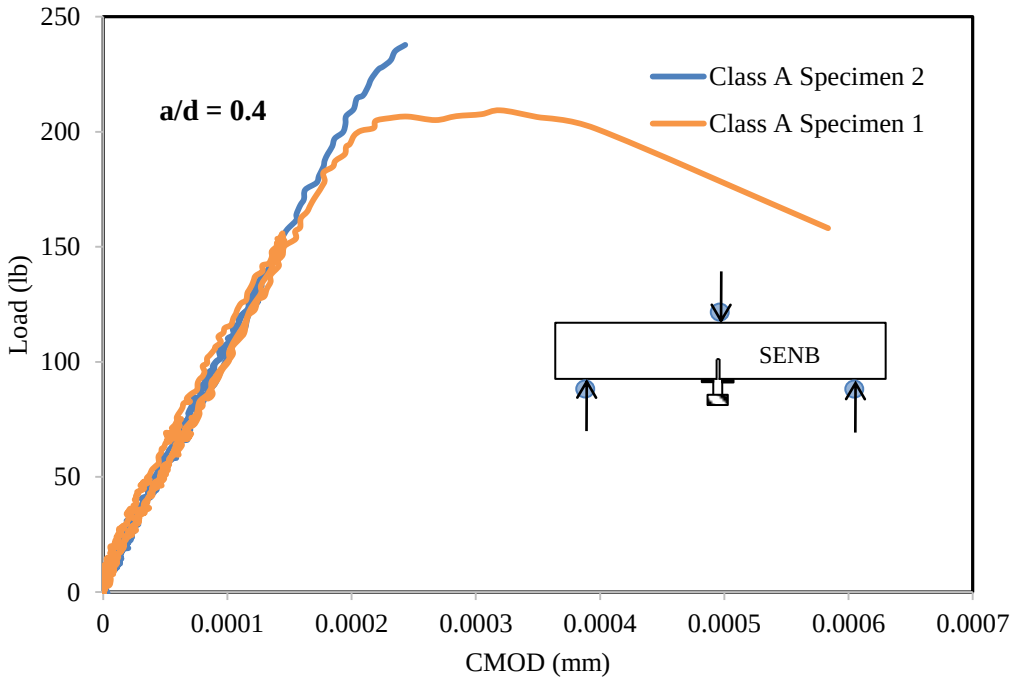

Figure 5-12: Variation of Load versus CMOD of Class A Oil Well Cement for a/d = 0.4

Variation of load versus CMOD of class A cement is shown in Figure 5-13 for a/d ratio of 0.4.

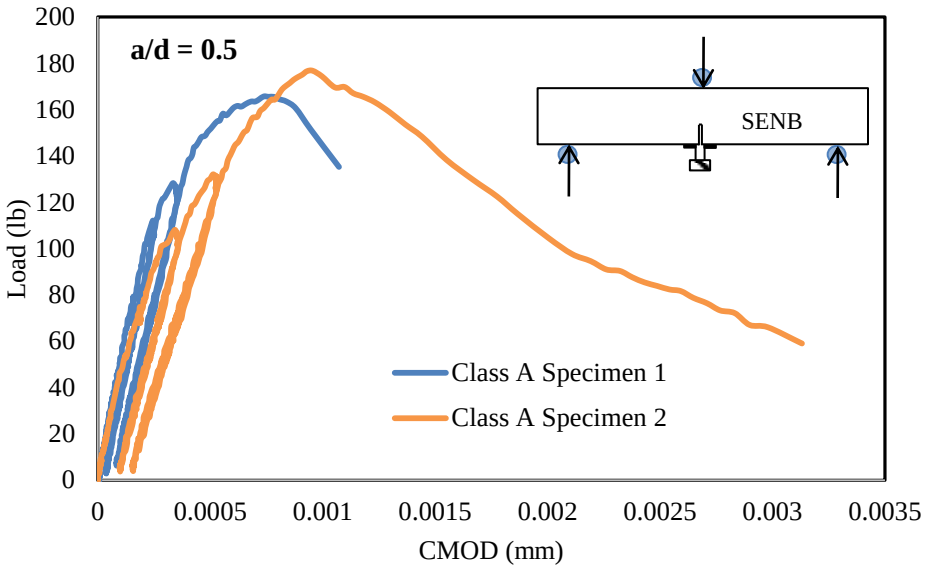

Figure 5-13: Variation of Load versus CMOD of Class A Oil Well Cement for a/d = 0.5

Figure 5-14 (Dharmarajan and Vipulanandan, 1988) shows a schematic of load versus CMOD which explains the components of total CMOD ($CMOD^T$).

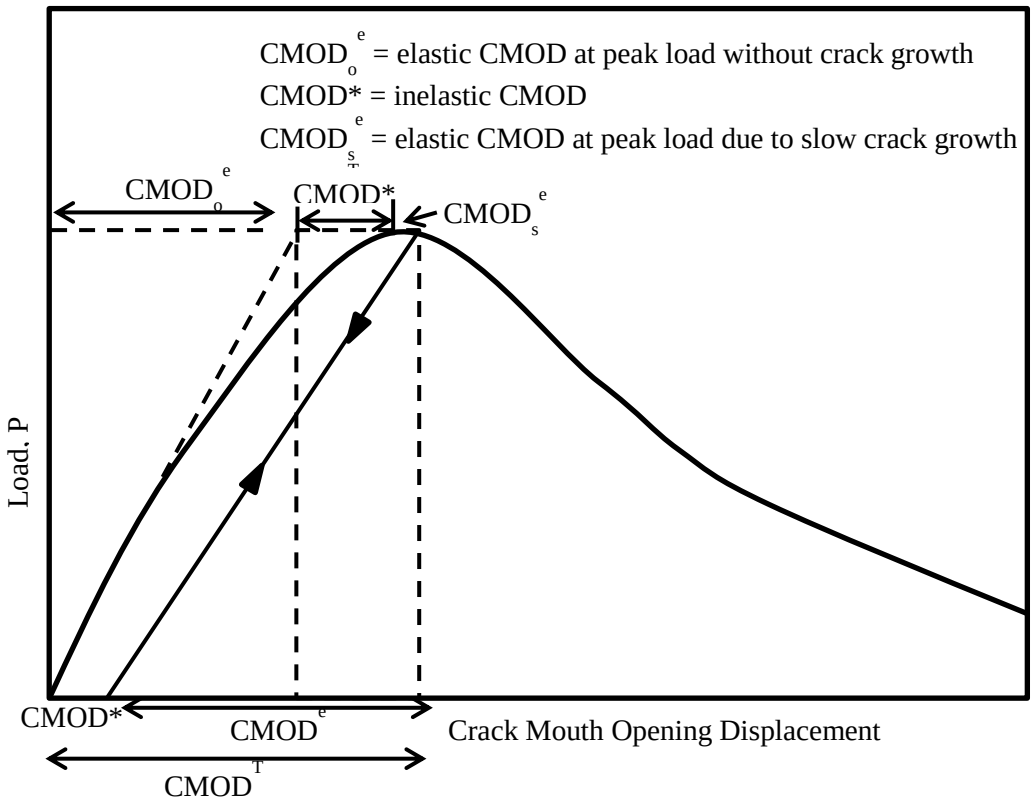

Figure 5-14: Schematic Diagram of load versus CMOD with the components of $CMOD^T$

If the material behaves elastically up to the peak load without any crack extension, the relationship between load and CMOD would be linear as shown in the Figure 5.4. By unloading the specimen immediately after the peak load it can be seen that there is inelastic displacement (CMOD*). At peak load the $CMOD^T$ is composed of the elastic displacement (no crack extension, $COMD^e_o$), inelastic displacement (CMOD*) and the elastic displacement due to slow crack growth ($COMD^e_s$).

In order to apply LEFM, the inelastic CMOD (CMOD*) should be extracted from the total COMD ($CMOD^T$) at peak load. The total elastic COMD ($COMD^e = COMD^e_o + COMD^e_s$) at peak load is obtained by unloading the specimen at 95% of the peak load.

Knowing σ, a and $F(\alpha)$ K_I was calculated for different types of cement as shown in Table 5-1.

Table 5-1: K_I for Different Types of Oil Well Cement in MPa.√m

Notch to Depth	Specimen	Class H	Class G	Class A
0.3	1	0.34	0.29	0.30
	2	0.32	0.30	0.27
0.4	1	0.38	0.43	0.58
	2	0.45	0.34	0.17
0.5	1	0.57	0.28	0.45
	2	0.47	0.43	0.51

Stress intensity factor for class H cement varied from 0.32 to 0.57 MPa.√m with an average of 0.42 MPa.√m. Stress intensity factor for class G cement varied from 0.28 to 0.43 MPa.√m with an average of 0.35 MPa.√m. Stress intensity factor for class A cement varied from 0.17 to 0.58 MPa.√m with an average of 0.38 MPa.√m.

K_I variation for each a/d ratio is presented for each types of cement in Figure 5-15. The values considered were average of two specimens.

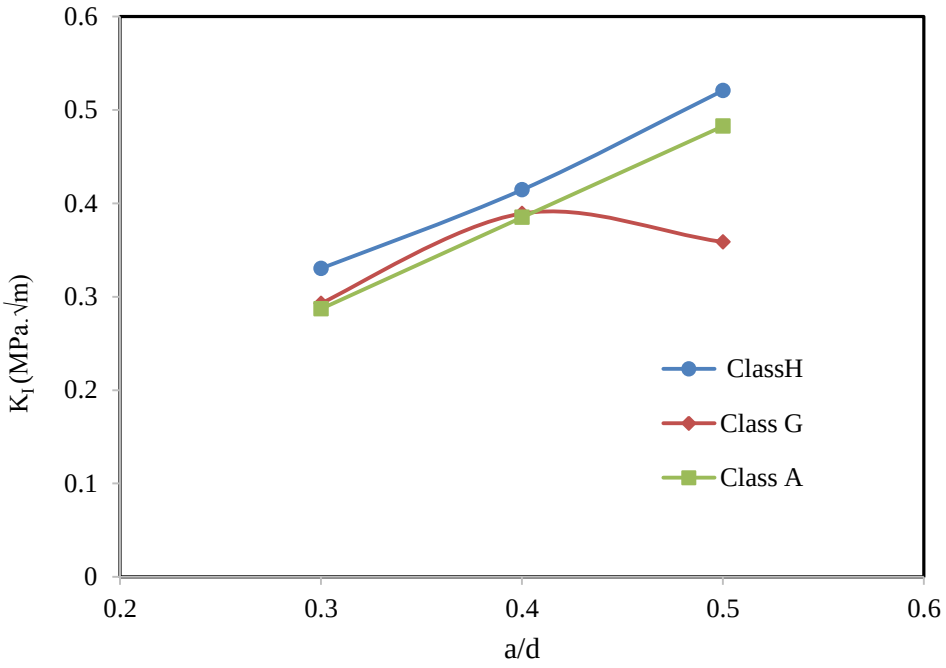

Figure 5-15: Variation of K_I with a/d for Different Types of Oil Well Cement

In general K_I increased with increasing notch to depth ratio which does not agree the literature trend (Heiza, 2009; Vipulanandan, 1994). K_I values of this study varied between 0.28 and 0.58. In the literature, K_{IC} for cement pastes, cement mortar and cement concrete has been reported to vary between 0.1 to 1.7 MPa.√m (John et al., 1987; Swartz et al., 1982; Vipulanandan et al., 1994; Ziegeldorf, 1983) which agrees with the findings of this study. Materials variations, scatters in experimental results and limitations in the applicability of fracture mechanics concepts were suggested to be the reasons for the wide range of K_{IC} values.

5.1.2 Crack Tip Opening Displacement (CTOD)

The crack tip opening displacement (CTOD), is defined in Figure 5-16, which is a measure of fracture toughness of solid materials that undergo ductile-brittle transition and elastic-plastic or fully plastic behavior as in larges structures. It is a measure of the distance which makes right angle as shown in the figure.

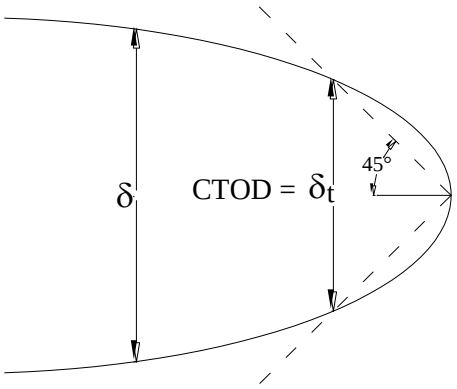

Figure 5-16: Definition of Crack Tip Opening Displacement, CTOD

Elastic Crack Tip Opening Displacement ($CTOD^e$) is calculated using Equation 5-12 (Jeng et al., 1985; Vipulanandan et al., 1989)

$$CTOD^e = CMOD^e Z(\alpha, \beta), \quad 5\text{-}12$$

where

$$CMOD^e = \frac{4\sigma a V(\alpha)}{E}, \quad 5\text{-}13$$

$$Z(\alpha, \beta) = \left[(1-\beta)^2 + (1.081 - 1.149\alpha)(\beta - \beta^2)\right]^{\frac{1}{2}}, \quad 5\text{-}14$$

and

$$\beta = \frac{a_0}{a_e}. \quad 5\text{-}15$$

Using the effective crack depth in Equation 5-8, $CTOD^e$ was determined for different types of cements. Figure 5-17 shows the variation of $CTOD^e$ with initial notch to depth ratio. In

general CTOD^e also decrease with increase in notch to depth ratio. The average value of CTOD^e is summarized in Table 5-2.

Table 5-2: CTOD^e for Different Types of Oil Well Cement in µm

Notch to Depth	Specimen	Class H	Class G	Class A
0.3	1	2.80	2.60	3.01
	2	2.80	2.68	3.24
0.4	1	3.77	5.17	5.82
	2	4.52	3.35	1.01
0.5	1	4.67	3.08	5.63
	2	4.48	5.40	6.49

CTOD^e for class H cement varied from 2.80 to 4.67 µm with an average of 3.84 µm. CTOD^e for class G cement varied from 2.60 to 5.40 µm with an average of 3.71µm. CTOD^e for class A cement varied from 1.01 to 6.49 µm with an average of 4.20 µm.

Average CTOD^e for each a/d ratio are presented for each types of cement in Figure 5-17

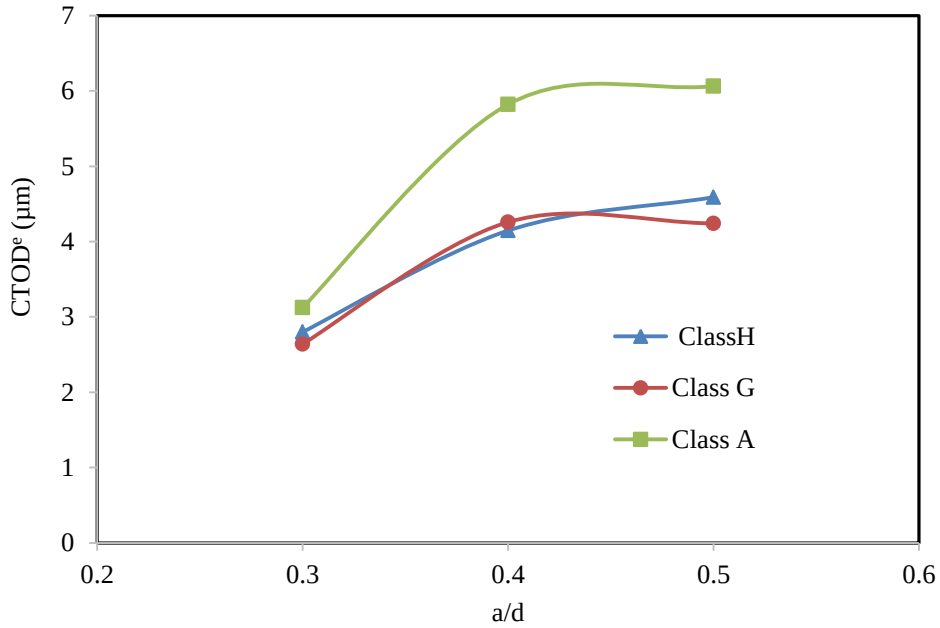

Figure 5-17: Variation of CTOD^e with a/d for Different Types of Oil Well Cement

In general $CTOD^e$ increased with increasing a/d ratio for all types of oil well cement studied. Class G cement had a small variation in trend compared to others.

5.2 Non-destructive Methods of Crack Monitoring

The crack growth was monitored using non-destructive methods also. Pulse wave and resistance change were monitored for this purpose. Figure 5-18 shows a typical variation of pulse wave travelling time between two observed points.

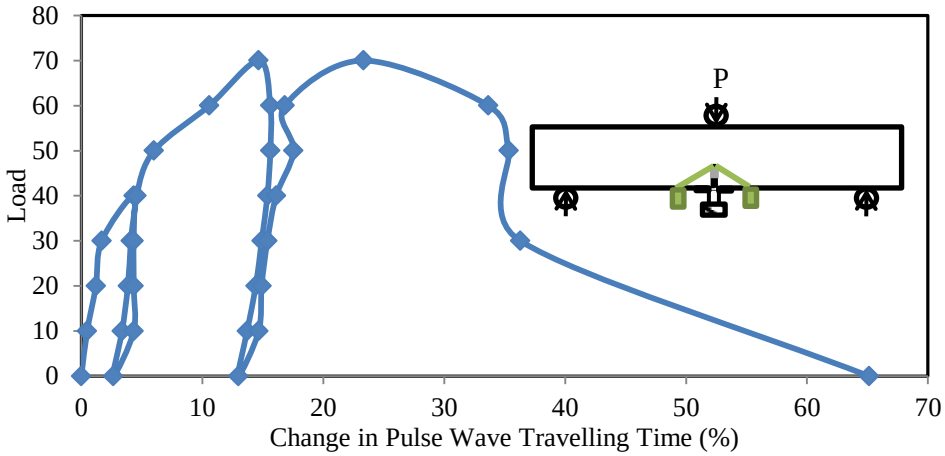

Figure 5-18: Change of Pulse Wave Travelling Time with Load

Figure 5-19 shows typical change of resistance with applied load. Resistance was monitored close to the crack propagation path.

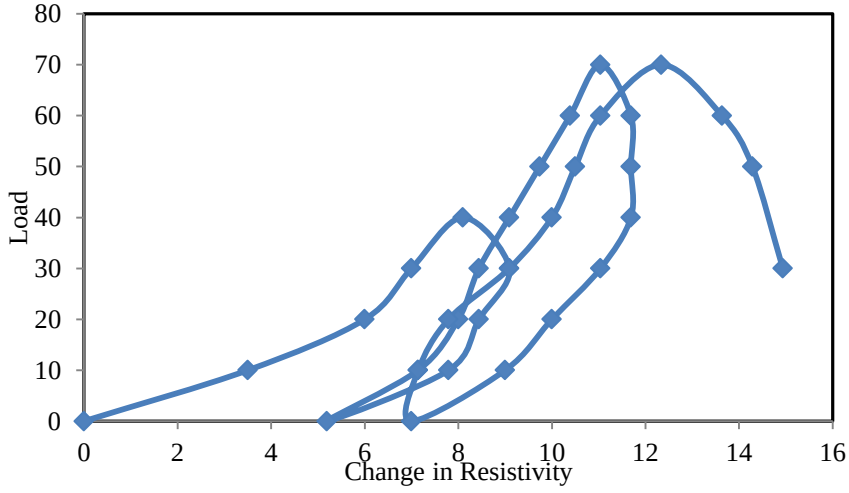

Figure 5-19: Typical Change in Resistance with Load

5.2 Numerical Modelling of Fracture

In fracture studies, a crack growth parameter can be calculated analytically or numerically and compared to values from experiments. It is possible to calculate fracture parameters using numerical methods (FEM) for practical problems.

Finite element programs such as ABAQUS are widely available for numerical calculation of crack growth parameters. Although special procedures are developed and implemented, the use of standard elements is possible after a minor adaptation of the element mesh. Using ABAQUS fracture toughness of class H, class G and class A cements were studied for a/d ratios of 0.3, 0.4 and 0.5 and compared to experimental.

5.2.1 Geometry

The schematic geometry of the model is shown in the Figure 5-20. This is two dimensional plane stress model with three point bending case. The load was applied on top of the specimen and vertical displacement was restrained.

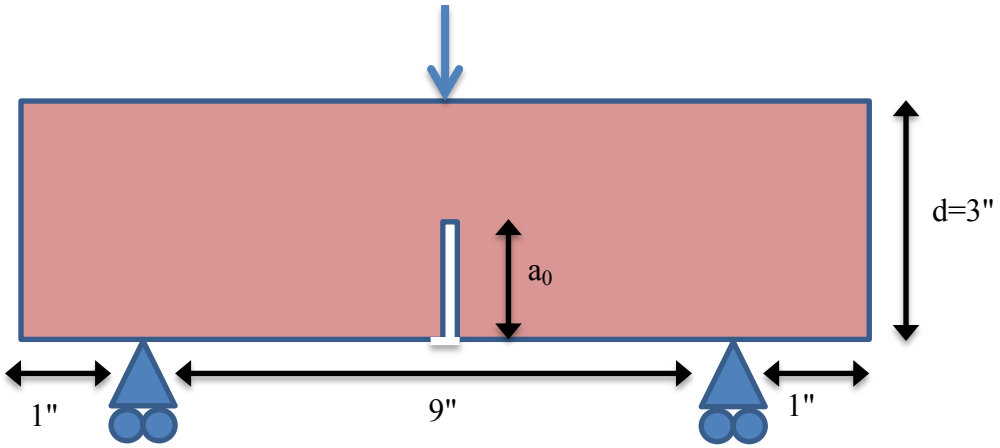

Figure 5-20: Schematic Geometry of the Finite Element Model Used

Figure 5-21demonstrated counter integral method of modeling the fracture behavior. The number of counter integrals considered was 4.

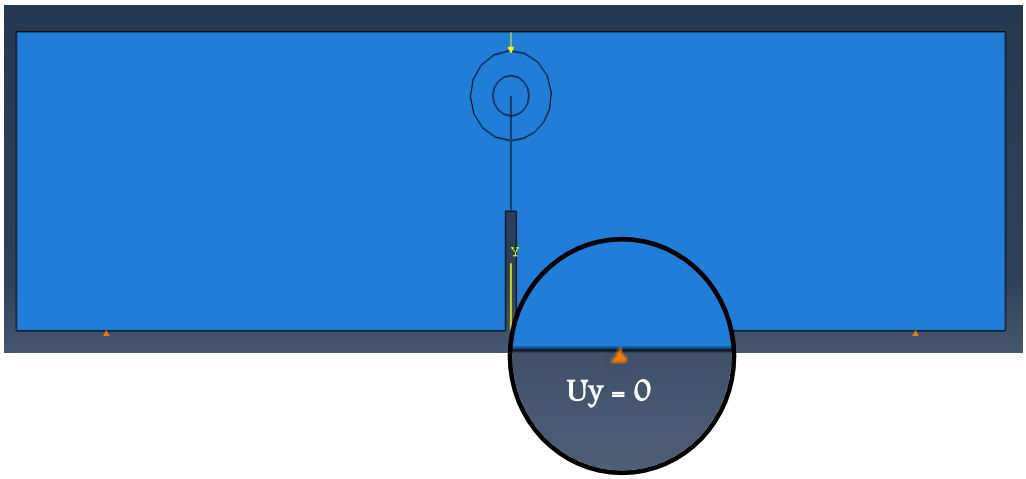

Figure 5-21: Counter Integral Method of Modeling Fracture Behavior

5.2.2 Input Data

The maximum loads applied were selected to be equal to the experimental data for each a/d ratio. The properties of the specimens including elasticity modulus, poison's ratio are shown in Table 5-3.

Table 5-3: Material Properties Considered

Type of Cement	E (psi)	Poisson's Ratio
Class H	3,500,000	0.19
Class G	2,800,000	0.19
Class A (OPC I)	2,730,000	0.15

5.2.3 Element types

For two-dimensional finite element analyses, the 8-node plane stress or plane strain element gives accurate results for most of the mechanical problems. The displacement of an internal element point is interpolated quadratically between the nodal displacements. Although initially the element edges were straight lines, after deformation they become parabolic. Used elements are described below.

- CPS6, 6-node quadratic plane stress triangle

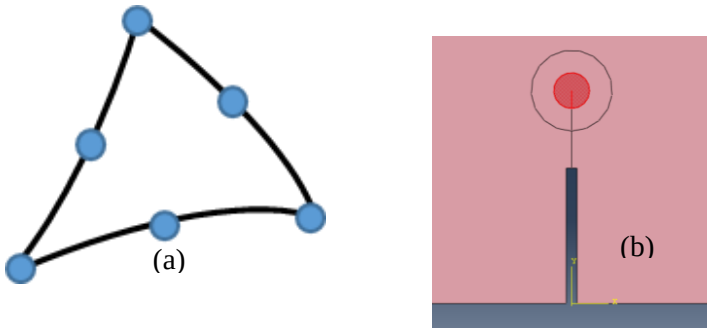

Figure 5-22: (a) 6-Node Quadratic Plane Stress Triangle (b) Used Region in the Model

- CPS8, 8-node biquadratic plane stress quadrilateral

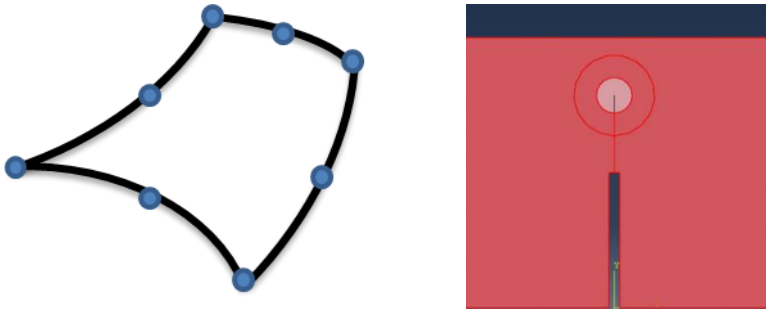

Figure 5-23: 8-Node Biquadratic Plane Stress quardrilateral (b) Used Region in the Model

5.2.4 Results and Discussion

Typical undeformed and deformed models are shown in Figure 5-24 and 5-25. Contours in Figure 5-25 related to von misses stresses.

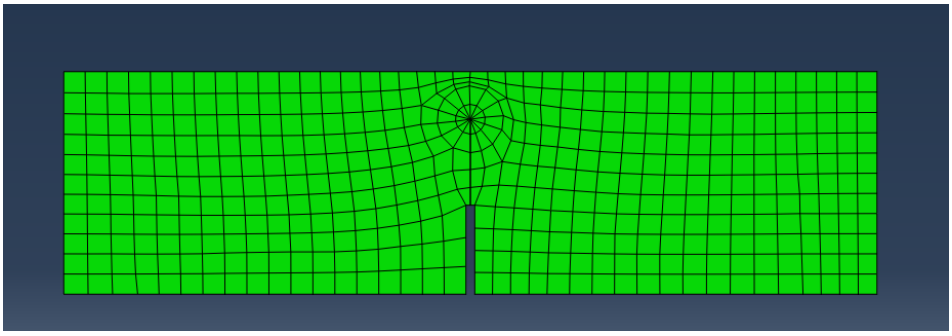

Figure 5-24: Typical Undeformed Model

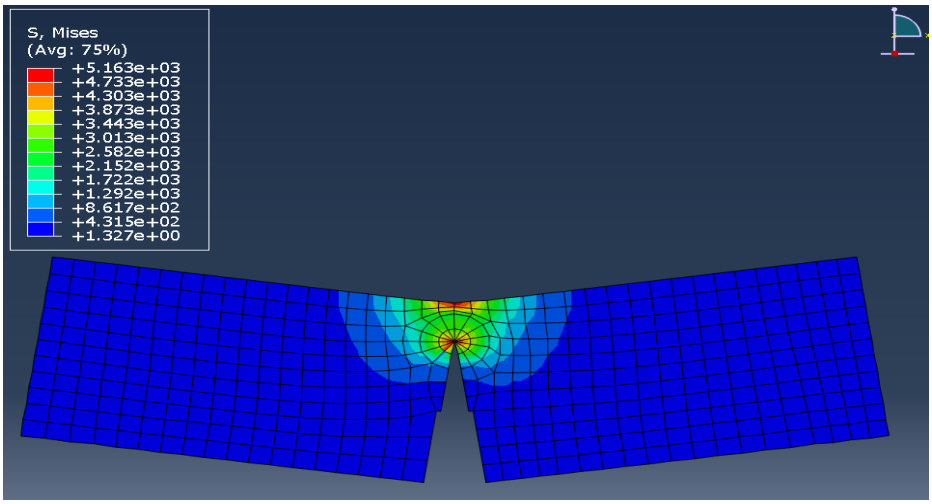

Figure 5-25: Figure 5 22: Typical Deformed Model

Figure 5-26 compares the experimental and FEM parameter of K_I value. Generally at 0.5 a/d value the experimental and FEM values did not match each other. However, other K_I values are in good agreement.

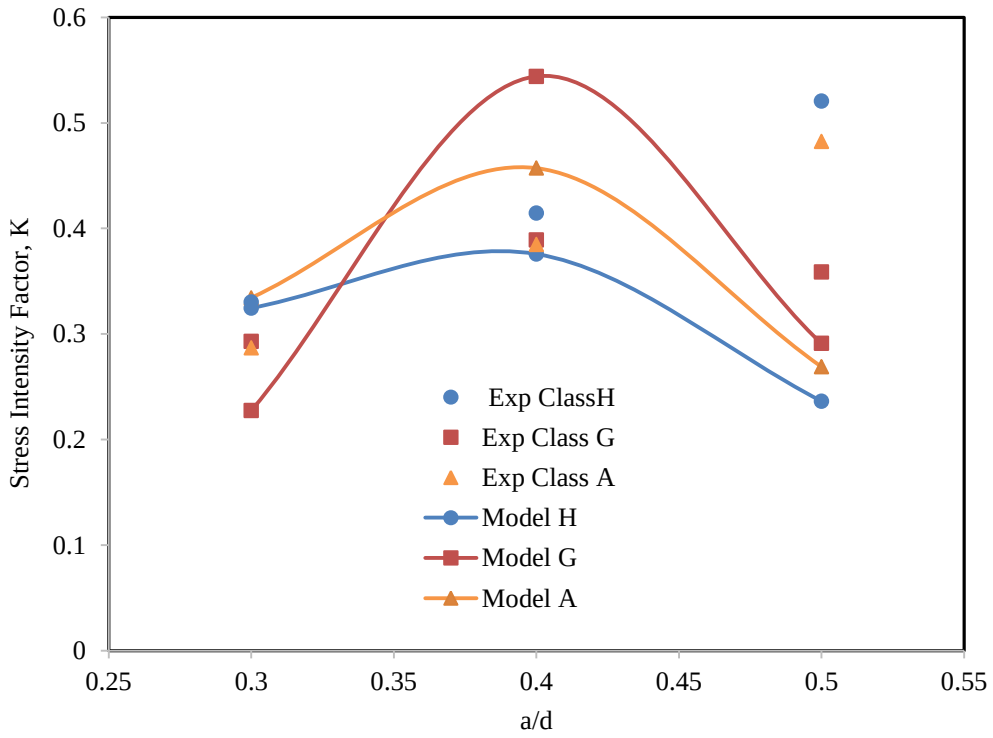

Figure 5-26: Experimental and FEM Values of K_I

Summary

1. Class H, class G and class A oil well cements were tested for fracture properties with notch to depth ratios of 0.3, 0.4 and 0.5.
2. Stress intensity factors varied from 0.28 to 0.58 MPa.√m for considered classes of oil well cement.
3. Elastic crack tip opening displacement varied from 2.60 to 6.49 µm
4. Change of Pulse wave travelling time and change of resistance were observed to monitor the growth of growth
5. Experimental and numerical values of K_I are generally in good agreement except a/d of 0.5

CHAPTER 6 BEHAVIOR OF LABORATORY SCALE MODEL OF OIL WELL

Real time monitoring of cementing in the annulus of lab scale oil well models are discussed in this chapter. Four different models of oil well were experimented at the laboratory to monitor the placement of cement and behavior of the cement sheath. Model 1 was a preliminary study to check the basic concepts of sensing the level of slurry using electrical properties and identifying the presence of free water. Displacement of oil based mud by spacer fluid and spacer fluid by cement slurry was studied using Model 2. Contamination also was detected using this model. Model 3 was calibrated to predict the resistance of the cement sheath to monitor the level of the cement slurry while it was being placed and after placement. Model 4 was comparatively large scale model than other three models. Level of cement placement was monitored real time and stress conditions were monitored. The trend of change in resistance enables to find out the depth at which the cement or drilling fluid is at. Each model is discussed one by one in this chapter.

6.1 Oil Well Model 1(Water as Drilling Fluid, Cement Slurry with W/C: 0.8)

Preliminary studies were conducted using model 1, for real time monitoring of the depth of cement at which it was being placed. This model helped to establish a trend of change in electrical resistance between selected sensors with the depth of cement being placed.

The model was built using poly methyl methacrylate tube which is a transparent thermo plastic and is known as Plexiglas in the industry. This Plexiglas tube simulated the formation of the oil well. A steel casing as shown in Figure 6-1 used to simulate the casing of the well. The casing was instrumented with electrical wires to monitor the resistance change. The distance between two sensors was 4 inches and there were six levels of sensors as shown in the Figure.

Different combinations of the sensors were connected to a 300 kHz LCR device to measure the resistance.

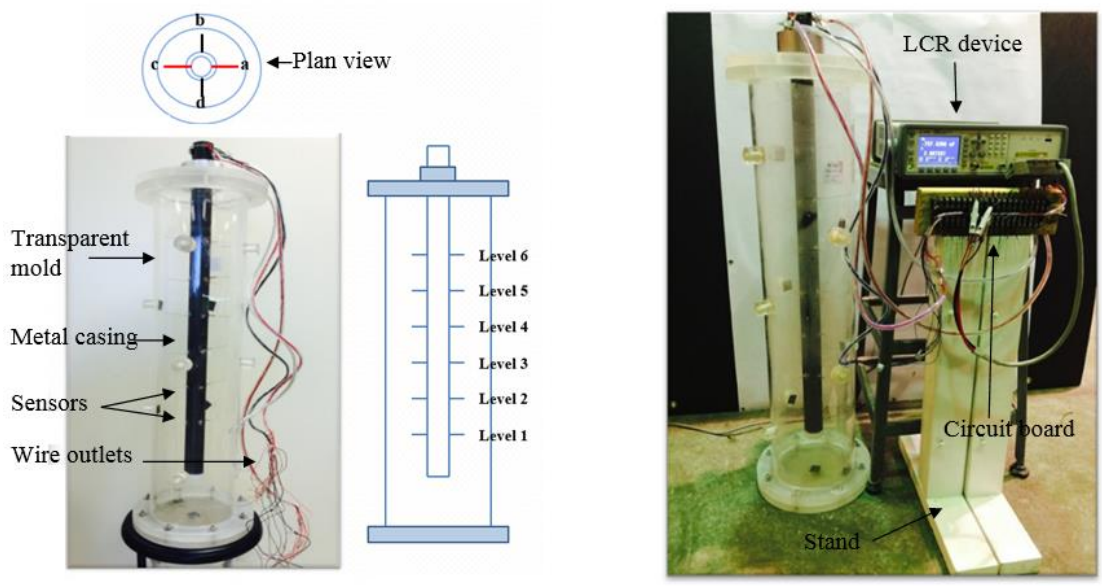

Figure 6-1: Monitoring System of Model 1

The vertical electrical resistance sensors were named a, b, c and d as shown in the Figure. Horizontal levels were named from 1 to 6. Figure 6-2 shows different depth of slurry in the well model.

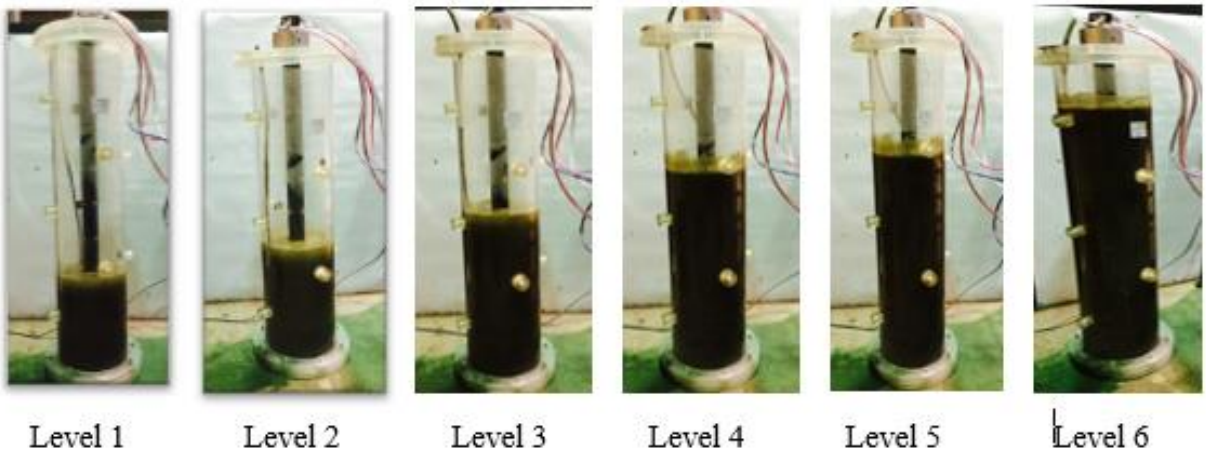

Figure 6-2: Different Depths of Slurry in the Oil Well Model

Depth of slurry was divided into six based on the level of the sensors. Cement was placed step by step.

6.1.1 Placement of Cement Slurry into the Well Model

Before the placement of cement, water was placed gradually in the model to represent drilling mud, while electrical resistance between sensors were monitored. Approximately 26 l of water was filled in the model using a tube of which open end was at the bottom of the well model. By placing the open end of the water filling tube, water was allowed to fill from the bottom of the well model towards upwards. The electrical resistance was measured with depth when water reached each level.

After measuring the resistance for all six levels of depth, water was removed and study was continued with cement slurry. Same amount of oil well cement class H slurry was used with a water to cement ratio of 0.8. The cement was modified with an addition of 0.075% Carbon fiber as discussed in Chapter 3. The same procedure was followed as for water and resistance measurements were taken when the slurry reach each levels.

6.1.2 Monitoring the Depth of Drilling Mud (Water)

Figure 6-3 shows the variation of measured resistance measured with depth. When there was no water in the well (at 0 level of water) the resistance was in the range of 450 to 650 kΩ which can be considered as the air resistance for the particular distance monitored at the relative humidity of the lab. When water level reached level 1, all vertical resistances dropped down to the range between 80 and 120 kΩ. This sudden change clearly showed that the depth of water reached level 1.

When water reached level 2, all vertical resistance combinations observed a small reduction in their values. But sensors c1-c2 (resistance in c vertical line between level 1 and 2) observed dramatic change in the resistance and dropped down to about 1000 Ω from about 95 000

Ω. It showed that earlier air resistance was replaced by water resistance when water completed the circuit between level 1 and 2 while the others still experienced air resistance.

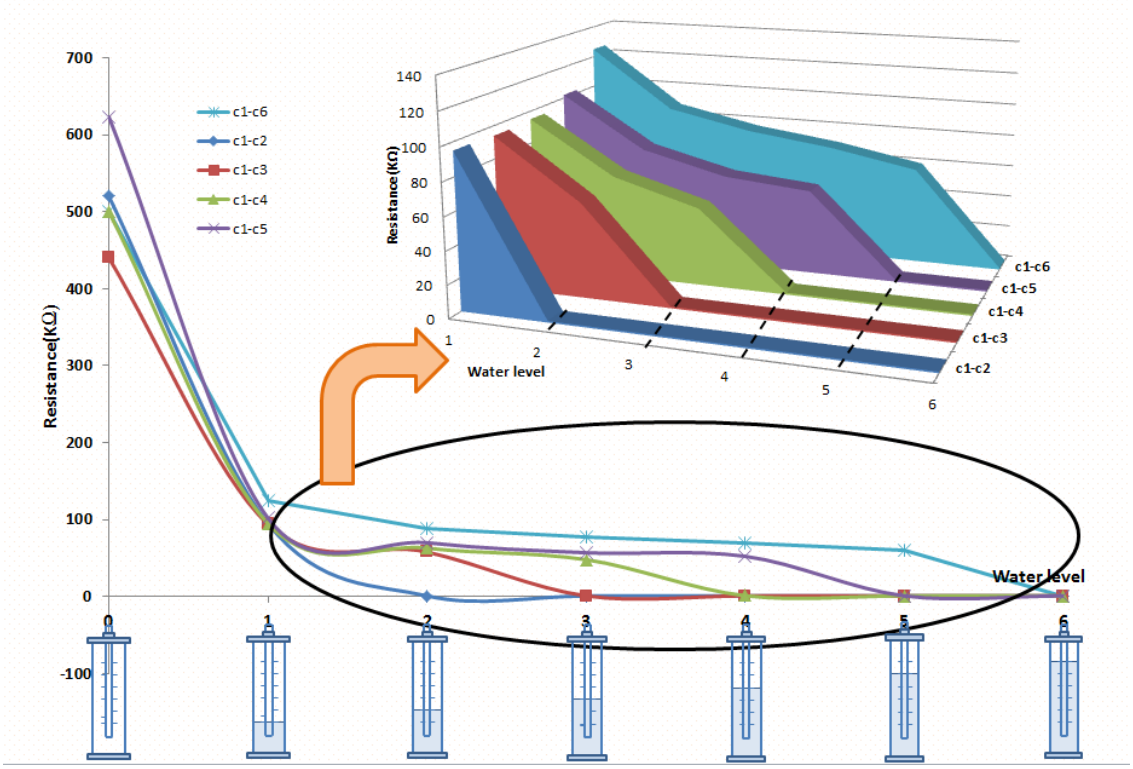

Figure 6-3: Vertical Resistance Measurements in the Oil Well Model 1

When water reached level 3, resistance between c1-c3 dropped down drastically as it happened to c1-c2 when water depth reached level 2. Same trend was observed for other combinations of sensors too, as shown in Figure 6-3. This consistent behavior showed that the depth of the drilling fluid can be monitored by measuring the resistance.

Continuous reduction in measured resistance was observed with increasing water level. When the water level was moving upwards, air was gradually replaced by water. Water has relatively lesser resistance than air. If water and air are assumed to be connected in series, the resulting resistance of water and air equivalent circuit should reduce when water level increases. Continuous reduction in resistance observed in the model when one sensor was in water and other

in air, supported this assumption. Dramatic drop in resistance was observed when the circuit was completed with water, replacing air.

Figure 6-4 shows the variation of resistance of horizontal level of sensors. When water reached each horizontal level, the resistance dropped from several hundred kΩ to few ohms. This sudden change in the resistance indicated the level of the water reached up to that particular level.

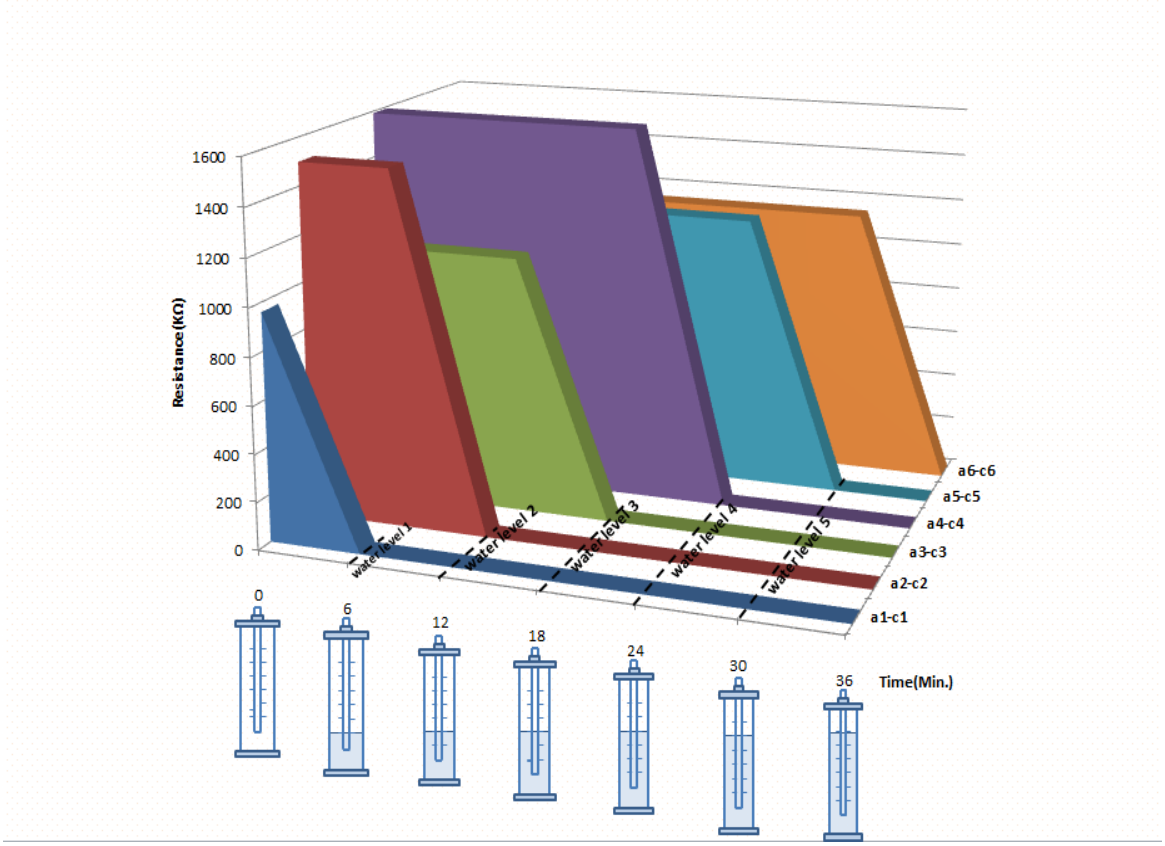

Figure 6-4: Variation of Horizontal Resistance with Depth of Water Level

Figure 6-5 illustrates variation of resistance with depth of water for horizontal levels monitored. When the water level reached each level, resistance for that level reduced suddenly. For example, resistance between sensors a3 and c3 (at horizontal level 3) reduced drastically when the water reached level 3.

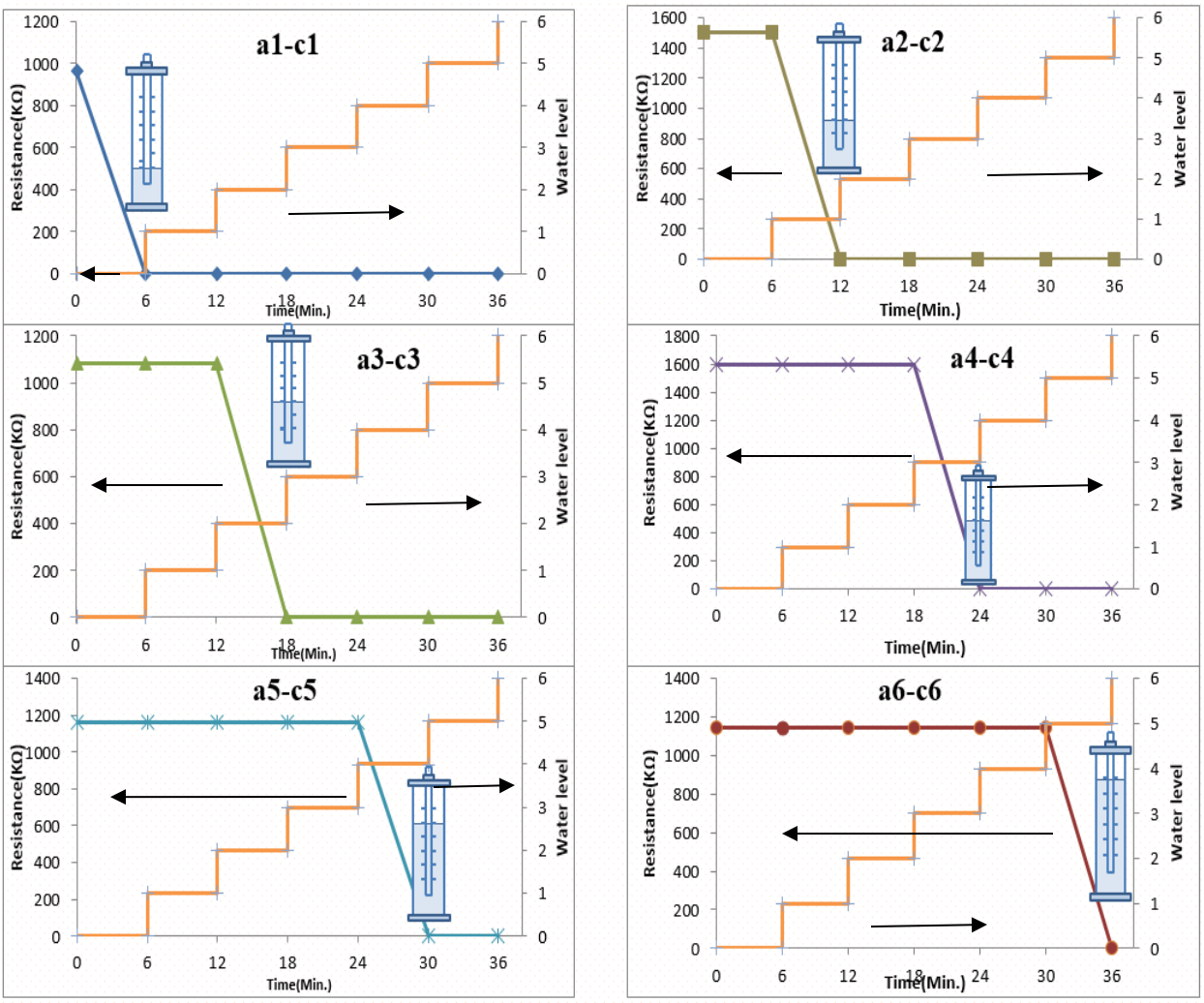

Figure 6-5: Variation of Resistance with Water Level

6.1.3 Monitoring the Depth of Cement Slurry

The same procedure was followed for cement as it was done for water. Variation of vertical resistance versus depth of the slurry is reported in Figure 6-6. A trend similar to drilling fluid (water) was observed. The similar trend proved that the level of the cement slurry or drilling fluid can be sensed using the method explained above by monitoring the resistance between two sensors.

In contrast to 1000 Ω resistance of the drilling mud (water) the range of resistance of cement slurry was between 20 to 50 Ω for the time interval monitored for the slurry with 0.8 water to cement ratio. This observation showed that the material in the annulus can be distinguished based on the resistance value while identifying the depth of the slurry.

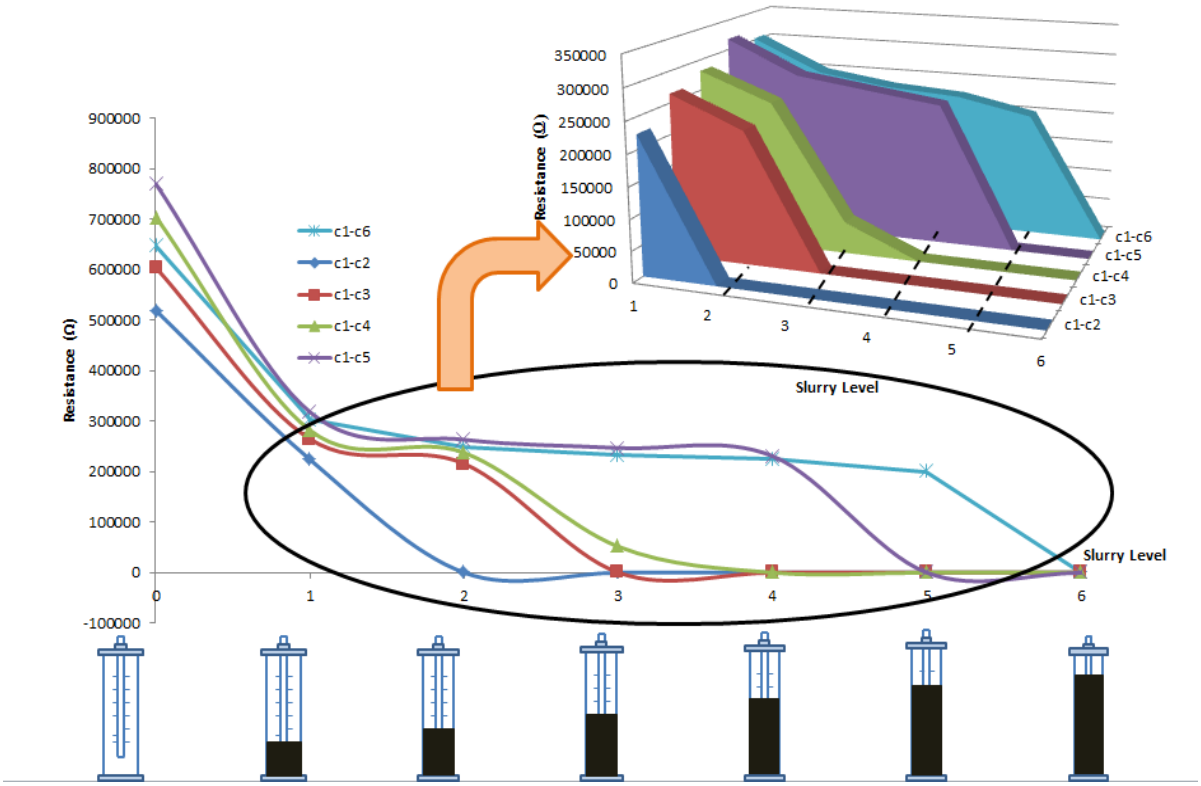

Figure 6-6: Variation of Vertical Resistance with Depth of Cement Slurry

Due to bleeding effect, free water accumulated above the cement or separated from cement with time as shown in Figure 6-7. This effect was exaggerated by using water to cement ratio 0.8, to study the sensing ability of resistance method in detecting the depth of the free water. Figure 7 shows that the monitoring method based on resistance clearly distinguishes between free water and cement. When water was used as drilling fluid, the water resistance was found to be in the range of 1000 Ω. But the resistance value of free water from cement slurry was in the range of 30 to 40 Ω because of the mixed ions from cement slurry.

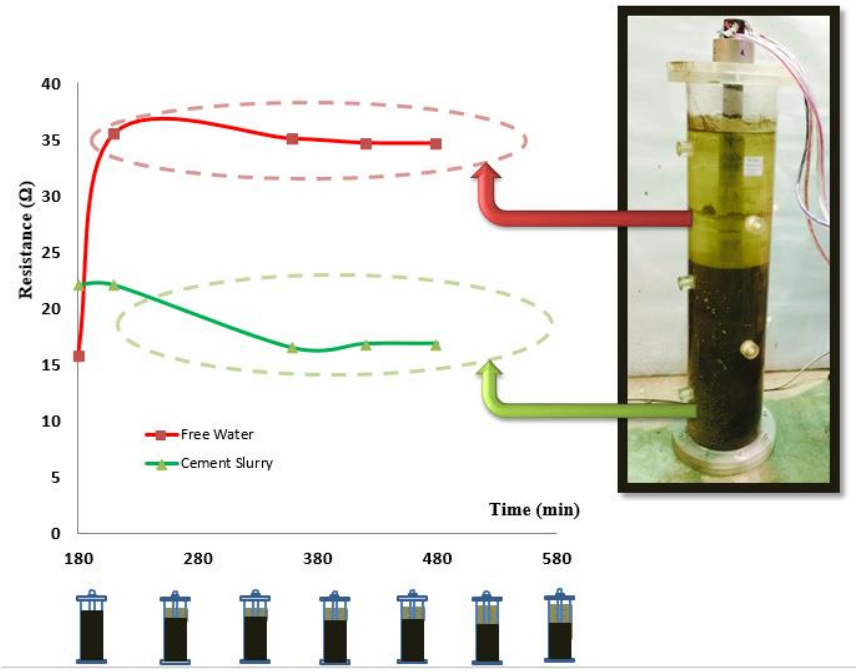

Figure 6-7: Resistance for Free Water and Cement Slurry

Resistance variation between horizontal sensors for cement slurry is reported in Figure 6-8, which shows similar pattern to horizontal monitoring for drilling mud. This observation again confirmed that the depth of drilling fluid or cement can be detected using resistance measurement.

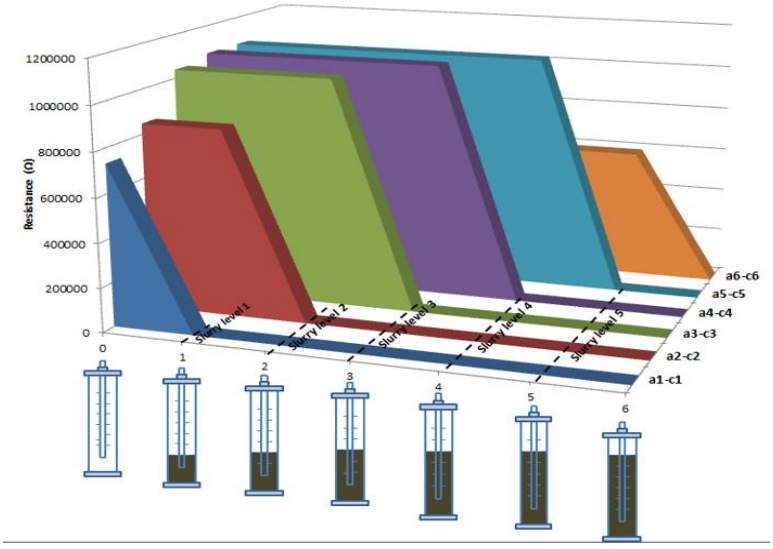

Figure 6-8: Horizontal Slurry Resistance with Slurry Level

Figure 6-9, shows the resistance variation of cement slurry with the depth of slurry being placed. The trends were similar to that of drilling fluid.

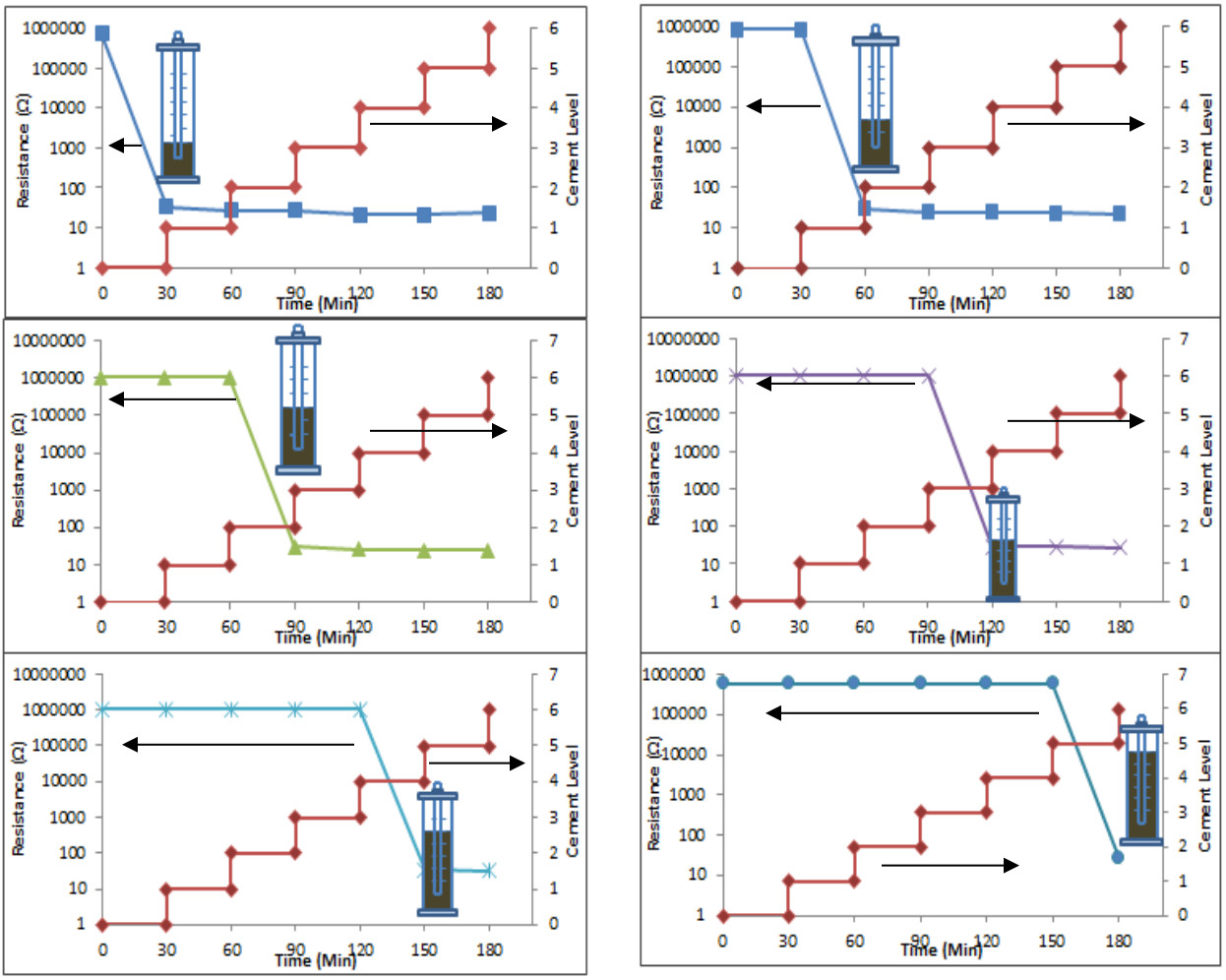

Figure 6-9: Variation of Horizontal Resistance Cement with Time and Slurry Level

6.2 Oil Well Model 2 (Oil Based Drilling Mud, Spacer and W/C: 0.38 Cement Slurry)

A similar model as model 1 was built to study the real time monitoring ability of resistance based sensing method in monitoring displacing drilling mud with spacer and spacer with cement slurry. Instead of six sensors used in last time, seven levels of sensors were used in model 2.

The vertical electrical resistance sensors were named with a, b, c and d. Horizontal levels were named 1 to 7. The distance between two vertical sensors was 4 inches. Different combinations of the sensors were connected to a 300 kHz LCR device to measure the resistance.

Oil based mud was prepared by mixing mineral oil, water and cetyltrimethylammonium bromide (CTAB) surfactant together. The ratio of oil to water ratio was 4: 1. Firstly, 1% of CTAB surfactant was mixed slowly with water and then oil was added gradually to the water and surfactant solution. The density of the oil based mud was 0.86 kg/l (7.2 ppg) and the resistivity was 110Ω.m.

The spacer fluid was prepared by mixing 0.5% Guar gum, 0.4% Bio-Surfactant and 3% KCl. The density of the spacer fluid was about 1 g/cc. Oil well cement class H was used with a water to cement ratio 0.38. The cement was modified with an addition of 0.075% carbon fiber by total weight.

6.2.1 Placement of Cement in the annulus by displacing preexisting fluids

Oil based mud of about 10 l volume was first filled in the annulus of oil well model gradually. While the level of the mud raises from the bottom the well towards upwards, resistance between different combinations of sensors was monitored real time.

Then spacer fluid of about 10 l volume was filled in the pressurizing chamber and pressurized to about 20 psi to fill the model by displacing the pre-existed oil based mud as shown in Figure 6-10. Similar procedure was adopted for spacer fluid as before to measure the resistance when the spacer fluid reached each level.

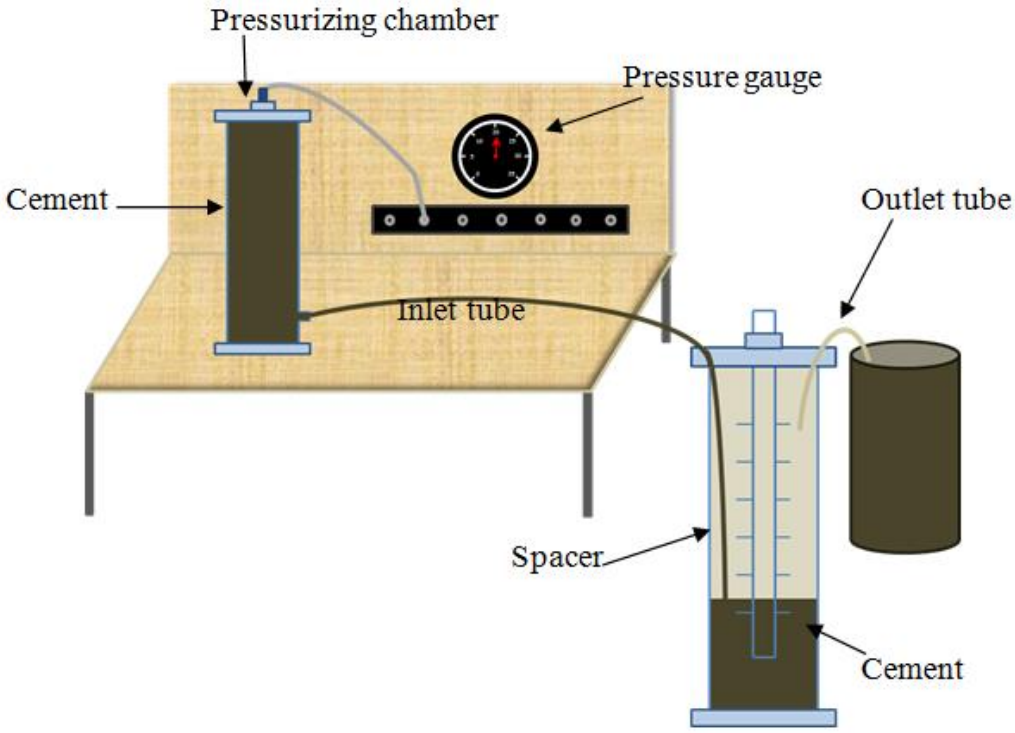

Figure 6-10: Experimental Setup of Oil Well Model 2

After measuring the resistance of spacer for all seven levels, cement slurry was filled in the chamber and pressurized to displace the spacer fluid which pre-existed in the oil well model. Similar procedure was followed as before to measure the resistance.

6.2.2 Monitoring the Placement of Oil Based Drilling Fluid

Resistance measured for different vertical levels of well is shown in Figure 6-11 with depth of oil based mud. When there was no fluid in the well (at 0 level of oil based mud) the resistance was in the range of 155 to 205 kΩ which can be considered as the air resistance for the particular distance monitored at the relative humidity of the lab. When oil based mud level reached level 1, all the vertical resistances dropped down to 35 to 60 kΩ range. This sudden change clearly shows that oil based mud reached level 1.

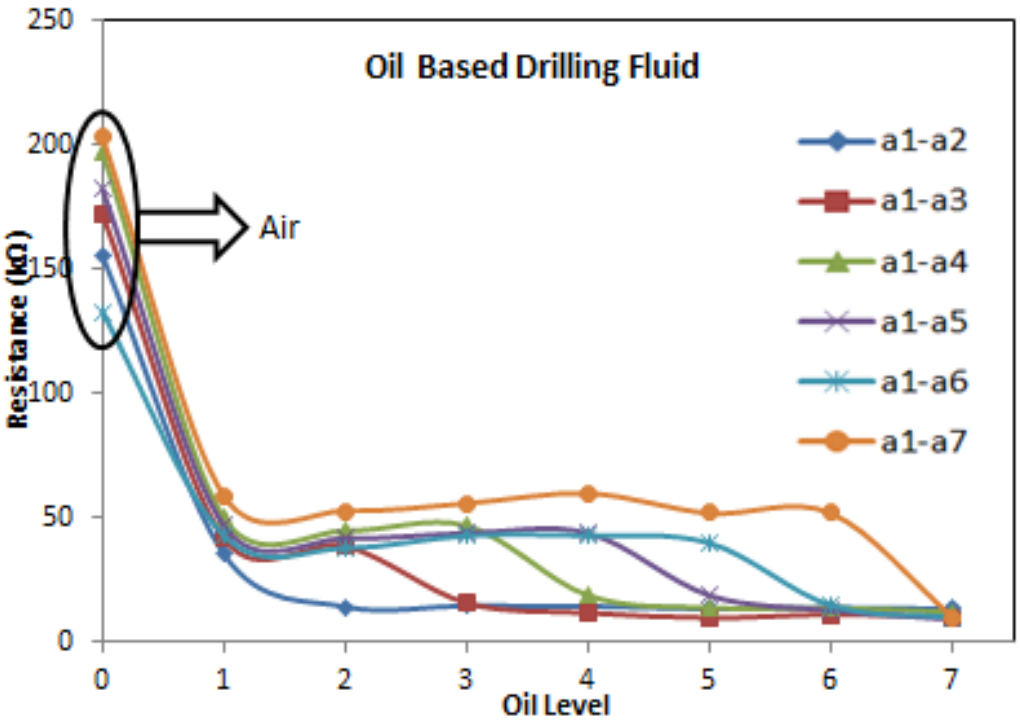

Figure 6-11: Variation of Vertical Resistance with Mud Depth for the Oil Based Mud

When oil based mud reached level 2, all vertical resistance combinations observed a small reduction in their values. But sensors a1-a2 (resistance in 'a' vertical line and between level 1 and 2) observed drastic change in the resistance. It dropped down to about 14 kΩ from about 36 kΩ. Drastic change happened because the air resistance between the two sensors was replaced by resistance of drilling mud when drilling mud completes the circuit between level 1 and 2 while the others still experience air resistance.

When mud reached level 3, resistance between a1-a3 dropped down drastically. The same pattern was observed for other set of readings too. This consistent pattern showed that the level of the drilling fluid can be monitored effectively by measuring the resistance. The trend was very similar to the first model.

6.2.3 Displacing Oil based mud by Spacer Fluid

Figure 6-12 shows the change of resistance with depth of spacer when spacer displaced drilling mud. Earlier it was full with drilling mud.

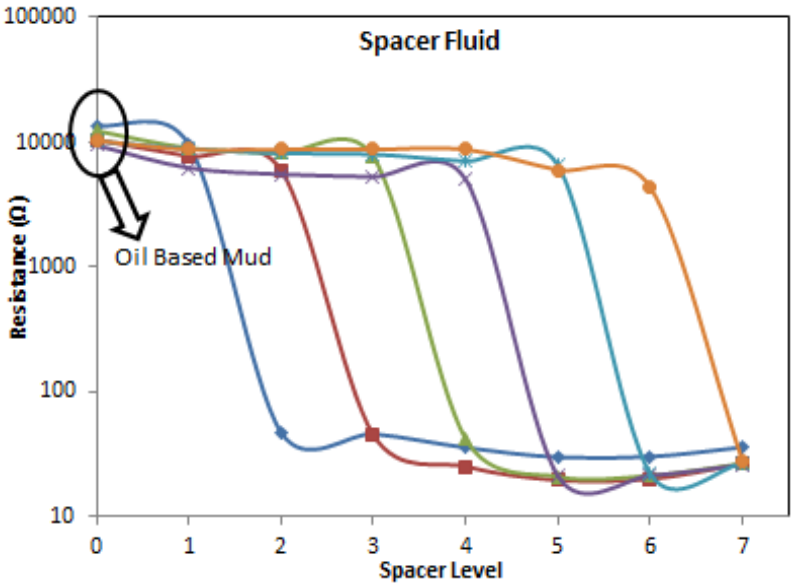

Figure 6-12: Change of Vertical Resistance with Depth of Spacer Fluid

When there was no spacer in the annulus of the well model, sensors measured the resistance of the oil based mud. While each level was displaced by spacer, resistance between corresponding sensors showed sudden change. This pattern again validated the previously observed pattern in detecting the level of the fluid. After the total depth of the well was displaced by spacer fluid, resistance reached the value of 25 to 35 Ω, which was the resistance of spacer.

6.2.4 Displacing spacer fluid by Cement Slurry

After filling up the well model totally with spacer fluid, spacer was displaced by cement slurry. Similar procedure as before was followed to monitor the depth of cement slurry. Figure 6-13 shows the resistance change with depth of cement slurry.

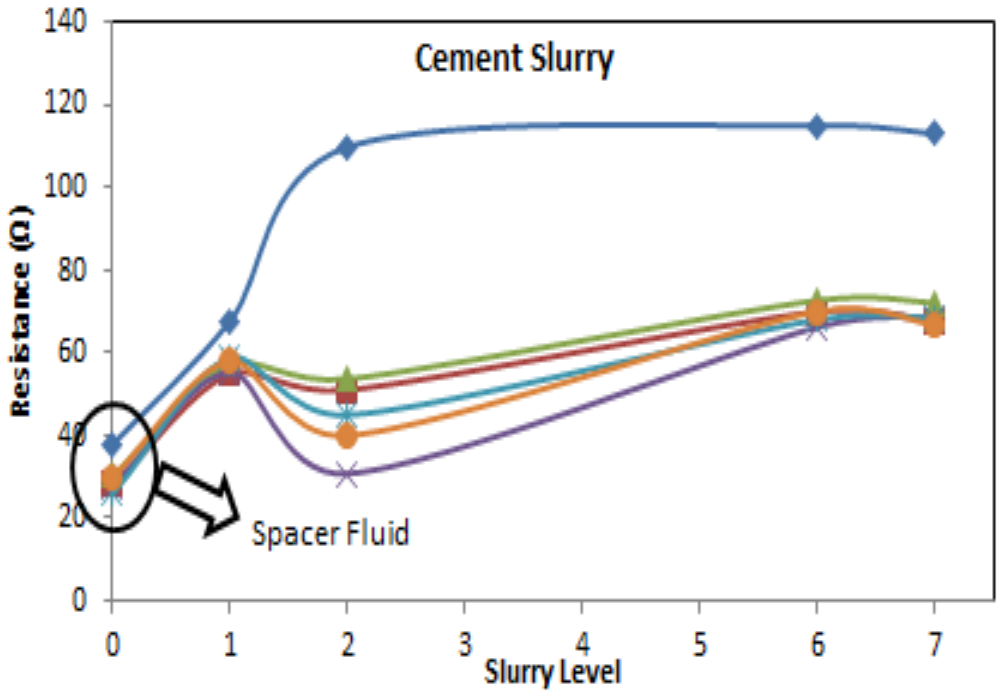

Figure 6-13: Vertical Resistance Measurements for Cement Slurry

When there was no cement slurry in the well (at 0 level of water) the resistance was in the range of 25 to 35 Ω which was the resistance of spacer. When cement slurry reached level 1, all the vertical resistances increased to 55 to 67 Ω range. This sudden change clearly showed that cement slurry reached level 1. The increase happened because the resistivity of the cement is higher than that of spacer fluid.

In the process of displacing spacer, cement got contaminated with spacer and therefor the following resistance values dropped to 30 to 50 Ω from 55 to 67 Ω. Contamination did not happen in the bottom level which is far away from the spacer level and it reflects in the result. Because of the hydration process, again the values started increasing as the resistivity of the cement increases with time. The above observation shows that, the contamination of cement slurry could be detected from resistance measurement method.

6.2.5 Continuous Monitoring of the Fluids used in the Model

Figure 6-14 shows the resistance change with time in the well for different types of the fluids used. Air resistance dropped to oil based drilling mud's resistance followed by resistance of spacer fluid and cement slurry. The variation of resistance with time clearly showed that the level of the slurry can be monitored by measuring the resistance.

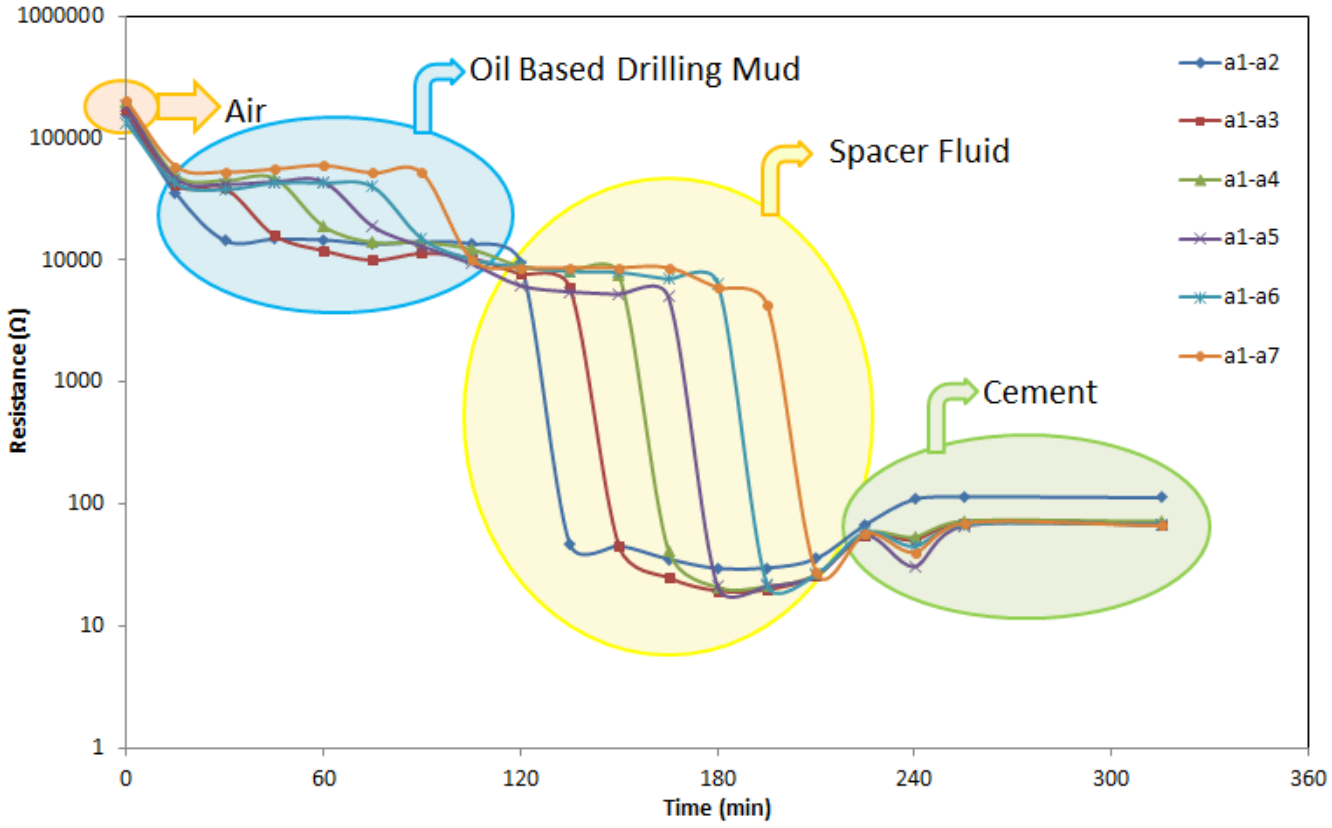

Figure 6-14: Vertical Resistance Measurements in the Oil Well Model

Figure 6-15(a) shows the resistance of the bottom sensors a1-a2 and Figure 6-15(b) shows the resistance of the top sensors a1-a7 while Figure 6-15(c) combines both of them. Because the bottom level sensors were filled with the fluid earlier than the top level sensors, the change of resistance of bottom level sensors happened before top level sensors.

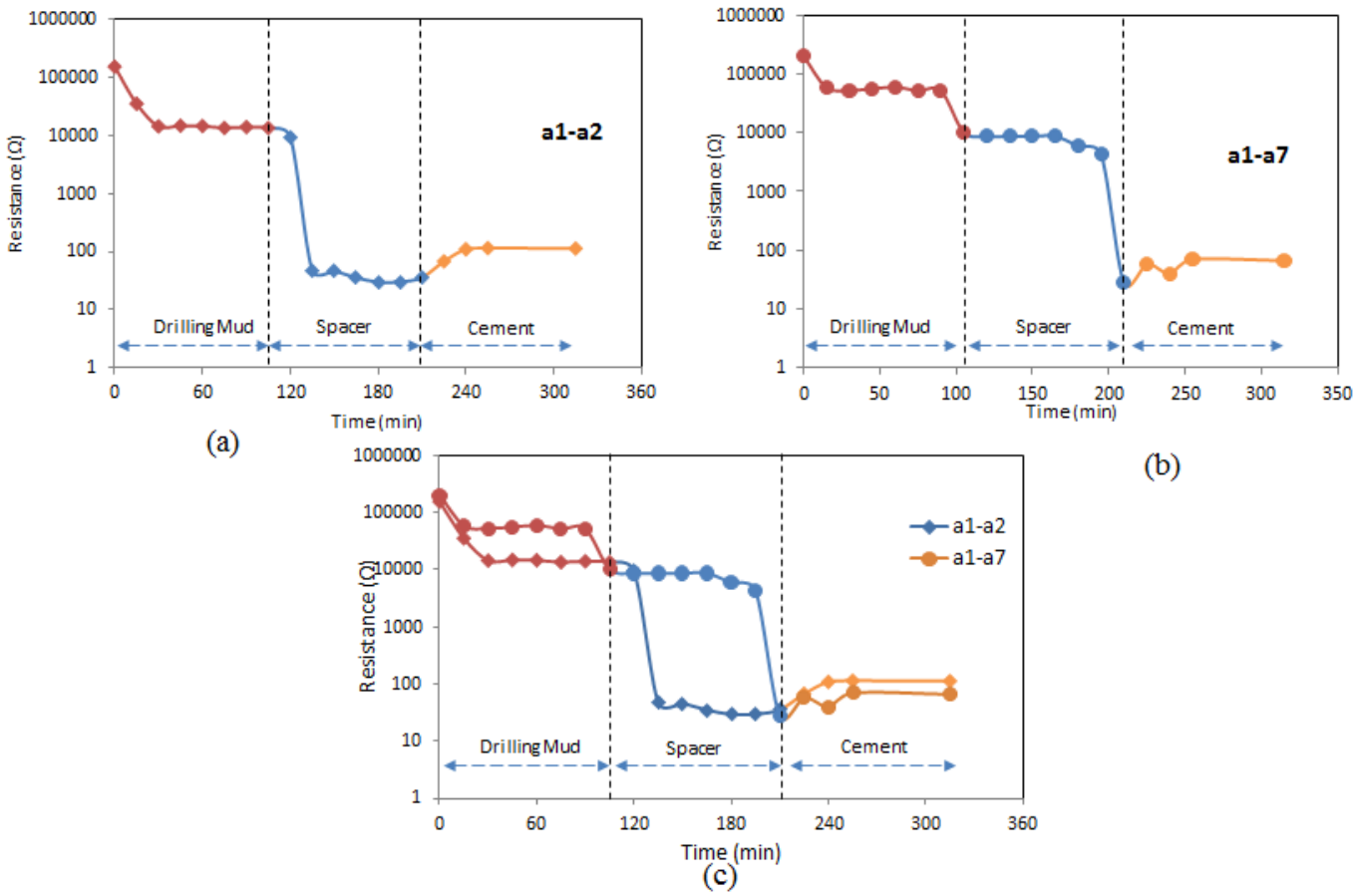

Figure 6-15: Resistance Change with Time for Selected Combinations of Sensors

Model 2 was useful in monitoring displacement of fluids by consequent fluids and contamination of cement slurry. It detected well the levels of different slurries.

6.3 Model 3 (Calibrated sensors with water and cement slurry, w/c: 0.38)

Model 3 was experimented in two steps, first step was to calibrate the sensors system and the second step was actual placement of cement in the annulus. Similar to previous well models, model 3 was built using a transparent mold, metal casing and a modified sensing system.

Previously the sensing system was connected to the steel casing. That could inter the operations in the field. Therefore model 3 sensing system was modified to have a separate sensing system with a steel angle.

The distance between two sensors was 6 inches and there were 5 levels of sensors. As opposed to previous models discussed, model 3 was instrumented with six lines of vertical sensors and the sensors were named with the letters a, b, c, d, e and f instead of four lines of vertical sensors. Horizontal levels were named 1 to 5.

Similar to previous models, different combinations of the sensors were connected to a 300 Hz LCR device to measure resistance between those sensors. Same amount of oil well cement class H slurry was used with a water to cement ratio of 0.38. The cement was modified with an addition of 0.075% Carbon fiber by total weight.

6.3.1 Calibration of the Sensing System

Sensing system was Calibrated in two steps one with water and then with cement slurry of w/c ratio 0.38. Carbon fiber also was added.

The modified sensing system was immersed in water and cement slurry separately and resistance was measured between different combinations of sensors. Resistivity of the water and cement slurry was measured using resistivity meter. Using Equation 6-1, k-factors for each sensor combinations were calculated

$$k = R / \rho, \qquad 6\text{-}1$$

where R refers to resistance between two sensors and ρ is resistivity.

Figure 6-16 shows the k-factor variation for 6 inch distance between sensors. It varied between 73 to 144 m-1 for water and 51 to 92 m-1 for cement. The mean value for water was 108 m-1 and for cement 69 m-1.

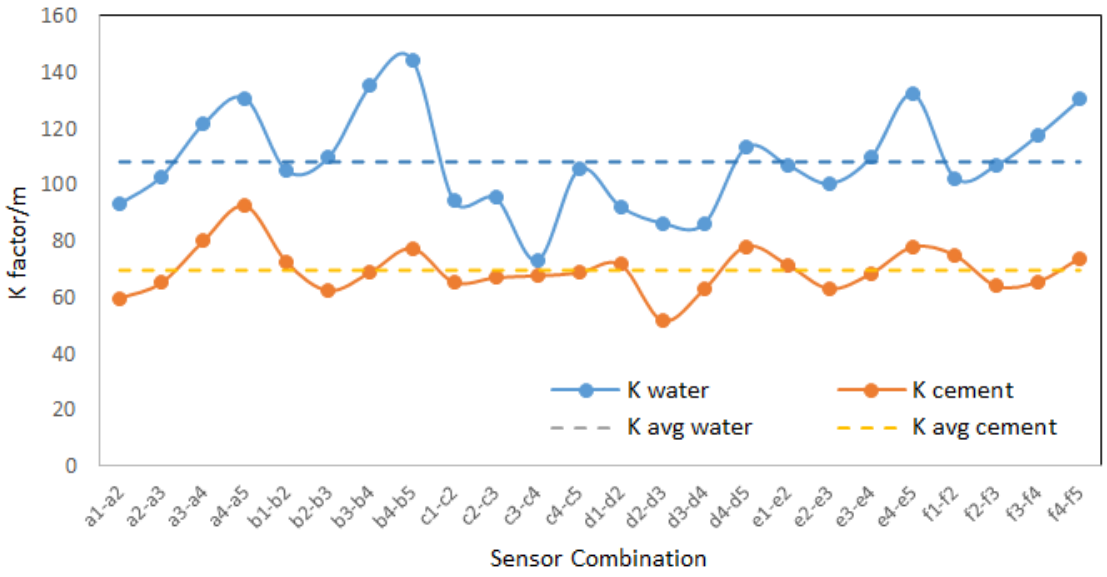

Figure 6-16: K-Factor Variation for 6 Inch Distance between Sensors

Figure 6-17 shows the k-factor variation for 12, 18 and 24 inch distance between sensors.

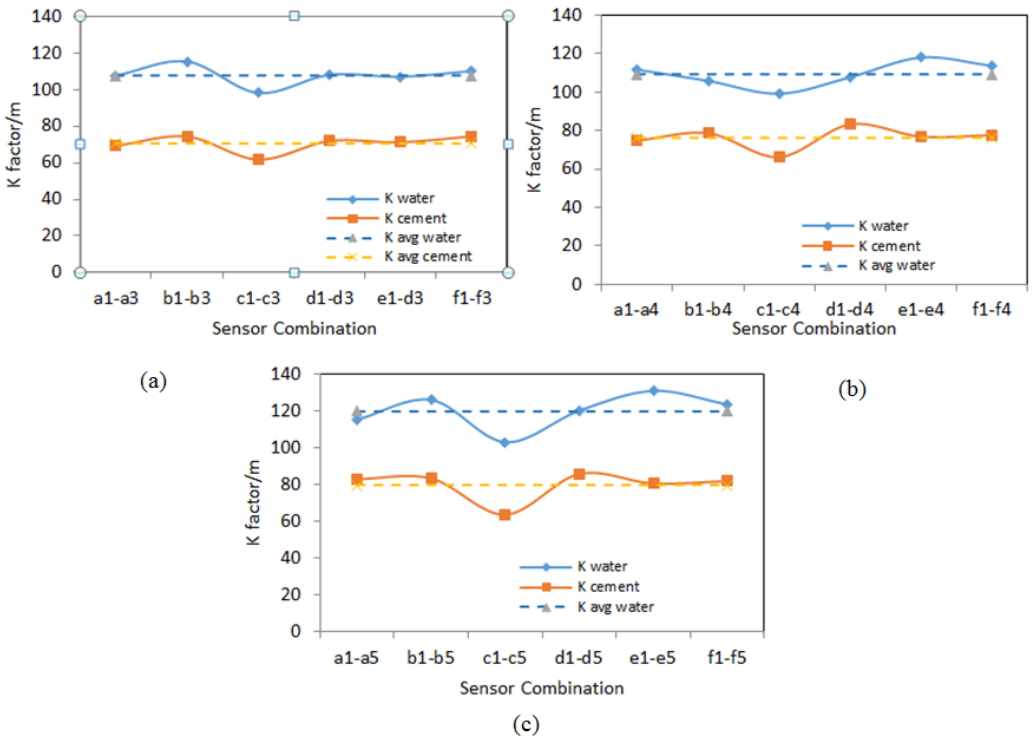

Figure 6-17: K-Factor for (A) 12 Inch (B) 18 Inch (C) 24 Inch Distance between Sensors

Figure 6-18 shows the k-factor variation for water and cement slurry with distance between sensors. The mean k-factor value of the water found to be higher than that of cement slurry in all cases.

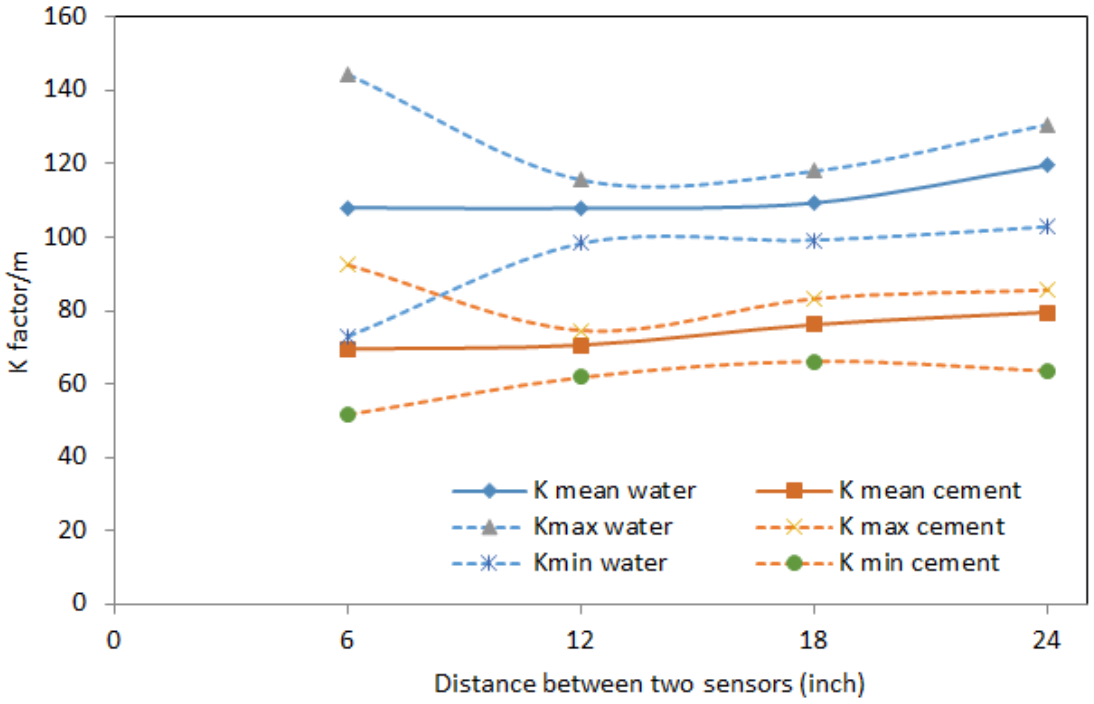

Figure 6-18: K-Factor Variation with Distance between Sensors

Table 6-1 summarizes the result for k-factor values for water and cement. The k-factor ratio between water and cement was about 1.5.

Table 6-1: K-Factor Values for Water and Cement

Distance (in)	K mean water (m)	K mean cement (m)	Kwater/Kcement
6	108.10	69.59	1.55
12	107.94	70.61	1.53
18	109.38	76.25	1.43
24	119.68	79.58	1.50

6.3.2 Actual Placement of Cement Sheath in the Annulus

Spacers were used to keep sensing system centered in the annulus of the well model. Then cement was placed in the annulus from the bottom of the model using a tube. The electrical resistance was measured as it was done in the previous cases.

From the calibration, the approximate resistance values for each combination of sensors were predicted before starting the actual placement of the cement in the annulus. The predicted resistance values were compared with the measured values. The predicted and measured values for sensors between level 1 and 2 are shown in Figure 6-19.

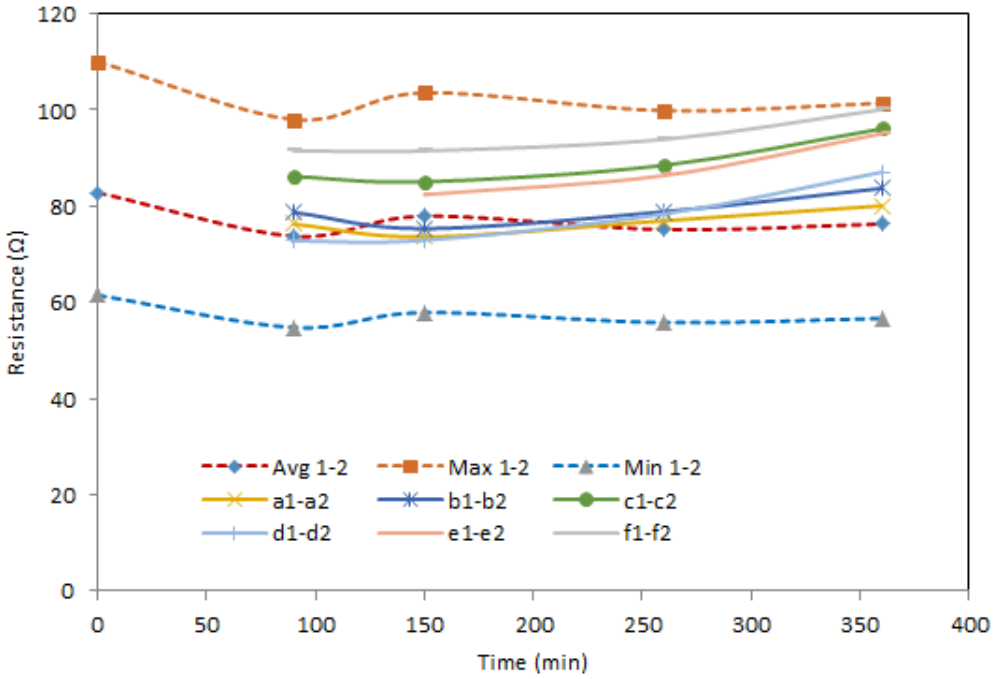

Figure 6-19: Variation of Predicted and Measured Resistance with Time

All the measured valued fell between the predicted maximum and minimum values and more close to the mean values. It shows the reliability of the calibration and any values falls apart the predicted region will indicate any defaults in the cementing procedure such as voids, early hardening due to high temperature, water loss.

Summary

Based on the experimental model study on determining the movement of drilling fluid, spacer fluid and cement slurry, following observations are advanced.

1. Measuring the change in the resistance with depth in the model borehole, it was possible to determine the movement of the drilling fluid, spacer fluid and cement slurry.
2. As the fluid reached a particular level, the corresponding vertical and horizontal resistance changed to indicate the arrival of the fluid to that level. Resistance of drilling mud was the highest followed by cement slurry and spacer fluid.

CHAPTER 7 PIEZORESISTIVE REPAIR MATERIAL FOR DAMAGED OIL WELL CEMENT SHEATH

This chapter describes about repairing damaged oil well cement using a piezoresistive material which helps to regain both the strength and piezoresistivity of the cement sheath, if the sheath had piezoresistive characteristics before the occurrence of the damage. Used materials, methods of repairing are outlined.

7.1 Importance of Repairing Damaged Oil Well Cement Sheath

As reported in Chapter 2, average life of an oil well is above 20 to 30 years. Within this long duration maintenance and repair is necessary to make sure the integrity of the cement sheath holding the casing to the formation.

Improper placement of cement, stress conditions in the wellbore due to operation and maintenance, stresses brought on by temperature and pressure cycling are some of the reasons for failure of cement sheath. When cement sheath loses its integrity, due to loss of zonal isolation, other formation fluids enter the annulus. It also possibly causes unwanted water production reduces the economic benefits of the well.

7.2 Materials and Methods

Considering cost, safety and regaining the strength at high pressure - high temperature conditions in the well, cementitious material can be a better repair material compared to epoxy resins, chemical gels, and silicate materials (Peter White, Prentice et al., 1997). For successful repair, repair material need to deep penetrate into the fracture. Hence, small-particle-size cement can be used as repair material. Since ultrafine cement contains very fine particles, it is capable of invading narrow openings that other standard cement cannot access. Ultrafine cement is defined

as d95 < 10 microns which is very smaller compared to Type I Portland cement of 70 microns and Blaine fineness of at least 900 m^2/kg.

Ultrafine cement was used as the repair material. To allow deep penetration into cracks, water to cement ratio was selected to be 0.6. To enhance piezoresistive behavior 0.075% carbon fiber was added to ultrafine cement. By conducting Vicat needle test, the setting time of the ultrafine cement slurry with added carbon fiber was found to be 8 hours.

Accelerating the setting time would help in rapid repairing. However, there should be enough time for the pumping and other process of repair. Addition of 5% Sodium Alumino Silicate reduced the time lap between initial and final setting times. Initial setting time of the slurry with the addition of Sodium Alumino Silicate to the above slurry was found to be about 4.5 hours and final setting time was found to be 5 hours.

To characterize the repair material during curing, resistivity was tested for about three hours. Figure 7-1 shows the change of resistivity with time.

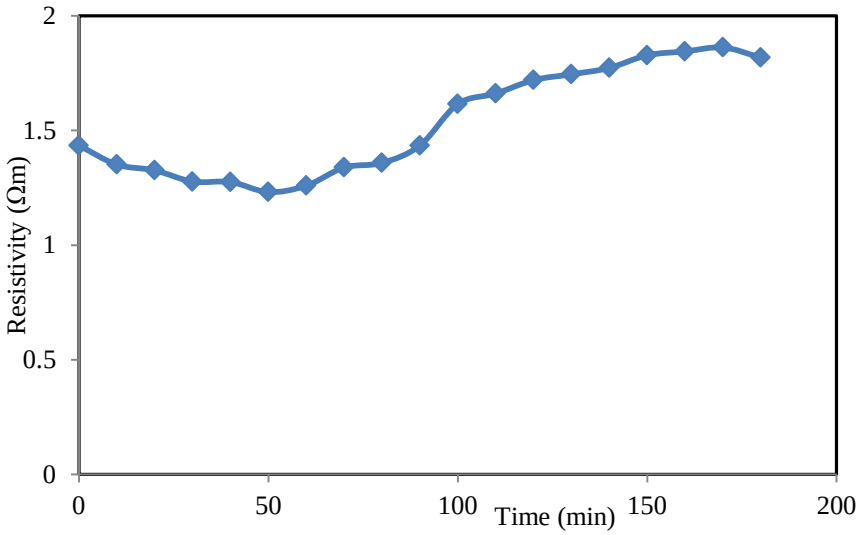

Figure 7-1: Change of Resistivity with Time

Figure 7-2 shows the variation of stress with piezoresistivity of specimen cured for 14 days in the atmospheric conditions. Specimens showed piezoresistivity above 300%.

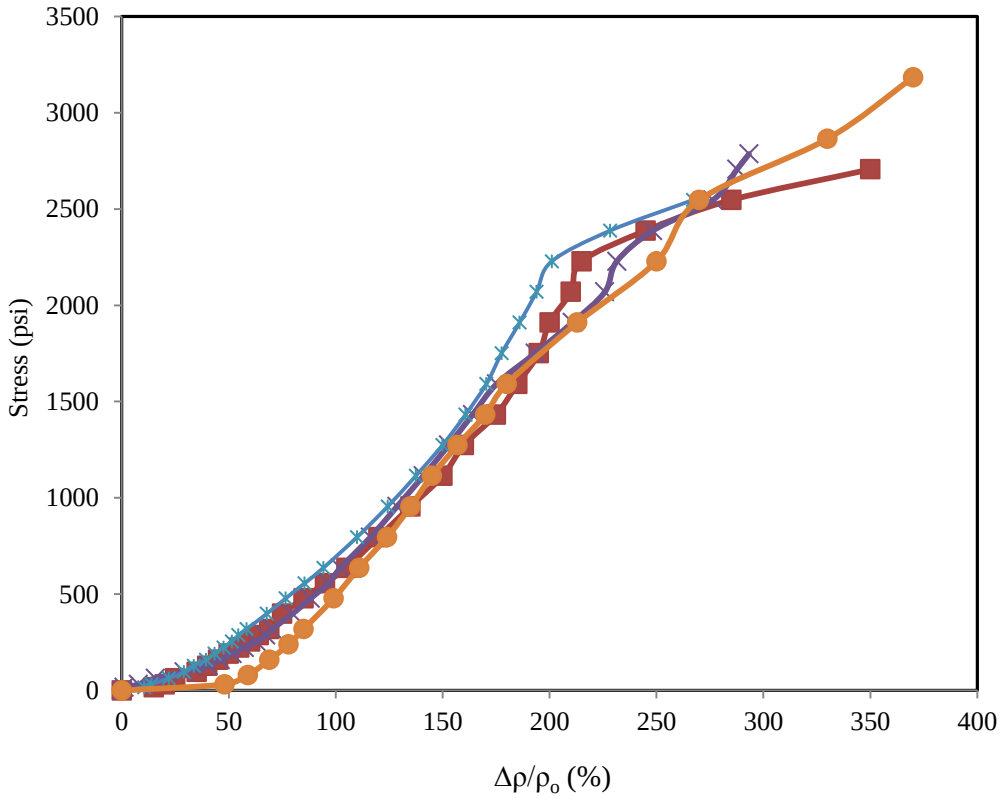

Figure 7-2: Piezoresistive Behavior of Repair Material Cured for 14 Days

Two-probe method with 300 kHz AC LCR device was used to measure piezoresistive behavior. Hollow specimen and beam specimen were repaired in this study.

7.3 Repairing Hollow Specimen

Modified class H oil well cement was used to prepare cylindrical hollow specimens of 2x4" (outer diameter 2" and inner diameter 0.75") with a water:cement ratio 0.4 by weight as shown in Figure 7-3(a). After hardening 3mm crack was made in between the sensing points as shown in Figure 7-3(b). The crack was deep enough to access through the hollow. The repair material was pressurized through the hollow and allowed to squeeze out through the crack so that it fills the crack. Figure 7-3(c) shows repaired sample.

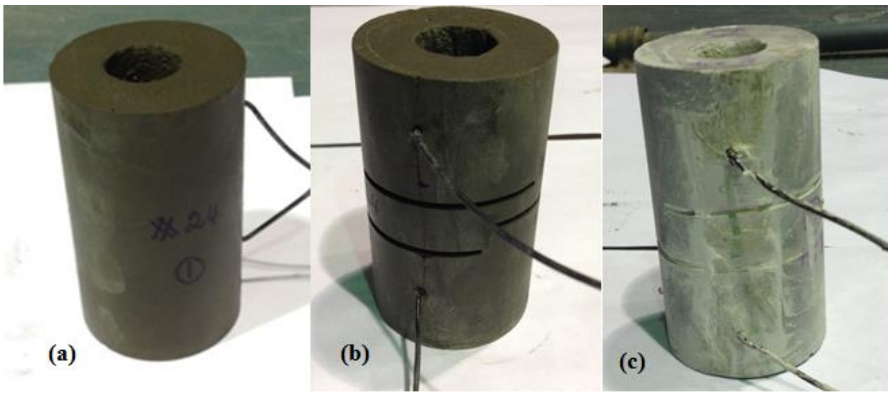

Figure 7-3: (a) Initial Specimen (b) Damaged Specimen (c) Repaired Specimen

To find out the strength and piezoresistivity of the specimen before damage, initial specimen was tested for compressive strength after 7 days of air curing. The piezoresistive behaviors reported in Chapter 4 are different from these values because of the different curing conditions. The same test was conducted on similar ultrafine cement hollow specimen and repaired specimen after 5 days of curing.

Immediately after the crack formation, relative resistivity increased by 65%. It showed the formation of the crack was sensed by the resistivity change. Figure 7-4 shows strength and piezoresistive behavior of initial oil well cement, ultrafine cement and repaired sample.

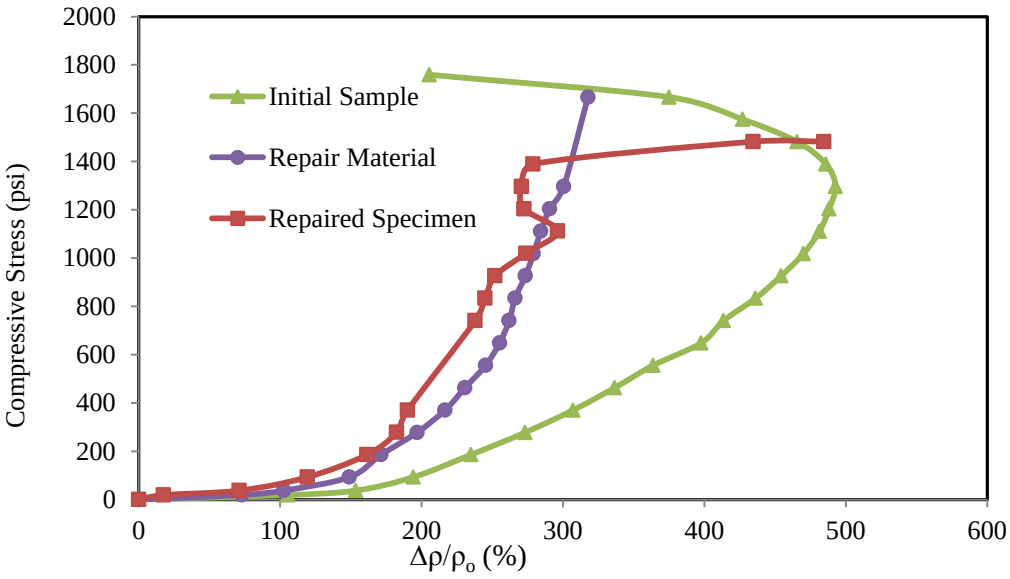

Figure 7-4: Effectiveness of Repair Method

Initial specimen showed about 500% of change in resistivity under atmospheric curing conditions, repair material showed about 300% of piezoresistivity under atmospheric curing conditions. Repaired specimen also regained piezo resistivity about 300% before failure. Also above 85% of the strength was regained through this method of repair.

7.4 Repairing broken beam Specimen

Modified class H oil well cement was used to prepare beam specimen of 11 x 3 x 3 inch with water:cement ratio 0.4 by weight. After 2 months of air curing, initial specimen was tested for three point load flexural strength shown in Figure 7-5(a). Figure 7-5(b) shows the initial specimen after failure. Figure 7-5(c) shows the specimen after repairing using modified ultrafine cement. 3 days after the repair it was again tested and is shown in Figure 7-5(d) after test. It was noted that, the repaired specimen failed not in the repaired location which shows the effectiveness of the repair.

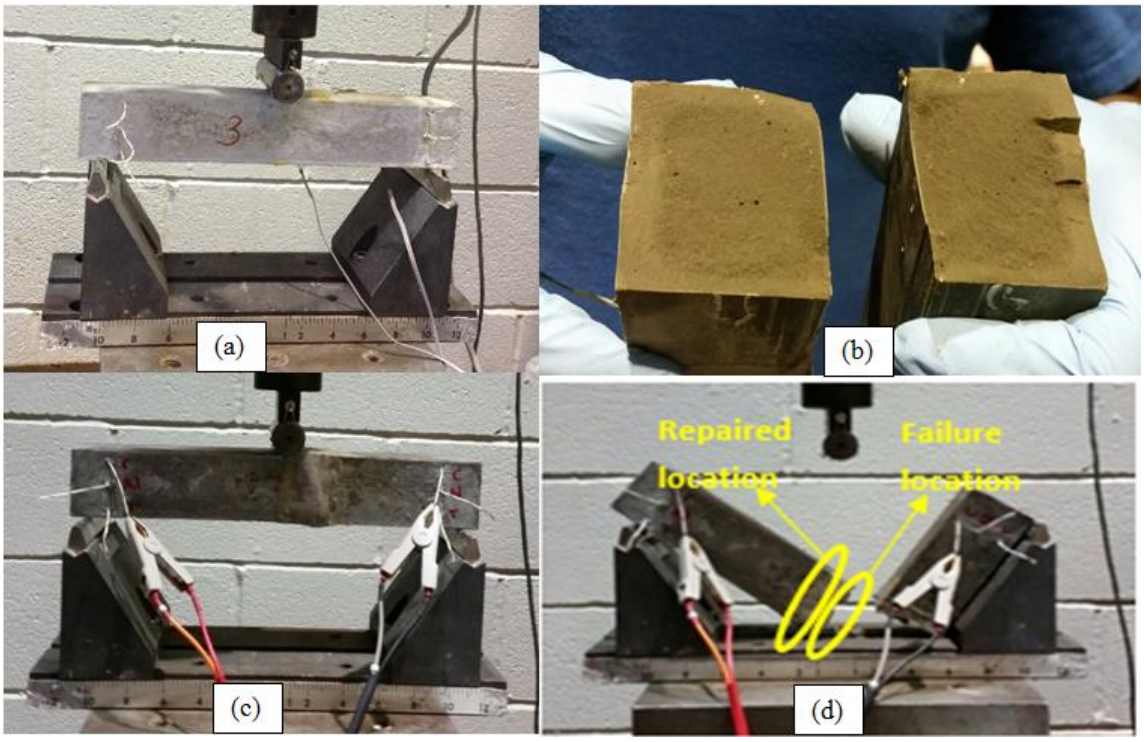

Figure 7-5: The Process of Beam Specimen Repair

Stress strain curve of the initial sample is shown in Figure 7-6, which shows the flexural strength of the initial sample to be 255 psi. Initial specimen showed maximum piezoresistivity of 60% while the corresponding failure strain was about 0.0003 which makes the self-sensing ability of the cement promising. The repaired sample showed above 125% piezoresistivity.

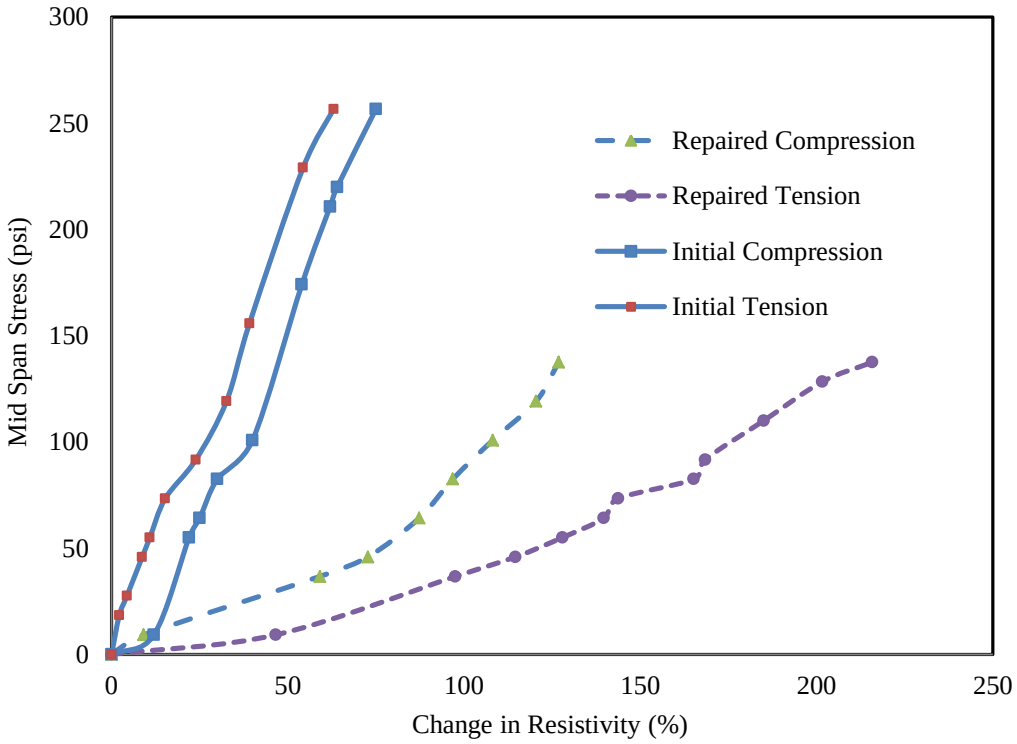

Figure 7-6: Tensile and Compressive Piezoresistivity of Initial and Repaired Beam

Initial resistance between the sensors was 22 kΩ for initial sample and 6 kΩ for repaired sample. The drop in initial resistance and increased in sensitivity before and after repair was because the cracked surface was soaked into water before repair and the repaired sample was cured in relative humidity 95%. Curing condition increased the piezoresistivity also.

Repaired specimen showed more than 75% of strength regaining and it recovered self-sensing ability. This repair method was found to be effective in regaining both strength and piezoresistivity.

Summary

1. Ultrafine cement modified with carbon fiber and Sodium Alumino Silicate with water to cement ratio of 0.6 was used to repaire hollow specimen and beam specimen.
2. Repaired hollow specimen showed 85% strength regaining. It regained piezoresistive behavior also.
3. Repaired beam specimen regained 75% strength and also piezoresistive behavior.

CHAPTER 8 CONCLUSIONS AND RECOMMENDATIONS

8.1 Conclusions

This study focused on characterizing the mechanical properties and piezoresistive behavior of different classes of modified oil well cements. API oil well Portland cement classification of class A (ASTM classification of type I Ordinary Portland Cement), class G and class H cements were studied. Fracture properties were studied and correlated with piezoresistive behavior. An innovative real time monitoring system was proposed to monitor the behavior of the cement sheath from the time of cement placement in the annulus to monitor the placement of slurry (drilling fluid, spacer and cement slurry) level and stress conditions. Based on the study, following conclusions can be advanced.

1. An addition of small amount of carbon fiber to oil well cement made it smart self-sensing piezoresistive material.
2. An indirect method of measuring the resistivity of hardened oil well cement was discussed. Resistivity of the tested oil well cement specimen increased from 1Ω.m to 35 Ω.m in 28 days in a decreasing rate.
3. Shrinkage of the class H cement about 8% while class G cement was about 3% under the tested conditions
4. Impedance characterization of different classes of smart oil well cement used in this study identified them as special bulk material (resistance only) at the tested curing times.
5. Impedance characterization of smart oil well cements used in this study proved that using high frequency AC current for piezoresistive studies has its advantage of avoiding the contact resistance and measures only the resistance of the bulk material which is the concern of the piezoresistive studies.

6. Different types of oil well cements tested in this study showed compressive strength between 5300 to 7100 psi, elastic modulus between 2,732,000 to 3,500,000 psi and poision ratio between 0.15 to 0.2.
7. Tensile strength of the tested cement specimen varied between 230 to 285 psi while flexural strength varied between 385 to 430 psi.
8. Compressive piezoresistance varied between 130 – 250 % while tensile piezoresistance varied between 85 – 240 %. Sett's piezoresistive analytical model predicted the piezoresistive behavior well.
9. P-q model predicted the stress strain variation of different oil well cements tested.
10. Fracture studies revealed the KI values to vary between 0.3 to 0.6 MPa.√m and CMOD between 2 to 6 µm.
11. The proposed real time monitoring of oil well model successfully monitored the slurry level and distinguished between oil based drilling fluid, spacer and cement slurry. It identified the contamination of spacer fluid in cement slurry.
12. The measured values of resistance in oil well model matched the predicted resistance which showed the well condition is good for the monitored period.

8.2 Recommendations

Based on the study conducted the following recommendations are proposed which may enhance the future research on this topic and make it more applicable.

1. Proposed resistance and resistivity based cement sheath monitoring system worked well in lab scale model. The same test should be conducted in the field to ensure the effectiveness in monitoring the method.
2. More studies should be conducted under high pressure, high temperature conditions to stimulate the wellbore conditions.

3. Possible contaminants should be studied with different percentages of contaminations and a relationship should be get for percentage of contamination to observed resistance (or resistivity) from which the percentage of contamination could be predicted.
4. The lab scale oil well models can be pressure tested and the stress levels can be estimated from piezoresistivity. Analytical and numerical methods can be used to calculate the stress levels at observed locations and experimental results can be verified.
5. The lab models of oil well can be tested to see the effect of different contaminants such as acids and oil.
6. After the pressure test on lab scale models any possible cracks can be repaired using the proposed repair material to check the efficiency in term of regaining the strength and piezoresistivity.

REFERENCES

ASTM (2012), “Standard Specification for Portland Cement”

ASTM, (2014). “Standard Test Method for Flexural Strength of Concrete (Using Simple Beam with Center-Point Loading)”

Benjamin Lee Weideman, (2014). “Investigation of Cased Wellbore Integrity in the Wabamun Area Sequestration Project,” Thesis, Master of Science in Petroleum Engineering, Missouri University of Science and Technology

Benjamin Weideman and Runar Nygaard (2014), “How Cement Operations Affect Your Cement Sheath Short and Long Term Integrity,” American Association of Drilling Engineers

Bernard Piot, (2007). “Cement and Cementing: An Old Technique with a Future,” Society of Petroleum Engineers, Distinguished Lecturer Program, www.spe.org/dl

Blacke, K.R., Llle, O. B. and Lyomov, S.K., (2001). “Characterizing Curing Cement Slurries by Electrical Conductivity”, Society of Petroleum Engineers, SPE 46216

Boukhelifa. L., Moroni. N., James. S. G., Le Roy Delage. S., Thiercelin. M. J., and Lemaire. G., (2004). “evaluation of cement systems for oil and gas well zonal isolation in full scale annular geometry,” IADC/SPE Drilling Conference, IADC/SPE 87195

Cairn Energy Plc., (2014). “Well Lifetime”

Calvert D.G., Dwight K. Smith, (1990). "Journal of Petroleum Technology,” pp. 1364-1373

Catalin Teodoriu, Mahmood Amani, Zhaoguang Yuan, Jerome Schubert, and Christian Kosinowski, (2012). “Investigation of Mechanical Properties of Class G Cement and Their Effect on Well Integrity,” International Journal of Engineering and Applied Sciences, Vol. 3, No. 2

Dominique Guillot, Nevio Moroni, Slavo Pastor and Augusto Zanchi, (2008). “Ensuring Zonal Isolation beyond Life of the Well,” Oilfield Review, pp. 18-31

Garnier, A., Saint-Marc, J., and Kermanac. Y., (2010). “An Innovative Methodology for Designing Cement Sheath Integrity Exposed To Steam Stimulation,” Society of Petroleum Engineers, SPE 117709

Garnier. A., Fraboulet. B., Saint-Marc. J., Bois. A. P., and Curistec, (2007). "Characterization of Cement System to Ensure Cement Sheath Integrity," Offshore Technology Conference, OTC 18754

Goodwin K. J., (1997). "Oil Well/ Gas Well Cement Sheath Evaluation" Society of Petroleum Engineers

Jandhyala, S., Barhate, Y. R., Anjos. J., Fonseka, C. E., and Ravi, K., (2013). "Cement Sheath Integrity in Fast Creeping Salts: Effects of Well Operations," Society of Petroleum Engineers, SPE 166622

John Campbell, (2012). "Activities and Risks," The International Association of Oil and Gas Producers

Kris Ravi, BR Reddy, Dennis Gray and Phil Pattillo, (2006). "Procedures to Optimize Cement Systems for Specific Well Conditions," American Association of Drilling Engineers, AADE-06-DF-HO-35

Malvar J., and Warren G., (1988). "Fracture Energy for Three-Point Bend Tests on Single-Edge Notched Beams," The Naval Civil Engineering Laboratory

Marathon Oil Co., (2000). "Eagle Ford: Oil and Natural Gas Fact Book"

Maurice B. Dusseault, Malcolm N. Gray, and Pawel A. Nawrocki, (2000). "Why Oil wells Leak: Cement Behavior and Long-Term Consequences," Society of Petroleum Engineers, SPE 64733

Phillip Pattilo, Kris Ravi, (2008). "Characterizing Cement Sheath Properties for Zonal Isolation," World Petroleum Congress

Ravi,K., Bosma, M., (2005). "Improve the Economics of Oil and Gas Wells by Reducing the Risk of Cementing Failure," CIPM

Simon Bittleston and Dominique Guillot, (1991). "Mud Removal: Research Improves Traditional Cementing Guidelines," Oilfield Review

Vipulanandan C., and Prashanth P., (2013). Impedance Spectroscopy Characterization of a Piezoresistive Structural Polymer Composite Bulk Sensor," Journal of Testing and Evaluation, Vol. 41, No. 6,

Vipulanandan. C, and Dharmarajan. N, (1989). “Critical Crack Tip Opening Displacement for Polymer Composites,” Engineering Fracture Mechanics, Vol 33, No 3, pp. 409-419

Walter Morris, Marcelo A. Criado, Jorge Robles and Gustavo Bianchi, (2003). “Design Of High Toughness For Effective Long Lasting Well Isolations,” Society of Petroleum Engineers, SPE 81001

Wei Wang, (2014). “Emergence of Delamination Fractures around Casing and Its Stability,” PhD Dissertation, Louisiana State University